

On the structure and reactivity of large complexes of metals and metalloids. A quantum chemical study.

Zur Erlangung des akademischen Grades eines

Doktors der Naturwissenschaften

(Dr. rer. nat.)

der Fakultät für Chemie und Biowissenschaften des
Karlsruher Instituts für Technologie (KIT) - Universitätsbereich
genehmigte

Dissertation

von
Magister

Adam Kubas

aus Zielona Góra, Polen

Dekan:	Prof. Dr. Martin Bastmeyer
Referent:	PD Dr. Karin Fink
Korreferent:	Prof. Dr. Willem Klopper
Tag der mündlichen Prüfung:	20.07.2012

CONTENTS

1	INTRODUCTION.....	5
2	THEORETICAL BACKGROUND.....	9
2.1	Basics of quantum chemistry	9
2.1.1	The Schrödinger equation	9
2.1.2	The variational principle	10
2.1.3	Many electron wave function: the Slater determinant.....	11
2.1.4	Some remarks about relativity	11
2.2	Single reference methods	13
2.2.1	The Hartree-Fock method	13
2.2.2	Møller-Plesset perturbation theory.....	15
2.2.3	Configuration Interaction and coupled-pair theories.....	17
2.2.4	Density functional theory.....	20
2.3	Multireference methods	24
2.3.1	Complete active space self-consistent field theory	24
2.3.2	Second order perturbation theory with CASSCF wave function	27
2.3.3	Multi reference configuration interaction	31
2.4	Common techniques.....	33
2.4.1	Basis sets.....	33
2.4.2	Resolution of the identity	34
2.4.3	Geometry optimisation.....	35
2.4.4	Normal mode analysis and thermodynamical corrections.....	37
3	APPLICATIONS – A THIN LINE BETWEEN COSTS AND ACCURACY.....	41
3.1	Additions of dialkylzinc to enals and iminals catalysed by paracyclophane-based ligands	41
3.1.1	Introduction.....	41
3.1.2	Computational details	45
3.1.3	NLE: formation of dimers.....	46
3.1.4	Interaction of substrate with complex A	48
3.1.5	Delocalization energy of substrates and transition states	50
3.1.6	Stereoselectivity	54
3.1.7	Regioselectivity.....	56
3.1.8	Thermodynamic vs. kinetic control.....	57
3.1.9	Screening of new ligands	58
3.1.10	Conclusions.....	60
3.2	Characterisation of unusual bonds in some germanium and tin clusters	62
3.2.1	Introduction.....	62
3.2.2	Computational details	64
3.2.3	Germanium cluster.....	64
3.2.4	Tin cluster	68
3.2.5	Conclusions.....	73

3.3	Nickel dimer and trimer: neutral and anionic states	74
3.3.1	Introduction	74
3.3.2	Computational details	75
3.3.3	Neutral and anionic states of the nickel dimer	76
3.3.4	Neutral and anionic states of the nickel trimer	83
3.3.5	Solvated nickel clusters	88
3.3.6	Conclusions	90
3.4	Molecular oxygen activation by β-diketonate cobalt complexes	92
3.4.1	Introduction	92
3.4.2	Computational details	94
3.4.3	Model	95
3.4.4	The ground state of the adduct	95
3.4.5	Oxygen uptake process	99
3.4.6	Conclusions	103
4	SUMMARY	105
5	ZUSAMMENFASSUNG (IN GERMAN)	109
6	PODSUMOWANIE (IN POLISH)	113
7	ACKNOWLEDGEMENTS	117
8	ACRONYMS	119
9	COPYRIGHT PERMISSIONS	121
10	LIST OF SCIENTIFIC PUBLICATIONS	123
11	BIBLIOGRAPHY	125

1 INTRODUCTION

Complexes, which are of particular interest in this work, are *molecular entities formed by loose association involving two or more component molecular entities*.¹ Coordination compounds of metals and ligands are the most prominent example of complexes. Such species, formed in the reaction of a Lewis acid (metal) and a Lewis base (ligand), are widespread in nature, e.g. in metalloproteins. The local environment of the metal centre influences its electronic structure and also determines the possible interactions with other molecules. The subsequent chemical transformation can then be very selective as only certain molecules can bind to the metal and react mainly in one direction. This idea underlays the premise of homogeneous catalysis with transition metals. In the early 80's it was anticipated that in the next 20 years homogeneous catalysis would be understood well enough to design new catalysts in a rational way.² Nowadays, this task is still a great challenge even though we have an understanding of a large number of reactions. Quantum chemical calculations can with this respect constitute an attractive alternative to expensive experimental trial and error.

In the present work the structures and reactivities of various polynuclear complexes are studied. The project has been carried out in the framework of the Transregio-Sonderforschungsbereich 88 "Cooperative Effects in Homo- and Heteronuclear Complexes (3MET)". In this context, theoretical calculations were undertaken to examine the electronic structure of a number of metal- and metalloid-containing systems in order to explain their properties and reactivities. The applications presented include the analysis of the reaction paths and the design of new paracyclophane-based ligands for the dialkylzinc additions to unsaturated aldehydes, the characterisation of unusual bonding patterns in large metalloid cluster compounds, accurate calculations of the structure of small nickel clusters as isolated molecules and solvated by alcohol molecules as well as studies of molecular oxygen activation by a cobalt complex. Important aspects of this work are careful benchmark studies which allow reliable predictions. It turned out that for some problems only expensive, highly correlated wave-function based methods were able to give qualitatively correct answers whereas for other properties more economical DFT computations provided satisfactory results. Furthermore, strong emphasis is put on the comparison with experimental findings. The topics presented in this work cover a wide range of structural problems (molecular geometry and electronic structure), calculations of spectroscopic data as well as the heart of chemistry – reaction mechanisms. The latter are not only used to explain observed phenomena but also to rationally design new, more selective and more efficient catalysts. In most cases a *less is more* strategy³ is applied to understand qualitatively the investigated systems, i.e. properties which are of particular interest are computed with the smallest possible model

systems. Such reductions allow to carefully check the methods, which are then applied to qualitative analysis of large, metal-containing systems.

The homogeneous metallic catalysts are complicated many-body systems and metallic nanoparticles are already in use as catalysts.⁴ On our way to fully understanding such nano-sized systems or clusters, which are midway between a molecule and the bulk material, like germanium and tin metalloid clusters discussed in chapter 3.2, we need methods that provide a compromise between accuracy and cost (time of calculations, computer resources needed). On the one hand very accurate methods have been developed over the years and we know how to systematically improve our results but on the other hand the size of the systems of interest limits the applicability of most of these methods. In the last two decades density functional theory (DFT), mainly in the Kohn-Sham formulation,⁵ was without doubts the most successful approach for these systems. However, Jacob's ladder proposed by Perdew,⁶ seems to be rather unstable – higher rungs (better functionals *by design*) do not always give better results for a property of interest.⁷ This was exactly the case in structural studies of small aluminium and tin clusters.⁸ Shortly, we will see that for the case of the nickel dimer, DFT can essentially give any bond distance. Another problem of DFT functionals is the absence of long range, weak interactions.⁹ Unfortunately, accurate geometry optimisation with post-Hartree-Fock methods for systems consisting of more than 50 atoms are extremely time consuming and – at some level of system size and method complexity – simply impossible. Also, calculations become a complicated task when static correlation starts to play an important role, i.e. the investigated system cannot be described by a single-determinant method (like DFT or HF) because of near degeneracies of the electronic states. This is particularly the case when molecules are far from the equilibrium geometries, e.g. if bonds are significantly elongated. Other prominent manifestations of static correlation are *3d* transition metal compounds with partially filled *d* shells. Once the static correlation problem is solved (or is not present) the dynamic correlation due to interaction of the electrons still remains an important contribution to the total energy. While DFT partially covers this type of correlation, the HF wave function must be augmented by excited configurations in order to account for dynamic correlation.

In most computations concerning homogeneous catalysis with metal complexes, DFT methods are employed due to the size of investigated systems.^{10,11} However, the unbalanced treatment of static and dynamic correlation make the transition metal chemistry a hard test for any functional because most of the popular exchange-correlation functionals were optimised and benchmarked mainly against compounds consisting of main group elements.¹² Many authors emphasize the need to test a set of DFT functionals before making final conclusions.^{10,12} A typical approach in computations of large, multimetallic systems is to compare various functionals with available experimental data. However, such an approach will certainly fail if experimental numbers have large uncertainties or are not available. This

work aims to go beyond the usual DFT calculations, i.e. for each system reliable wave function based reference data will be obtained and used to gain additional information about the investigated chemical structure or reaction.

This thesis is organised as follows. The presentation of results is preceded by the theoretical background of the methods used. This short outline focuses on the basics of selected quantum chemical concepts and aims to show the scope and limitations of various approaches. The application section is comprised of four topics. It begins with the investigation of the addition reactions of dialkylzinc to π -conjugated systems. The reaction is catalysed by bulky paracyclophane-based ligands and constitutes a challenging theoretical problem. On the one hand the long range interactions have to be handled properly because of the presence of bulky groups in the catalyst whereas on the other hand the correlation effects in the transition states have to be described consistently in order to predict the major product of the reaction quantitatively correct by transition state theory. Next, multireference calculations on large germanium and tin cluster compounds will give insights into the unusual bonding situation in these compounds. Unlike the transition states in the dialkylzinc additions, these molecules possess some significantly elongated bonds, but there is no compensation by formation of another bond. Consequently, multireference calculations have to be employed in order to explain the nature of this interaction. The third topic investigated in this thesis is the structure of small nickel clusters. To describe electron correlation in such systems in a balanced way a number of quantum-chemical methods are benchmarked with the complicated electronic structure of the nickel dimer. Selected methods are then used in studies of the electronic structure of Ni_2^- as well as in the geometry and ground state of the nickel trimer and its anion. The gained knowledge is then used in the calculations of the properties of small nickel clusters interacting with alcohol molecules. The obtained data can be directly compared with upcoming experimental measurements in order to derive the geometry of the clusters. The application section is closed by investigations of the molecular oxygen activation with a cobalt complex where the experience from all previously studied systems is combined in order to explain the reorganisation of spins in the analysed reaction. The energetic effect of the reaction as well as relative energies of states with various spin multiplicities are shown to be highly dependent on the method used. At the same time, the electronic structure of the final adduct with oxygen, e.g. the location and number of unpaired electrons, will directly reflect the reactivity of the system towards unsaturated alcohols. Final conclusive remarks can be found at the end in the summary.

2 THEORETICAL BACKGROUND

The aim of this chapter is to give an outline of the methods applied throughout this work. Theories which are well established and comprehensively described in text books are just briefly introduced. The focus is laid on recently developed methods as well as techniques that made them applicable to large molecular systems. The chapter is divided into four major parts. The first introduces the Schrödinger equation and discusses fundamental approximations which make quantum theory applicable to systems larger than the hydrogen atom. Moreover, through a short discussion of the Dirac equation we introduce approximate methods for the handling of relativistic corrections. The next two parts address two distinct approaches in quantum chemical calculations: single reference – HF-based and DFT – and multi reference (MR) methods. The chapter is closed with a description of the techniques common to all of the reviewed methods like basis sets, potential energy surface exploration or molecular vibrations and thermochemical calculations. For sake of simplification atomic units are used.

2.1 BASICS OF QUANTUM CHEMISTRY

2.1.1 THE SCHRÖDINGER EQUATION

Quantum chemistry was built on the time-independent non-relativistic Schrödinger equation:¹³

$$\hat{H}\Psi(\mathbf{x}, \mathbf{R}) = E\Psi(\mathbf{x}, \mathbf{R}) \quad (1)$$

where Ψ is a wave function of the space and spin coordinates \mathbf{x} of N electrons and spatial coordinates \mathbf{R} of M nuclei, E is the total energy associated with the system described by Ψ and \hat{H} is the Hamilton operator defined as:

$$\hat{H} = -\frac{1}{2} \sum_{i=1}^N \nabla_i^2 - \frac{1}{2} \sum_{A=1}^M \frac{1}{M_A} \nabla_A^2 - \sum_{i=1}^N \sum_{A=1}^M \frac{Z_A}{r_{iA}} + \sum_{i=1}^N \sum_{j>i}^N \frac{1}{r_{ij}} + \sum_{A=1}^M \sum_{B>A}^M \frac{Z_A Z_B}{R_{AB}} \quad (2)$$

In eq. (2) variables A and B run over all M nuclei of charge Z_M while i and j over all N electrons. The first two terms describe the kinetic energy of electrons (\hat{T}_e) and nuclei (\hat{T}_n). The next three terms define the potential energy of electron – nucleus interactions (\hat{V}_{en}), electron – electron interactions (\hat{V}_{ee}) and nucleus – nucleus interactions (\hat{V}_{nn}), respectively. In chemistry, we used to think about the molecules in context of their structure, i.e. spatial distribution of atoms. However, neither electrons nor nuclei are static particles. The conceptual bridge between chemistry and physics, that at the same time greatly reduces the complexity of the Schrödinger equation, is called adiabatic approximation.¹⁴ The idea here relies on the fact that even the smallest nucleus, a proton, is over three orders of magnitude

heavier than an electron. Thus, nuclei move much slower than electrons and it is assumed that the total wave function of the system can be expressed in the following form¹⁵

$$\Psi(\mathbf{x}, \mathbf{R}) \approx \Psi_e(\mathbf{x}, R)f(\mathbf{R}) \quad (3)$$

In the above equation, $\Psi_e(\mathbf{x}, R)$ parametrically depends on the fixed positions R of the nuclei, i.e. for any R there is a certain mathematical form of $\Psi_e(\mathbf{x}, R)$. The function $f(\mathbf{R})$ depends not only on R but also on the direction of the vector \mathbf{R} and therefore can be used in the description of molecular vibrations and rotations. We then group the Hamiltonian into two groups – electronic (\hat{H}_e) and nuclear ($\hat{T}_n + \hat{V}_{nn}$):

$$\hat{H} = (\hat{T}_e + \hat{V}_{en} + \hat{V}_{ee}) + (\hat{T}_n + \hat{V}_{nn}) = \hat{H}_e + (\hat{T}_n + \hat{V}_{nn}) \quad (4)$$

In the adiabatic approximation, $\Psi_e(\mathbf{x}, R)$ is an eigenfunction of the electronic Hamiltonian \hat{H}_e . In calculation of $f(\mathbf{R})$ we assume that the movement of nuclei and electrons is uncoupled, i.e. the nuclei ‘feel’ the average field arising from the fixed configuration of electrons for certain R and therefore the position of electrons determine the potential energy of the nuclei. The last statement is a subject of the Born-Oppenheimer approximation¹⁶ which allows to use such concepts like the shape of a molecule or potential energy surface of a chemical system.

From now on we will focus solely on the electronic problem

$$\hat{H}\Psi(\mathbf{x}) = E\Psi(\mathbf{x}) \quad (5)$$

where $\hat{H} = \hat{H}_e$ as defined in eq. (4), E is electronic energy and $\Psi(\mathbf{x}) = \Psi_e(\mathbf{x}, R)$ for clarity.

2.1.2 THE VARIATIONAL PRINCIPLE

The Schrödinger equation can be solved exactly only for a small number of model problems. If a many-body problem has to be solved then an approximate wave function is needed. It is easy to show that the energy ε , calculated with any trial wave function Φ will be always larger or equal to the energy of the ground state E_0 :

$$\varepsilon[\Phi] = \frac{\langle \Phi | \hat{H} | \Phi \rangle}{\langle \Phi | \Phi \rangle} \geq E_0 \quad (6)$$

If we now assume that Φ is a finite, continuously differentiable and normalized function (is a Q -class function) then we have a clear prescription of obtaining approximate wave function which is the variational principle. Such a trial wave function is usually constructed from a linear combination of P known basis functions $\{\Psi_i\}$:

$$\Phi = \sum_{i=1}^P c_i \Psi_i \quad (7)$$

The variational parameters c_i are optimised in order to get the lowest possible energy in the given set of basis functions. This method, firstly formulated by Ritz,¹⁷ paved the way for a

class of quantum-chemical methods called variational where the energy is minimised by a systematic refinement of the trial wave function.

2.1.3 MANY ELECTRON WAVE FUNCTION: THE SLATER DETERMINANT

The variational principle introduced in the previous paragraph is a lighthouse for the search of an optimal wave function. However, it says nothing about the form of this function. Analytical solutions of Schrödinger equation for model systems give some one-electron wave functions but the many electron analogues are not known. From physical considerations we only know that they have to be functions of Q -class that depend on the same variables like the exact solution as well as have to be antisymmetric under permutation of electrons (change the sign upon relabeling of an electron pair). Slater¹⁸ proposed N -electron function of the following determinant-form:

$$\Psi_{\text{Slater}} = \frac{1}{\sqrt{N!}} \begin{vmatrix} \phi_1(1) & \dots & \phi_1(N) \\ \vdots & \ddots & \vdots \\ \phi_N(1) & \dots & \phi_N(N) \end{vmatrix} \quad (8)$$

In this definition ϕ_i are orthonormal one-electron spinorbitals (products of orbitals and spin functions) and the factor before the determinant is a normalization factor. The Slater determinant (8) has desired properties:

- changing the labels of electrons means exchange of columns of the determinant – the function is antisymmetric,
- two electrons cannot occupy the same spinorbital (Pauli principle) – in this case two columns are equal and the determinant vanishes.

Most of the quantum chemical methods use the Slater approach either in one-determinant form (single reference methods) or in multi-determinant formulation (multireference methods). Nevertheless, one should have in mind that the wave function in form of eq. (8) does not depend on the interelectronic distance r_{12} . Therefore, in order to at least approximately describe the electronic cusp one has to use large orbital basis sets. A different approach is to explicitly correlate the motion of electrons which can be achieved for example by means of f_{12} methods.¹⁹ However, due to its mathematical complexity this approach is still limited to medium-sized molecules containing main-group elements.

2.1.4 SOME REMARKS ABOUT RELATIVITY

Ground state energies and properties of molecular systems obtained with eq. (5) suffer from the non-relativistic treatment of motion. While this effect is negligible for light elements, it contributes significantly to the chemical behaviour of heavy elements mainly through contraction of orbitals.²⁰ Recently, an extreme example of the importance of relativistic correction has been shown for the calculation of the standard voltage of the lead-acid battery.²¹ It appeared, that only 20% of the voltage can be recovered in non-relativistic calculations.

The treatment of a finite speed of light with all its consequences requires the usage of the electron-positron Dirac equation:²²

$$[\boldsymbol{\beta}c^2 + c(\boldsymbol{\alpha} \cdot \mathbf{p}) + V]\psi = i\hbar \frac{\partial}{\partial t} \psi; \psi = \begin{bmatrix} \psi^L \\ \psi^S \end{bmatrix} \quad (9)$$

where c is the speed of light, V an external potential, \mathbf{p} the momentum operator, and $\boldsymbol{\alpha}$, $\boldsymbol{\beta}$ are the 4×4 Dirac matrices.²³ The spinor ψ which appears in eq. (9) in place of Schrödinger's wave function consists of a so-called small (ψ^S) and large (ψ^L) component. In Dirac theory we are mainly interested in the stationary electronic solution. The Dirac equation for an electron in a molecular field has the following form:

$$\begin{aligned} h_D \psi &= E^+ \psi \\ h_D &= \boldsymbol{\beta}' c^2 + c(\boldsymbol{\sigma} \cdot \mathbf{p}) + V = \begin{bmatrix} V & c(\boldsymbol{\sigma} \cdot \mathbf{p}) \\ c(\boldsymbol{\sigma} \cdot \mathbf{p}) & V - 2c^2 \end{bmatrix} = \begin{bmatrix} h_{LL} & h_{LS} \\ h_{SL} & h_{SS} \end{bmatrix} \\ \boldsymbol{\beta}' &= \boldsymbol{\beta} - \mathbf{I}_4 \end{aligned} \quad (10)$$

where $\boldsymbol{\sigma}$ is a vector that collects the Pauli spin matrices and \mathbf{I}_4 denotes a 4×4 identity matrix. The one-electron Dirac operator h_D can be used in place of the nonrelativistic one-electron operator in the electronic structure calculations. To take into account the relativistic effects in the two electron repulsion terms, $g(1,2)$, the Breit terms²⁴⁻²⁶ have to be considered in addition to the classical $1/r_{12}$ term:²⁷

$$g(1,2) = \frac{1}{r_{12}} - \frac{\boldsymbol{\alpha}(1) \cdot \boldsymbol{\alpha}(2)}{r_{12}} + \frac{1}{2} \left[\frac{\boldsymbol{\alpha}(1) \cdot \boldsymbol{\alpha}(2)}{r_{12}} - \frac{(\boldsymbol{\alpha}(1) \cdot \mathbf{r}_{12})(\boldsymbol{\alpha}(2) \cdot \mathbf{r}_{12})}{r_{12}^3} \right] \quad (11)$$

In conjunction with h_D for the one electron part, the resulting Hamiltonian is the Dirac-Coulomb-Breit (DCB) Hamiltonian.

The small and large components of the spinor ψ are coupled through eq. (9) by the coupling operator \mathbf{R} :

$$\psi^S = \mathbf{R}\psi^L; \mathbf{R} = (2c^2 - V + E^+)^{-1} c(\boldsymbol{\sigma} \cdot \mathbf{p}) \quad (12)$$

Thus, the one-electron operator h_D can be block-diagonalised by some unitary transformation:

$$\mathbf{U}^\dagger h_D \mathbf{U} = \mathbf{U}^\dagger \begin{bmatrix} h_{LL} & h_{LS} \\ h_{SL} & h_{SS} \end{bmatrix} \mathbf{U} = \begin{bmatrix} \tilde{h}_{++} & 0 \\ 0 & \tilde{h}_{--} \end{bmatrix} \quad (13)$$

The operator \tilde{h}_{++} will then only act on the large, electronic component. The exact unitary transformation is given as:

$$\mathbf{U} = \begin{bmatrix} \Omega_+ & -\mathbf{R}^\dagger \Omega_- \\ \mathbf{R} \Omega_+ & \Omega_- \end{bmatrix}; \Omega_+ = \frac{1}{\sqrt{1 + \mathbf{R}^\dagger \mathbf{R}}}; \Omega_- = \frac{1}{\sqrt{1 + \mathbf{R} \mathbf{R}^\dagger}} \quad (14)$$

However, the unitary transformation (14) is usually done in an approximate way because the coupling \mathbf{R} depends explicitly on the electronic energy (see eq. (12)). For example by taking

$$\mathbf{R} = (2c^2 - V + E^+)^{-1} c(\boldsymbol{\sigma} \cdot \mathbf{p}) \approx \frac{1}{2c} (\boldsymbol{\sigma} \cdot \mathbf{p}) \quad (15)$$

and applying the unitary transformation to the Dirac Hamiltonian one obtains the Pauli one-electron Hamiltonian:²⁸

$$\hat{h}^{Pauli}(i) = V + T_i - \frac{p_i^4}{8c^2} + \frac{1}{4c^2} \boldsymbol{\sigma} [(\nabla V) \times \mathbf{p}_i] + \frac{1}{8c^2} (\nabla^2 V) \quad (16)$$

where only terms to $O(c^{-2})$ were retained. In the Hamiltonian (16), the non-relativistic terms are extended by three relativistic corrections: mass-velocity, spin-orbit and Darwin term, respectively.²³ The Hamiltonian which combines the Pauli approach to the one-electron part and the Breit correction to the two-electron interactions is called the Breit-Pauli Hamiltonian.²⁹ However, the computations with the resulting operator are rather demanding, especially for the spin-orbit terms. Thus, in many cases the effective nuclear charge approximation is used.³⁰ Alternatively, the mean-field approach of Hess *et. al.*³¹ can be employed. Other possibilities to carry out the unitary transformation (14) include the zeroth-order regular approximation (ZORA)³²⁻³⁴ or the Douglas-Kroll-Hess (DKH) method.³⁵⁻³⁷ In the latter, the spin-dependent terms are usually neglected (scalar DKH).²⁹ Therefore, the spin-orbit effects can be included in the next step, e.g. from the spin-orbit operator based on the Pauli Hamiltonian (16):

$$h^{SO}(i) = \sum_{A=1}^N \frac{Z_A e^2}{4c^2 r_{iA}^3} \boldsymbol{\sigma} \cdot \mathbf{l}_{Ai} \quad (17)$$

where the orbital angular momentum operators \mathbf{l}_{Ai} are defined with respect to each nucleus A . Even more routinely, scalar relativistic effects are introduced into non-relativistic calculations using relativistic effective core potentials (ECP).³⁸ This approach is based on the observation that relativistic effects have the largest influence on the low lying, core electrons, which in chemical reactions do not play as important a role as the valence electrons. Therefore, core electrons can be substituted by a special effective potential which then is used in the Hamiltonian from eq. (5) while valence shells are described in the usual way with accordingly optimised exponents of the basis sets.

2.2 SINGLE REFERENCE METHODS

2.2.1 THE HARTREE-FOCK METHOD

The Hartree-Fock method belongs to the class of variational methods with a trial function consisting of a Slater determinant. By minimising the energy with respect to spinorbitals one can derive the canonical Hartree-Fock equations:

$$\hat{F} \phi_i = \epsilon_i \phi_i \quad (18)$$

where ϕ_i are canonical Hartree-Fock orbitals (molecular orbitals, MOs) and ϵ_i are respective orbital energies. The Fock operator, \hat{F} , is an effective one-electron operator defined as a sum of three operators:

$$\hat{F} = \hat{h} + \hat{J} - \hat{K} \quad (19)$$

The first operator on the right side of the eq. (19) gives a sum of the kinetic energy of the electron and its attraction potential to all nuclei. The Coulomb operator \hat{J} is associated with the average repulsion between an electron i and all electrons while the exchange operator \hat{K} does not have a classical interpretation. It arises from the antisymmetric nature of the single determinant wave function and, in contrary to the Coulomb operator, has a nonlocal character. Both Coulomb and exchange operators define the so-called mean-field potential and therefore Hartree-Fock theory is sometimes referred to as a mean-field approximation.

The Hartree-Fock equations can be conveniently solved when the unknown MOs are expressed in terms of a basis set expansion. In most cases we employ the linear combination of K atomic orbitals (LCAO)³⁹ to form MOs:

$$\phi_i = \sum_{\mu=1}^K c_{\mu i} \chi_{\mu} \quad (20)$$

where $c_{\mu i}$ are the expansion coefficients and χ_{μ} are the atomic orbitals. Thus, the LCAO approach reduces the Hartree-Fock ansatz to finding the best expansion coefficients for a given finite basis set (for $K = \infty$ the solution is exact if the basis is complete). According to Roothaan⁴⁰ and Hall,⁴¹ for closed-shell molecules (restricted Hartree-Fock method, RHF) this can be written in matrix form as

$$\mathbf{FC} = \mathbf{SC}\epsilon \quad (21)$$

In eq. (21) \mathbf{F} denotes the Fock matrix, \mathbf{S} is an array of overlap integrals between basis functions χ_{μ} , \mathbf{C} is a matrix of coefficients searched and ϵ denotes the orbital energies. For open-shell systems, like for many of the transition metal compounds, the unrestricted Hartree-Fock (UHF) problem has to be solved. While in the restricted case two electrons on the same molecular orbital have the same spatial function and differ only in spin functions (α and β), in unrestricted formalism both parts can be different and therefore two sets of molecular orbitals are needed. For each set one simply solve the unrestricted analogues of eq. (21) – the Pople-Nesbet equations:⁴²

$$\mathbf{F}^{\alpha}\mathbf{C}^{\alpha} = \mathbf{S}\mathbf{C}^{\alpha}\epsilon^{\alpha} \quad (22)$$

$$\mathbf{F}^{\beta}\mathbf{C}^{\beta} = \mathbf{S}\mathbf{C}^{\beta}\epsilon^{\beta} \quad (23)$$

The main difficulty within the UHF approach is that the resulting wave function is no longer necessarily eigenfunction of the \hat{S}^2 operator. The deviation from the ideal expectation value of this operator ($\langle\langle\hat{S}^2\rangle\rangle = s(s+1)$, where s denotes total spin) can serve as a tool for diagnosing the stability of the UHF solution. When large differences are obtained (high spin contamination) then one has to use either spin-projection techniques⁴³ or switch to the restricted open-shell Hartree-Fock method (ROHF).⁴⁴ Briefly, it introduces a special form of the Fock operator where doubly occupied orbitals are treated separately from singly occupied orbitals and coupled by additional terms. The MOs are then obtained with eq. (21). The main

disadvantage in the ROHF method is the form of the Fock matrix which is not unique and various orbitals can lead to the same total wave function and total energy. However, if an orbital-invariant post-HF method is to be used with ROHF reference then this is not a particular problem. It should be emphasised that ROHF orbitals are usually a good starting point in complete active space self-consistent field (CASSCF) calculations as discussed in next chapters.

The Fock operator depends on the coefficients used in the basis set expansion and therefore the Roothaan-Hall equations have to be solved in an iterative way. In the first step we assume a set of arbitrary MO coefficients solve the eq. (21) and obtain corresponding intermediate molecular orbitals. Then we use them to get new coefficients and corresponding new orbitals. Such self-consistent field (SCF) procedure is converged when the total energy change between two consequent iterations is smaller than a given threshold. Moreover, when a high accuracy is desired, also the change of the coefficients can be controlled.

In the conventional SCF method all two-electron integrals are calculated and stored on the hard disk. However, this increases the number of I/O operations and is rather ineffective for large systems (formal scaling of N^4). Here, the *direct* SCF approach is preferred and two-electron integrals are calculated *on demand* and with pre-screening techniques (formal scaling is reduced to N^3).⁴⁵ To save time, the starting or guess orbitals should be already close to the proper solution and usually one employs some semiempirical method, like extended Hückel theory (EHT) used in this study, in order to obtain good starting point for SCF iteration.

The Hartree-Fock method with its chemically intuitive form (with molecular orbitals and corresponding energies) has unfortunately many limitations. In HF theory the only effect which correlates the movement of electrons is the electron exchange (Fermi correlation) which prevents two electrons with parallel spins to occupy the same point in space. The probability of finding electron i at some point does not change upon movement of another electron j if they have opposite spins. The dynamic correlation is missing in this case. Moreover when more than one electronic configuration is important for the description of the certain electronic state (near degeneracy) then one-determinant methods are no longer valid and have to be exchanged with multi-determinant based approaches.

2.2.2 MØLLER-PLESSET PERTURBATION THEORY

When the Hartree-Fock method is a good approximation to the real wave function, then the remaining correlation energy can be approximated through a series of small perturbations to the ground state HF wave function ψ_0^{HF} . In this case, the real Hamiltonian \hat{H} can be divided into two contributions – a large non-perturbed Hamilton operator $\hat{H}^{(0)}$ and a small perturbation operator $\lambda\hat{H}^{(1)}$ where λ is a perturbation parameter ($0 \leq \lambda \leq 1$):

$$\hat{H} = \hat{H}^{(0)} + \lambda\hat{H}^{(1)} \quad (24)$$

We assume that the 0th order Hamiltonian has a form of a sum of known one-electron Fock operators:

$$\hat{H}^{(0)} = \sum_i \hat{F}(i) \quad (25)$$

It is readily visible that acting with $\hat{H}^{(0)}$ on the $\psi_0^{HF} = \psi_0^{(0)}$ one obtains the 0th order energy $E_0^{(0)}$, being the sum of the energies of the occupied HF spinorbitals:

$$\hat{H}^{(0)}\psi_0^{(0)} = E_0^{(0)}\psi_0^{(0)} = \left(\sum_i \epsilon_i \right) \psi_0^{(0)} \quad (26)$$

According to the perturbation expansion the change of $\psi_0^{(0)}$ upon application of the perturbation has a form:

$$\psi_0(\lambda) = \psi_0^{(0)} + \lambda\psi_0^{(1)} + \lambda^2\psi_0^{(2)} + \dots \quad (27)$$

with corresponding expansion of the total energy:

$$E_0(\lambda) = E_0^{(0)} + \lambda E_0^{(1)} + \lambda^2 E_0^{(2)} + \dots \quad (28)$$

When equations (24), (27) and (28) are now combined in the Schrödinger equation one obtains an infinite sequence of perturbation equations, one for each power of λ .

Assuming intermediate normalization ($\langle \psi_0^{(0)} | \psi_0^{(n)} \rangle = \delta_{0n}$), first and second order energy corrections can be written:

$$E_0^{(1)} = \langle \psi_0^{(0)} | H_0^{(1)} | \psi_0^{(0)} \rangle \quad (29)$$

$$E_0^{(2)} = \langle \psi_0^{(0)} | H_0^{(1)} | \psi_0^{(1)} \rangle \quad (30)$$

Because $\psi_0^{(1)}$ is unknown we expand it as a linear combination of the known eigenfunctions of $H_0^{(0)}$, i.e. we expand it in terms of doubly excited Slater determinants ψ_{ab}^{pq} (here a, b and p, q denote occupied and unoccupied spinorbitals in $\psi_0^{(0)}$, respectively). The use of only doubly excited determinants is a consequence of Brillouin's theoremⁱ and the Slater-Condon rules.ⁱⁱ It is here clear that the sum of 0th and 1st order energies defines the Hartree-Fock energy. The sum of this reference energy and the 2nd order correction gives the second-order energy, the Møller-Plesset energy at second order:

$$E_{\text{MP2}} = E_{\text{HF}} + \sum_{a < b, p < q} \frac{|\langle ab|pq\rangle - \langle ab|qp\rangle|^2}{\epsilon_a + \epsilon_b - \epsilon_p - \epsilon_q} \quad (31)$$

ⁱSingle excitations do not contribute to the total ground state energy.

ⁱⁱIf two determinants differ by more than two spinorbitals then the expectation value of a two-electron operator calculated with these determinants equals zero

One can expect that the addition of higher order corrections to the E_{MP2} should improve the energy and, consequently, lead to the limit of the non-relativistic, single determinant ansatz (at some intermediate order, however, the energy can drop below the exact solution because the MP energy is not variational). This is true for ground state geometries of molecules which are already well described at HF level. However, this is not true in general. In problems, where the correlation effects play a major role (e.g. during bond breaking) the $\text{MP}n$ series likes to oscillate and higher corrections sometimes lead to pathological behaviour.⁴⁶ It is therefore common to stop at the relatively economic MP2 level (formal scaling with system size of N^5) for ground state properties of closed shell molecules consisting mainly from main-group elements.

Recently, Grimme proposed the spin-component scaled variants of MP2⁴⁷ and MP3⁴⁸ calculations (SCS-MP2/MP3) that constitute a significant improvement over the conventional approaches at no additional cost. Particularly, the SCS-MP2 method was widely tested for structure and properties of weakly bounded systems^{49,50} as well as for other molecular structures, vibrational frequencies and thermodynamical properties of a wide group of closed and open shell molecules.^{51,52} Basically, the SCS-MP2 energy is defined as

$$E_{\text{SCS-MP2}} = E_{\text{HF}} + c_{os}E_{os} + c_{ss}E_{ss} \quad (32)$$

where the second term from eq. (31) was exchanged by a sum of the opposite-spin contribution to the second-order correlation energy, E_{os} , and the corresponding same-spin contribution, E_{ss} , weighted by parameters c_{os} and c_{ss} , respectively. When $c_{os} = c_{ss} = 1$, eq. (32) is equivalent to eq. (31) because the second-order energy can be easily decomposed into contributions from electron pairs.⁵³ Grimme⁴⁷ fitted the parameters c_{os} and c_{ss} to a set of known reaction energies and obtained scaling factors of 6/5 and 1/3 for E_{os} and E_{ss} , respectively. Following the original argumentation, the first parameter is larger than one because α,β -pair contributions are underestimated by MP2 by about 20% while the same-spin energy has to be scaled down in order to keep the second-order energy contribution at about MP2 level. However, depending on the applications, several other parameterizations have been proposed and tested.⁵⁴

2.2.3 CONFIGURATION INTERACTION AND COUPLED-PAIR THEORIES

The $\text{MP}n$ theory constitutes a significant improvement over the Hartree-Fock approximation but does not offer a general way of systematic convergence to the non-relativistic limit in a given basis set. This is fulfilled by a method called configuration interaction (CI) where the wave function of the system is constructed from the linear combination of all possible Slater determinants:

$$\psi = \sum_{I=0} c_I \psi_I = c_0 \psi_0 + \sum_{ap} c_a^p \psi_a^p + \sum_{\substack{a<b \\ p<q}} c_{ab}^{pq} \psi_{ab}^{pq} + \sum_{\substack{a<b<c \\ p<q<r}} c_{abc}^{pqr} \psi_{abc}^{pqr} + \dots \quad (33)$$

In (33), the reference ψ_0 is usually taken as a Hartree-Fock wave function and the following determinants are constructed by varying the occupations of spinorbitals in the reference determinant. This is successively done by including higher and higher excitations from occupied orbitals a,b,c,\dots to unoccupied (virtual) orbitals p,q,r,\dots of the zeroth-order wave function. The linear parameters c are optimised according to the general Ritz procedure. This involves calculations of Hamiltonian matrix elements between *all* pairs of ψ_I determinants. If all possible excitations are included then the method is called *full* CI (FCI). However, even for small molecules this become unfeasible because the number of determinants that has to be handled increases rapidly with the system size and basis set. The largest FCI calculations up to date included about 10^{10} Slater determinants and were applied to energy calculations of N_2 molecule (still with rather moderate basis set).⁵⁵

In order to reduce the complexity of FCI problem a number of truncations to the CI expansion were proposed. Practically, the list of excitations is limited to some prescribed order, e.g. up to quadruple excitations. The method is then named after the excitations that are included in the CI expansion: CISD means configuration interaction – singles and doubles, CISDT stands for configuration interaction – singles, doubles and triples etc. Unfortunately, any truncated CI method is not size consistent in general, i.e. the energy of two non-interacting molecules is not a simple sum of the energies of both of them, calculated within the same approximation. With increasing system size, higher excitations have to be included. In practise, however, for small systems the CISDTQ is effectively size consistent (nonetheless, prohibitively expensive).

Further truncation of the CI expansion can be achieved in a basis of natural orbitals (NOs) as introduced by Löwdin.⁵⁶ Here, after the first CI iteration the density ρ is constructed:

$$\rho(1) = \int \psi^*(1,2,\dots,N)\psi(1,2,\dots,N)d\tau_2d\tau_3\dots d\tau_N = \sum_{ij} D_{ij} \phi_i^*(1)\phi_j(1) \quad (34)$$

where the summation runs over all spinorbitals. Next, the density matrix \mathbf{D} is diagonalised to yield a new set of orbitals – NOs – and corresponding occupation numbers (diagonal elements of the density matrix). The orbitals occupied in the reference state ψ_0 are called *strongly occupied* and the virtual *weakly occupied*. The CI expansion is then performed by means of exciting electrons within the space of natural orbitals which in most cases is truncated at some point by restricting excitations only to weakly occupied NOs with occupation number higher than a certain threshold. However, this approach is not efficient for large systems because in order to get good NOs one needs to perform some CI calculations without truncation (NOs coming from HF calculations are a rather poor choice). For the CI approaches which consider only single and double excitations a more convenient approximation has been proposed by Meyer^{57,58} and subsequently extended by Ahlrichs and co-workers.⁵⁹ They suggested the use of PNOs (pair natural orbitals sometimes called also pseudo natural orbitals) in order to reduce the CI-expansion length. The PNOs are most conveniently defined by firstly

introducing the so-called independent electron pair approximation (IEPA) where in the primary step all individual pair correlation energies ε_{ab} are calculated:

$$\psi_{ab} = c_0 \psi_0 + \sum_{p<q} c_{ab}^{pq} \psi_{ab}^{pq} \Rightarrow \varepsilon_{ab} = \langle \psi_{ab} | \hat{H} | \psi_{ab} \rangle \quad (35)$$

Thus, the total correlation energy is a sum of all ε_{ab} . The IEPA is equivalent to doing CID calculations for each pair separately. In a next step one constructs approximate natural orbitals for each electron pair function ψ_{ab} .ⁱ By introducing a threshold for occupation numbers of weakly occupied PNOs and rejecting pairs with negligible pair correlation energy (this can be corrected perturbatively) one ends up with a very compact PNO-IEPA expansion that roughly approximates the FCI.

The IEPA method, in contrast to CID, is size consistent but usually significantly overestimates the correlation energy which would be obtained by means of FCI in a given basis set, mainly due to the lack of inter-pair correlation. In his pioneering work on PNOs,⁵⁸ Meyer proposed a relatively simple way to include the correlation between pairs, namely the CEPA (coupled electron pair approximation) method. He noted, that the quadruple excitations $abcd \rightarrow pqrs$ can be well approximated by assuming that they can be accounted for by a combination of double excitations. Similar to the coupled cluster approximation (CC), the coefficients of such terms are then expressed by a simple product of respective coefficients of double excitations ($c_{abcd}^{pqrs} \cong c_{ab}^{pq} c_{cd}^{rs}$). The pair correlation energy within CEPA approximation can be then expressed as:

$$\varepsilon_{ab} = \sum_{p<q} \langle \psi_0 | \hat{H} | \psi_{ab}^{pq} \rangle c_{ab}^{pq} \quad (36)$$

while the equation that has to be solved in order to get the coefficients c_{ab}^{pq} becomes:

$$\langle \psi_{ab}^{pq} | \hat{H} | \psi_0 \rangle + \sum_{\substack{c<d \\ r<s}} \langle \psi_{ab}^{pq} | \hat{H} - E_0 | \psi_{cd}^{rs} \rangle c_{cd}^{rs} = \varepsilon_{ab} c_{ab}^{pq} \quad (37)$$

The solution of the CEPA equations (36) and (37) is more complicated than in the case of IEPA because the pair correlation energy ε_{ab} depends on the coefficients of all other pairs c_{cd}^{rs} and must be determined in the iterative procedure. The total energy of the system is the sum of all pair correlation energies:

$$E_{CEPA} = \sum_{a<b} \varepsilon_{ab} \quad (38)$$

However, the CEPA correlation energy has to be corrected by removing terms that violate the exclusion principle (EPV terms), i.e. we have to subtract energy terms that arise from double excitations out of occupied or into an empty orbital of the reference determinant from the correlation to avoid double counting. The strict correction is performed in the CEPA/3

ⁱ The PNOs obtained in this way can then be iteratively improved. For details see R. Ahlrichs, F. Driessler, *Theor. Chim. Acta* 1975, **36**, 275.

approach while CEPA/2 and CEPA/1 account for this only partially. CEPA/0 totally neglects this problem. However, the ordering of CEPA approaches is a bit misleading because CEPA/1 is a more rigorous approximation than CEPA/2. Any type of CEPA is superior to CID or IEPA by virtue of coupling between double excitations and approximately size consistency (if based on localized internal orbitals). Moreover, when augmented with single excitations it can be successfully applied for ground state property calculations as well for excited states. For further details of CEPA versions and technical details we refer to excellent review of Ahlrichs.⁶⁰

The CEPA method together with the PNO approach (PNO-CEPA) was successfully applied to electronic structure description of some small molecules like acetylene cation⁶¹ or silicon hydride.⁶² However, it has been abandoned for years in favour of more rigorous coupled – cluster methods which are unfortunately more expensive. In this context, it should be noted that CEPA results are close to CCSD(T) numbers (today’s “gold standard” in quantum chemistry) and are obtained in significantly shorter computation time. Lots of effort have been made towards locally correlated CC methods⁶³ based on the idea of Pulay’s *correlation domains*.⁶⁴ Nevertheless, recently Neese and co-workers revived the PNO approach in context of CEPA⁶⁵ and CCSD⁶⁶ framework. They showed, that in this way one retrieves more correlation energy than in locally correlated methods, the potential energy surfaces are very smooth as well as the computation effort scales much better with the number of basis function (the number of PNOs stays rather constant with basis set extension). The scaling of the method is unfortunately far from being linear (like in local correlated methods) and the most expensive step reaches N^5 where N is the number of basis functions. It is still much less than canonical calculations and the method can be applied to systems of about 100 atoms with up to 2500 basis functions. Calculations performed in this work support the statement that PNO-CEPA method yields qualitative agreement with experimental data and is superior to latest DFT functionals and to the SCS-MP2 approach.

2.2.4 DENSITY FUNCTIONAL THEORY

Density functional theory (DFT) represents a different approach to the electron correlation than wave function based methods so far discussed. Here, the central quantity is the electron density $\rho(\mathbf{r}_i)$ defined as an integral of the module of a wave function over all space and spin variables of all but one electrons and spin variable of electron i , multiplied by the number of electrons N :

$$\rho(\mathbf{r}_1) = N \int |\Psi(\mathbf{r}_1, \mathbf{r}_2, \mathbf{r}_3 \dots, \mathbf{r}_N)|^2 ds_1 d\mathbf{r}_2 d\mathbf{r}_3 \dots d\mathbf{r}_N \quad (39)$$

The integration of the electron density over space gives the number of electrons and the density of a molecule has cusps at positions of nuclei.

The slope of the cusp is determined by the nuclear charge. Hohenberg and Kohn⁶⁷ proved that the electron density uniquely defines the interaction between nuclei and electrons, i.e. there is only one external potential $v(\mathbf{r}_i)$,

$$v(\mathbf{r}_i) = - \sum_{A=1}^M \frac{Z_A}{r_{iA}} \quad (40)$$

that results in the density $\rho(\mathbf{r}_i)$. Therefore, all the information about the molecule is incorporated in the electron density and the total energy of the system can be written as a functional of the density:

$$E[\rho] = V_{en}[\rho] + T[\rho] + V_{ee}[\rho] = \int \rho(\mathbf{r})v(\mathbf{r})d\mathbf{r} + F[\rho] \quad (41)$$

In equation (41) the electron-nucleus interaction can be expressed by the integral of the density because \hat{V}_{en} contains only one-electron operators and electrons are indistinguishable. The $F[\rho]$ is called universal functional and consists of the kinetic energy and electron-electron repulsion functionals. There exists an electron density analogue of the variational principle and is called the second Hohenberg-Kohn theorem.⁶⁷ It says that the energy obtained with any trial density $\tilde{\rho}$ that defines its own wave function $\tilde{\Psi}$ will be larger than or equal to the energy that corresponds to the exact density ρ :

$$E[\tilde{\rho}] = \langle \tilde{\Psi} | \hat{H} | \tilde{\Psi} \rangle = \int \tilde{\rho}(\mathbf{r})v(\mathbf{r})d\mathbf{r} + F[\tilde{\rho}] \geq E[\rho] \quad (42)$$

The relation (42) holds only for the exact universal functional that has an unknown form. However, a useful approach was proposed by Kohn and Sham.⁵ They suggested that the electron density of N electrons moving in the external field $v(\mathbf{r})$ arising from nuclei and interacting between each other through Coulombic forces can be obtained by setting up a fictitious system of N *non-interacting* electrons moving in the external field $\hat{v}_0(\mathbf{r})$ matched in this way that it yields the electron density of the real system. The total energy of the system can then be written in the form:

$$E = \int \rho(\mathbf{r})v(\mathbf{r})d\mathbf{r} + T_s[\rho] + J[\rho] + E_{xc}[\rho] \quad (43)$$

where $T_s[\rho]$ is the sum of kinetic energies of all non-interacting electrons and $J[\rho]$ is a classical Coulomb repulsion:

$$J[\rho] = \frac{1}{2} \iint \frac{\rho(\mathbf{r}_1)\rho(\mathbf{r}_2)}{r_{12}} d\mathbf{r}_1 d\mathbf{r}_2 \quad (44)$$

Such repulsion functional does not include the Coulomb holes of individual electrons. This is moved to the exchange-correlation functional $E_{xc}[\rho]$ which additionally incorporates also the correction for a Fermi hole, so that electrons of the same spin avoid themselves as well as includes some small kinetic energy correction to the real kinetic energy of electrons. Despite that it is known that the latter is small, the exact form of this functional is not known. As a

consequence, some *a priori* defined exchange-correlation functional has to be used in molecular calculations. In the analogy to HF equations, the Kohn-Sham approach involves the self-consistent solution of the Kohn-Sham equations:

$$\left(-\frac{1}{2}\nabla^2 + v(\mathbf{r}) + \frac{\delta J[\rho]}{\delta\rho(\mathbf{r})} + \frac{\delta E_{xc}[\rho]}{\delta\rho(\mathbf{r})} \right) \varphi_i(\mathbf{r}) = \epsilon_i \varphi_i(\mathbf{r}) \quad (45)$$

The Kohn-Sham orbitals – $\varphi_i(\mathbf{r})$ – are then used to construct the total electron density that can be used in total energy calculations (see eq. (43)).

The DFT methods are usually classified according to the exchange-correlation functional they involve. Furthermore, the functionals are often split into an exchange and a correlation part and new functionals can be formulated by any combinations of them. In the simplest local density approximation (LDA) the exchange functional is taken as a function of the density deduced from the uniform gas model (S and $X\alpha$ functionals⁶⁸). The correlation energy is then approximated usually in form of the Vosko-Wilk-Nusair (VWN)⁶⁹ correlation functional which is also just a function of the density. Although this approach was successful in physics where spatially uniform (local) form of the density is a good model for some solids, the molecular density has a non-local character and LDA is here certainly limited. Thus, another class of functionals were developed based on the generalised gradient approximation (GGA). They depend not only on the density but also on its gradient that in most cases is scaled by some parameter and used to correct the chosen LDA exchange and correlation terms. Some prominent examples of exchange functionals fitted in this way are those due to Becke (B)⁷⁰ or Perdew and Wang (PW)⁷¹ while popular correlation functionals also developed in this groups are B88,⁷² P86⁷³ or PW91.⁷⁴ There are also correlation GGA functionals without empirical parameters like PBE.⁷⁵ The popular LYP (Lee-Young-Parr)⁷⁶ correlation functional was constructed also with a different philosophy. Instead of correcting LDA correlation it was fitted to reproduce the correlation of electrons in the helium atom. The GGAs constitute significant improvements over LDA in all chemical applications of density functional theory. Particularly, they give reasonable molecular structures especially in cases where metals are present in the molecule. Moreover, in combination with an approximate treatment of Coulomb terms by the resolution-of-identity (RI) technique⁷⁷ the calculation costs are significantly lower than those with the standard Hartree-Fock method. In some applications, improvements can be gained by incorporation of the Laplacian of the density into a functional (for example in the TPSS functional⁷⁸). Such meta-GGA functionals can also be implemented in a very efficient way.

Further search for better exchange-correlation functionals led to a series based on the so-called adiabatic connection method (ACM).^{79,80} These functionals, developed in the ACM framework, are called hybrid because they mix LDA/GGA exchanges and correlations with some fitted amount of exact Hartree-Fock exchange. Probably the most popular representative of this group is Becke's three parameter correlation functional combined with a fraction of a

LYP exchange and 20% of HF exchange (B3LYP).⁸¹ Its use had tremendous impact on chemistry. B3LYP is nowadays the first choice when studying organic closed shell molecules and their reactions⁸² even if calculations are considerably more expensive than with GGA due to the calculations of the exchange integrals. However, investigations of metallic complexes showed that superiority of hybrid functionals over GGAs is either much less pronounced or even disappears. Especially in open shell cases where the spin state of the system is to be determined by the calculation of energy differences between possible multiplicities, the *a priori* inclusion of some HF exchange influences the ordering of spin states. In transition metal complexes the splitting of spin states is in many cases linearly dependent on the amount of exact exchange due to gradual inclusion of Fermi correlation.⁸³ This is the reason why hybrid functionals favour high spin states while pure GGAs (0% HF exchange) overestimate the stability of low spin configurations. In connection with the fact that Kohn-Sham theory is a single-determinant method (even with exchange functionals that through exchange holes introduce to some degree static correlation) it is clear that DFT calculations on open shell systems have to be treated with special care.

There is another source of errors in most of the present functionals, namely long-range interactions (van der Waals-type forces). To fix this problem one has to increase the amount of long-range exchange which cannot be simply done by increasing the portion of exact exchange because short range properties would degrade. One way to go is to split the functional into short range and long range parts as it is done in range separated approaches like CAM-B3LYP.⁸⁴ However, the additional computation time does not guarantee consistently better results than uniform hybrids (apart from some long range properties like charge transfer excitation energies etc.). A much more economical way to correct for van der Waals interactions was recently proposed by Grimme (DFT-D).⁸⁵ This approach, similar to well-known empirical corrections to the HF energy,^{86,87} is based on the R^{-6} dependence of the dispersion energy with respect to interatomic distance. The DFT-D model corrects the DFT energy by an empirical energy correction E_{disp} :

$$E_{DFT-D} = E_{DFT} + E_{disp} \quad (46)$$

where

$$E_{disp} = -s_6 \sum_{i=1}^{M-1} \sum_{j=i+1}^M \frac{C_6^{ij}}{R_{ij}^6} f_{damp}(R_{ij}) \quad (47)$$

depends on the dispersion coefficients C_6^{ij} for all ij pairs within M atoms constructed by averaging tabularised coefficients for individual atoms. The dumping function f_{damp} is used to decay the correction at small R (covalent bond) and s_6 is a functional-dependent parameter. The equations above define the so-called DFT-D1⁸⁵ and DFT-D2⁸⁸ models that differ only by the parameters used. On the way to less empirical and more system-dependent corrections

Grimme and co-workers proposed recently DFT-D3⁸⁹ model where the dispersion energy is split into two- and three body terms:

$$E_{disp} = E^{(2)} + E^{(3)} \quad (48)$$

The two-body term, $E^{(2)}$ is analogous to the total dispersion energy defined in eq. (47):

$$E^{(2)} = - \sum_{ij} \sum_{n=6,8} s_n \frac{C_n^{ij}}{R_{ij}^n} f_{damp,n}(R_{ij}) \quad (49)$$

Introduction of the second set of 8th order coefficients gives larger flexibility at medium distances between atoms. The crucial change here comes from the C_6^{ij} coefficients which are now calculated and corrected by some rationally chosen coordination-number dependent function. The C_8^{ij} coefficients are then calculated recursively from the lower order ones. The three-body term $E^{(3)}$ arises from the fact that the interaction energy of three atoms is not exactly equal to the of sum pair interaction energies. It has a rather complicated and not well known form and the simplified form assumed by authors causes in fact a slight deterioration of the results. Thus, it is rarely used in standard calculations.

The dispersion corrected DFT method is particularly well suited for interaction energies.⁹⁰ With this respect it uniformly and significantly improves all GGA and hybrid functionals. Moreover, comparison with high-level methods such as CC proved the adequacy of the DFT-D3 methods for calculations of binding energies of ligands to metals.⁹¹ This is much less pronounced in thermochemical benchmarks but this is rather expected that the dispersion error will be here much smaller and therefore less space for improvements is left with this respect. The situation is more balanced when medium-range interatomic distance is described more accurately. For example, the recently developed double-hybrid methods that incorporate some amount of MP2-like correlation energy provide already a good description of thermochemistry and kinetics.⁹² When augmented with dispersion correction they yield a balanced description of most chemical problems.^{52,93} However, they are still internally limited by the single-reference KS determinant, the amount of correlation recovered by MP2 method as well as by some degree of empiricism in the chosen parameters.

2.3 MULTIREFERENCE METHODS

2.3.1 COMPLETE ACTIVE SPACE SELF-CONSISTENT FIELD THEORY

Single reference approaches break down in cases, where an orbital near-degeneracy problem appears. In such situations, there will be at least two Slater determinants that are needed for a proper description of the system of interest. A prominent example that requires a multideterminant reference wave function is bond dissociation. Even in the simple case of the H₂ molecule where the ground state is well described by a single determinant the gradual increasing of bond length should decrease the energy span between σ and σ^* orbitals. In the

limit two hydrogen atoms should be obtained, each with one electron in 1s orbital. Not surprisingly, at the dissociation limit the RHF energy explodes to the value of over 300 kcal/mol larger than twice the energy of an hydrogen atom – the RHF limit is an ionic state consisting of H^- and H^+ ions. Usage of the UHF approach helps only at large interatomic distances while at intermediate bond lengths the energy is still badly described. In fact, the UHF spin-up and spin-down determinants mimic a multideterminant wave function but at the cost of significant spin-contamination. At infinite distance, the UHF wave function is a 1:1 mixture of pure singlet and triplet Slater determinants with $M_s=0$.

This serious problem can be avoided if a wave function is used, which is constructed from a series of Slater determinants and is an eigenfunction of the \hat{S}^2 operator. In the multiconfigurational self-consistent field theory (MCSCF)⁹⁴ the wave function is represented by a chosen combination of m determinants:

$$\Psi_{MCSCF} = \sum_m c_m \Psi_m \quad (50)$$

In contrast to a CI wave-function, where only the c_m coefficients of the expansion are optimised, the orbitals that build the determinants Ψ_m are also optimised in a variational manner. Obviously, the c_m coefficients are subject to normalisation with $\sum_m c_m^2 = 1$. Furthermore, it is often convenient to express each Slater determinant, representing certain situation of orbital occupations, with a set of configuration state functions (CSF) that differ in spin-orbital occupations but correspond to the same orbital occupations. While Slater determinants are eigenfunctions of the projected spin only, the spin-adapted CSFs are simultaneously eigenfunctions of the total and projected spins.

In the early applications of the MCSCF method, the selection of configurations that enter equation (50) was performed on the base of physical insight and intuition. This sometimes led to problems because the orbitals were not invariant under unitary transformations carried out during the orbital optimisation process. Nowadays, a more systematic approach is usually taken. The complete active space self-consistent field method⁹⁵ – CASSCF – divides the orbital space into three parts: inactive, active and secondary orbitals. The total CASSCF wave function is then constructed by assuming the inactive orbitals to be always doubly occupied, secondary orbitals occupations are set to zero and expanding the active space by means of full CI. Therefore, any rotations inside the active space are invariant. The occupation numbers from state-specific calculations (SS-CASSCF) are usually different from 0 or 2 as far as the expansion (50) does not trivially reduce to the RHF case. This information, along with the weights of most important configurations is then used for characterisation of the molecular system. Not surprisingly, the number of active orbitals and electrons that can occupy these orbitals is limited by a number of possible configurations, i.e. the (30,20) active space of 30 electrons distributed among 20 orbitals results in quite a large but still accessible FCI expansion, the CASSCF(14,14) calculations with just 14 electrons on 14 orbitals yield in

several millions of configurations and are a limit of the method on powerful computers. Moreover, one has to take into account the size of a chemical system (total number of electrons) as well as the basis set used.

The active space in CASSCF calculations is usually selected on the basis of the chemical problem that has to be solved. For example dissociation of a single bond, like in the H_2 system, requires at least two electrons distributed over two orbitals (bonding and antibonding). Transition metal complexes are more demanding because at least in a first approximation all valence d (and s if applicable) orbitals with all corresponding electrons have to be included in the active space which in some cases has to be extended by a number of occupied or virtual orbitals of ligands. However, these are extreme examples where additionally a second set of d orbitals have to be added to the active space in order to obtain reasonable results.⁹⁶

The starting orbitals are usually obtained with HF calculations but KS orbitals can also be useful. The situations where active orbitals do not arise naturally around the HOMO-LUMO gap are rather a rule than an exception. The usual strategy involves calculation of the high-spin state, localization of the orbitals and selection of the active space based on the intermediate results. More problematic are molecules in which it is not clear at all which orbitals should enter the active space. Solution can be provided by performing some inexpensive, correlated single reference calculations, e.g. MP2 or CEPA/0, and a subsequent formation of natural orbitals. The active space is then constructed from those natural orbitals which have an occupation number highly different from 2 and 0. After a few CASSCF optimisation steps it should be clear which orbitals can be excluded from the calculation. However, even with a large number of starting active orbitals it can happen that some important contributions are missed. Therefore, it is common that the final active space results from a series of trials. The interested reader is referred to the paper of Verazov and Malmqvist⁹⁷ devoted to the pioneer of the CASSCF method – B. O. Roos – where some general remarks about the art of selection of an active space are given.

An important field of the application of the CASSCF method is calculation of several electronic states of the same molecule. This can be achieved in two different ways, either by individual calculations for each state or by state-averaging over different states in one calculation (SA-CASSCF). The second approach has the advantage that the resulting wavefunctions of the electronic states are orthogonal to each other and can be conveniently used in subsequent calculations involving various coupling matrix elements like in response theory. The wave function in SA-CASSCF calculations consists of blocks of a certain multiplicity and space symmetry which are usually equally weighted, although some flexibility is left for their adjustment on the base of physical arguments. Of course, the final orbitals are not optimal for each state but the energy differences are usually very well reproduced. The latter would not be true if the active space is not flexible enough to describe all desired states. This

can happen for example in the calculation of absorption spectra of molecules that involve charge-transfer states where the active space of the ground state is certainly not large enough. It should be also emphasised that in contrast to occupation numbers derived in SS-CASSCF calculations, average occupation numbers of the average orbitals have a rather limited physical meaning.

A crucial point which limits the accuracy of the CASSCF method is the minimal amount of dynamic correlation covered (only inside the active space through FCI). In some cases even the CASSCF will fail qualitatively. Well known is an example of the chromium dimer Cr_2 ,⁹⁸ which by this level of theory is considered as non-bonded system. The remedies were designed in close analogy to the single reference methods. However, because of already complicated reference state, they are much more demanding.

2.3.2 SECOND ORDER PERTURBATION THEORY WITH CASSCF WAVE FUNCTION

In analogy to HF theory, a natural way to extend the CASSCF method should be the application of perturbation theory. While the obvious choice of $\psi_0^{(0)}$ is the CASSCF multideterminant wave function, the form of the zeroth-order Hamiltonian is less straightforward. This is due to the fact that CASSCF orbitals do not diagonalize any particular set of one-electron operators (*vide supra*). Several different choices have been made in the literature but only few became widely used. Probably the most popular one is the CASPT2 method of Anderson *et al.*^{99,100}

The $\hat{H}^{(0)}$ operator in classical MP theory is chosen in such a way that the HF wave function $\psi_0^{(0)}$ is an eigenfunction of this zeroth-order Hamiltonian defining that:

$$\hat{H}^{(0)} = \hat{P}_0 \hat{F} \hat{P}_0 + \hat{P}_X \hat{F} \hat{P}_X \quad (51)$$

where $\hat{P}_0 = |\psi_0^{(0)}\rangle \langle \psi_0^{(0)}|$ is a projection operator onto the reference function, \hat{P}_X is a projection operator for the rest of the configuration space. The Fock operator \hat{F} is diagonal in the chosen orbital space and has a form given by eq. (25).

The philosophy of construction of the CASPT2 Hamiltonian is very similar.⁹⁴ $\hat{H}^{(0)}$ has the CASSCF wave function as a reference $\psi_0^{(0)}$ and the form in close analogy to (51):

$$\hat{H}^{(0)} = \hat{P}_0 \hat{F} \hat{P}_0 + \hat{P}_K \hat{F} \hat{P}_K + \hat{P}_{SD} \hat{F} \hat{P}_{SD} + \hat{P}_X \hat{F} \hat{P}_X \quad (52)$$

The CI space is divided into four subspaces:

- 0, the reference function,
- K, CAS CI space (restricted full CI),
- SD, subspace of all single and double excitations from reference,
- X, the rest of CI space.

The orbital energy operator \hat{F} is chosen with the condition that it should reproduce the results of MP theory in case of an empty active space. Thus, \hat{F} has a form of Fock-like one electron operator:

$$\hat{F} = \sum_{p,q} f_{pq} \hat{E}_{pq} \quad (53)$$

where $\hat{E}_{pq} = a_{p\alpha}^\dagger a_{q\alpha} + a_{p\beta}^\dagger a_{q\beta}$ are spin-averaged one electron excitation operator and the matrix elements f_{pq} are:

$$f_{pq} = h_{pq} + \sum_{r,s} D_{rs} \left[(pq|rs) - \frac{1}{2}(pr|qs) \right] \quad (54)$$

The matrix f is a 3x3 blocks matrix each corresponding to certain combination terms from the subspaces inactive, active, and secondary. The orbitals are then determined by diagonalization of these blocks one by one. With this definition of the $\hat{H}^{(0)}$ only those configurations which interact directly with the reference wave function have to be included into the first order wave function. All this configurations belong to the SD subspace and $\psi_0^{(1)}$, called CASPT1 wave function correction, is constructed as:

$$\psi_0^{(1)} = \sum_{p,q,r,s} C_{pqrs} \hat{E}_{pq} \hat{E}_{rs} \psi_0^{(0)} \quad (55)$$

All single and double excited states are included in the first-order wave function, except of those with all $pqrs$ indices corresponding to active orbitals. These states are already covered in the subspace K . Because triples and higher excitations from $\psi_0^{(0)}$ do not interact with the reference function they are also neglected. The coefficients C_{pqrs} are determined by solving equations of the general form:

$$(\mathbf{F} - E_0 \mathbf{S})\mathbf{C} = -\mathbf{V} \quad (56)$$

where \mathbf{F} is the matrix defined in eq. (53), \mathbf{S} is the corresponding overlap matrix, \mathbf{C} collects the searched coefficients while \mathbf{V} is a vector representing the interaction between all single and double excitations and the reference wave function with elements $V_{pqrs} = \langle \psi_0^{(0)} | \hat{H} | \hat{E}_{pq} \hat{E}_{rs} \psi_0^{(0)} \rangle$. According to Wigner's $2n+1$ rule,^{46,101} the CASPT1 wave function (55) defines both first- and second-order energy corrections as defined in general by equations (29) and (30). The CASPT2 energy has a rather complicated mathematical form and interested reader is referred to the original work. We should here only note that all double excitations are classified by the number of external orbitals involved as internal (no excitations to external orbitals), semiinternal (one excitation to external orbital) and external (both excitations are going to external orbitals). The single excitations are formulated as linear combinations of double excitations. The second-order energy correction is then evaluated separately for all types inside each class of double excitation. Such components have similar form compared to single reference MP2 energy with *the difference being that the active*

orbital energies are replaced by a more complex expression involving a weighted sum over all active orbitals. The weights are given by linear combinations of one through four particle density matrix elements.⁹⁹

Although CASPT2 theory is widely used in theoretical chemistry, there is a significant problem embedded in this theory. If any of the excitations from the SD space is close in energy or even below the energy of the reference state, then the assumption of a *small* perturbation breaks down and the theory is no longer valid. This is referred to as an intruder-state problem.⁹⁴ When the weight of such an excitation is small then small level shifting can remove the problem but to some degree this will influence the final correlation energy. In all other cases there is no other way around apart from extending the active space. This however, is mainly constrained by the size of the active space, which can be handled.

Another deficiency of CASPT2 energy is the separability that is not conserved, i.e. energy and components of a wave function of non-interacting system A-B cannot be simple decomposed into the contributions from A and B. Both weak points (separability and intruder state problem) are removed if a Hamiltonian proposed by Dyall is used as zeroth-order energy operator.¹⁰² It consists of two parts, one for inactive and secondary orbitals \hat{H}_{in}^D and another for active orbitals \hat{H}_{act}^D (i,j,\dots – inactive orbitals, r,p,\dots – secondary orbitals, a,b,\dots – active orbitals):

$$\hat{H}^D = \hat{H}_{in}^D + \hat{H}_{act}^D \quad (57)$$

$$\hat{H}_{in}^D = \sum_i \epsilon_i a_i^\dagger a_i + \sum_r \epsilon_r a_r^\dagger a_r + C \quad (58)$$

$$\hat{H}_{act}^D = \sum_{ab} h_{ab}^{eff} a_a^\dagger a_b + \frac{1}{2} \sum_{abcd} \langle ab|cd \rangle a_a^\dagger a_b^\dagger a_d a_c \quad (59)$$

where $h_{ab}^{eff} = \langle a|h + \sum_i (J_i - K_i)|b \rangle$. In eq. (58) the constant C is defined as $C = \sum_i \langle i|h|i \rangle + 1/2 \sum_{ij} \langle ij||ij \rangle - \sum_i \epsilon_i$ and so the HF wave function is automatically eigenfunction of \hat{H}^D . It is clear that \hat{H}^D through the usage of a complete Hamiltonian for the active space electrons is invariant with respect to the rotation of orbitals within the active space and consequently – strictly size consistent and separable (as far as the reference wave function is). The first application of \hat{H}^D was in the framework of CASPT2 approach and the corresponding method was named CAS/A.¹⁰²

Recently, Angeli and co-workers introduced second order n -electron valence state perturbation theory (NEVPT2).¹⁰³ They also prefer Dyall's Hamiltonian as $\hat{H}^{(0)}$ even if the general formulation of the theory allows a full Hamiltonian. The CAS-CI wave function is here written as an antisymmetrized product of a core part (n_{cor} inactive electrons) and a valence part (n_{val} valence electrons, i.e. active electrons in CASSCF):

$$|\Psi_{CAS-CI}\rangle = |\Phi_{cor} \Psi_{val}\rangle \quad (60)$$

In this formulation, the perturbation functions have the form $|\Phi_l^{-k}\Psi_\mu^{v+k}\rangle$, where Φ_l^{-k} is an orbital product of $n_{cor} - k$ inactive electrons and Ψ_μ^{v+k} is a multireference valence function of $n_{val} + k$ electrons, while k denotes the number of electrons that are promoted from the inactive to the active space ($-2 \leq k \leq 2$). Each wave function $|\Phi_l^{-k}\Psi_\mu^{v+k}\rangle$ can be written as a linear combination of determinants with the core part of Φ_l^{-k} and all possible distributions of $n_{val} + k$ electrons in the active space. The perturbed functions are obtained by diagonalization of $\hat{H}^{(0)}$ in each determinant space S_l^k , where index l denotes the inactive part of the wave function and k is the number of electrons promoted to the active space. Through usage of \hat{H}^D , the inactive and secondary space is treated by \hat{H}_{in}^D while the eigenfunctions of the active space are independently obtained by applying \hat{H}_{act}^D to Ψ_μ^{v+k} . With this different treatment of external and active orbitals one assures core and active orbitals to be well separated and therefore the method is free of the intruder state problem. The exploration of the whole dimensionality of S_l^k was termed by the authors as *uncontracted* NEVPT2. This is a rather expensive treatment and usually the internal contraction scheme is applied. Thus, all double excitations from the orbitals i,j are contracted into one function where each excitation to the active space generates m functions in the contraction sum (m : number of orbitals inside the active space). The weights of the components are then calculated through diagonalization of the Hamiltonian with the resulting contracted wave function. This approximation is called *partially contracted* NEVPT2 (PC-NEVPT2) and together with the usage of \hat{H}^D is identical with the CAS/A model. A more drastic simplification is introduced through *strongly contracted* NEVPT2 method (SC-NEVPT2) where the perturbed function for a certain pair i,j in each subspace S_l^k is generated by taking a normalized non-weighted internally contracted wave function. The normalization factor incorporates the one particle density matrix and only elements with two active indices are required. With the latter approach one can straightforwardly calculate the first order correction to the wave function as well as the second-order energy. Both contracted versions can be efficiently implemented^{104,105} and a hierarchy of approximations allows for systematic improvements. It was shown, that already at the simplest SC-NEVPT2 level the results are comparable or even of better quality than those obtained with CASPT2 theory.¹⁰⁶ Some recent applications in the field of transition metal chemistry were summarised by Neese and co-workers.¹⁰⁷ It is noteworthy that once the CASSCF wave function has been obtained, the dynamic correlation can be well approximated by any of the discussed perturbation theories at a cost similar to MP2 calculations. However, they will almost certainly fail if dynamic correlation strongly affects the weights of the determinants in the CASSCF reference. In such cases, a much more demanding treatment has to be applied and the wave function has to be allowed to relax with respect to dynamic correlation.

2.3.3 MULTI REFERENCE CONFIGURATION INTERACTION

In the multireference configuration interaction method (MRCI) dynamic correlation is accounted in the same spirit as in single reference CI discussed in chapter 2.2.3. The full MRCI expansion (equivalent to FCI) is built by including all possible excitations from all m reference determinants (constructed usually from a CASSCF wave function):

$$\psi = \sum_m \left(c_{0,m} \psi_{0,m} + \sum_{ap} c_{a,m}^p \psi_{a,m}^p + \sum_{\substack{a<b \\ p<q}} c_{ab,m}^{pq} \psi_{ab,m}^{pq} + \sum_{\substack{a<b<c \\ p<q<r}} c_{abc,m}^{pqr} \psi_{abc,m}^{pqr} + \dots \right) \quad (61)$$

The usual way to simplify the expansion above is to restrict the excitation list only to single and double substitutions in the reference function. However, the MRCISD expansion explodes rapidly with the size of active space (number of reference functions). Therefore, additional truncations are introduced by exclusion of configurations with small CASSCF weights. The number of double excitations can be further reduced by a perturbative approximation of the interaction of doubly excited wave-functions with the reference and subsequent elimination of weak perturbers. Both selections introduce some truncation error and the truncation thresholds should be carefully tested in each calculation. It can also happen that some excitations will be accidentally identical. The preferable method should properly handle such redundancies. Additionally, the excitations from the same orbitals can be conveniently grouped and contracted either in external^{108,109} or internal manner¹¹⁰⁻¹¹² what lead to more compact version of function (61).

In analogy to CISD, the MRCISD also suffers from exclusion of triple and higher excitations. The size-consistency error can be minimised in at least two ways: by correcting the CI equations or by including a posteriori correction to the energy. The first strategy is closely related to the CEPA approaches previously discussed. It should be emphasised that the lack of a widely accepted MR version of coupled – cluster method leads to the fact that CEPA-type corrections are preferred. A large number of MR coupled electron pair approximations have been proposed over the years. Probably the most popular approach – MRACPF (multireference averaged coupled pair approximation) – was proposed by Gdanitz and Ahlrichs.¹¹³ In this method an averaged CEPA/2 compensation for the EPV terms is used. Later, a similar strategy was undertaken but with a more strict EPV correction of CEPA/1-type and led to MRAQCC (multireference averaged quadratic coupled cluster).¹¹⁴

Another possibility to correct for the size consistency is to include a posteriori correction to the total energy. Widely used is one due to Davidson:¹¹⁵

$$E_{Davidson} = (1 - c_0^2) \Delta E \quad (62)$$

In eq. (62) the correction is proportional to the correlation energy ΔE and to the square norm of the correlation part of the wave function (c_0^2). In the multireference case, c_0^2 is usually

defined as a sum of the coefficients of the reference functions in the MRCI wave functions. The use of this correction is usually indicated by '+Q' suffix added to the method abbreviation, i.e. MRCISD+Q. However, one has to be careful when comparing results from different programs or publications because various choices of c_0^2 and ΔE are present in the literature. Recently, Szalay *et al.*¹¹⁶ reviewed multireference methods along with possible corrections and applications and the interested reader is referred to this comprehensive work.

At the end of this chapter it should be underlined that multireference methods are much more demanding in terms of both computational resources and man power. On the one hand careful selection of the active space has to be performed while on the other hand a number of preselection thresholds can significantly influence the results. MR methods are not of *black box* manner like most of the single reference methods, especially DFT. Systematic improvements are possible but they are up to now limited by the inclusion of excitations higher than two and the typical one-electron finite basis set expansion. Significant progress to remove both limitations has been recently achieved by the development of MRCC methods^{117,118} and application of some F12 techniques in multireference calculations.¹¹⁹ The latter two techniques have in common high computational demands and are so far limited to systems consisting of just a few main-group atoms. Additionally, there is no uniform approach to MRCC calculations and each has its pros and cons. This dilemma was recently discussed by Jagau.¹²⁰

2.4 COMMON TECHNIQUES

2.4.1 BASIS SETS

In practical calculations the atomic spin-orbitals ϕ_i , used later to construct the Slater determinants, are expressed through a set of known basis functions $\{\eta_\mu\}$. Each basis function is composed from a radial $R(r)$ part as well as an angular part $Y(\theta, \phi)$:

$$\eta_\mu = R(r) Y(\theta, \phi) \quad (63)$$

where r , θ and ϕ denote radial coordinates. The most natural choice for $R(r)$ is to use Slater type orbitals (STOs), i.e. the functions of the form $\exp(-\alpha r)$. α is a parameter which indicates the degree of compactness of the function – large α means compact function while diffuse functions have small exponents. STOs generally show a proper behaviour with changing of r and closely resemble hydrogenic functions. However, there is no analytical solution of many-centre two-electron integrals. This is why Gaussian type orbitals (GTOs) are preferred over STOs. They involve functions with r^2 in exponent, i.e. $\exp(-\alpha r^2)$. Unfortunately, GTOs suffer from the improper description of the cusp at $r=0$. This is handled approximately by contraction (taking a linear combination with optimised coefficients) of a set of GTOs into one contracted Gaussian (CGTO). Furthermore, for typical chemical applications each single orbital is described by a set of CGTOs which leads to a hierarchy of basis sets with increasing complexity: double- ζ , triple- ζ , quadruple- ζ etc. Following the chemical observation that valence electrons are significantly influenced by the molecular environment while core electrons are rather inert. For most applications it is reasonable to construct a basis set for an atom of a small number of CGTOs for the inner shells (usually just one) and larger number of CGTOs describing the valence shells. Such split-valence basis sets perform very well in HF, DFT and CASSCF calculations. The basis sets of choice in this study are those of Ahlrichs and co-workers: def2-SVP,¹²¹⁻¹²³ def2-TZVP,¹²²⁻¹²⁴ def2-QZVP,¹²³ where ‘def2’ means ‘default’ (for historical reason augmented with suffix ‘2’), S, T, and Q denote the number of CGTOs in the valence shells (two, three, and four, respectively) and P is added for polarization functions. As shown by Neese and Valeev,¹²⁵ these basis sets of triple- ζ and quadruple- ζ quality can also be sufficient in correlated calculations. However, if high accuracy is desired the correlation-consistent basis sets can be employed, for example those of Dunning et al. (cc-pVXZ series)¹²⁶ or atomic natural orbitals basis sets (ANO series).¹²⁵ The proper treatment of core-valence correlation is even more demanding and augmentation of the core shells by some set of additional functions is highly advisable.¹²⁷ Nonetheless, the typical approach for large molecules would be to optimise the geometry of a molecular system at DFT level with def2-SVP or def2-TZVP basis set and then derive the properties of interest with a larger basis set suited for the property and the method used.

Unfortunately, the finite expansion in a basis set introduces other sources of error. The basis set superposition error (BSSE) arises in calculations of properties of molecular fragments and

is connected to the fact that the monomer in a whole molecule is artificially stabilised by the basis functions of the rest of complex. This problem is reduced with larger basis sets because ‘borrowed’ basis functions constitute a smaller fraction of the total expansion, which is already sufficiently flexible to describe the monomer properly. Although, increasing the basis set or application of F12 techniques can minimize the BSSE, a conceptually simple method was proposed by Boys and Bernardi.¹²⁸ The method introduces so-called counter-poise correction (CP) which for a dimer is defined as:

$$E_{CP} = E_{AB} - (E_{A(B)} - E_A) - (E_{B(A)} - E_B) \quad (64)$$

where E_{AB} , E_A and E_B are the energies of dimer and monomers A and B, respectively. $E_{A(B)}$ and $E_{B(A)}$ denotes the energies of both monomers calculated in the basis of dimer, i.e. with ghost orbitals of the absent monomer. Eq. (64) can be easily extended to larger number of monomers and works with any quantum chemical method. The main deficiency in this approach is the definition of a monomer. While it is clear for weakly interacting non-bonded systems, monomers connected via covalent bonds are still challenging. Of course one can divide the system into atoms and perform the calculation of the CP correction but this is a rather demanding task. Mayer¹²⁹ proposed the chemical Hamiltonian approach (CHA) for both intra- and intermolecular interaction but this method is not widely used, mainly because it has always to be adopted to the method that is used. Nonetheless, a typical approach is to increase the basis set to the reachable limit (maybe for some small model) and compare obtained results with smaller basis set.

2.4.2 RESOLUTION OF THE IDENTITY

Nearly all applications presented in this work benefit from the resolution-of-the-identity approximation (RI).¹³⁰ This technique is used for the decomposition of four index many-electron integrals into three-index integrals. It has been implemented for most modern *ab initio* methods and allows significant speedups in the integral evaluation.¹³¹ Probably the most successful application was to Coulomb integrals (J) that are four centre objects. Briefly, 4-centre-2-electron integrals of type:

$$(ij|kl) = \int \phi_i(r_1)\phi_j(r_1)\frac{1}{r_1 - r_2}\phi_k(r_2)\phi_l(r_2)d\tau_1 d\tau_2 \quad (65)$$

are replaced by an expansion in terms of atom centred functions α and β , usually called the auxiliary basis:

$$(ij|kl) \approx \sum_{\alpha, \beta} (ij|\alpha)(\alpha|\beta)^{-1}(\beta|kl) \quad (66)$$

Equation (66) represents one of the possibilities of such an insertion but the general features are common. The relation (66) would be exact in case of a complete auxiliary basis set. While this is impossible, the usual way is to employ another basis set as an auxiliary basis in addition to the one used for the orbital expansion. They are typically fairly large in

comparison to their orbital counterparts and should be used only with basis sets for which they were optimised. For the aforementioned def2 basis sets, corresponding auxiliary basis sets^{122,132,133} exist and the typical reduction of computational costs is about one order of magnitude. In particular, the RI approximation allows significant time savings in DFT calculations with popular gradient-corrected functionals where the computation of the J -terms is a bottleneck. Post-HF methods also benefit from the RI technique. It allows to perform integral transformations in cases where the exact procedure would be much more expensive or even impossible.

The error introduced by RI is usually negligible if the auxiliary basis set is sufficiently large. Moreover, it can be applied also to the exchange integrals¹³⁴ but the time savings here are much less pronounced. Recently, Neese and co-workers¹³⁵ explored some numerical techniques together with the RI approximation to speedup the calculations of the exchange terms. They introduced a method called RIJCOSX ('chain-of-spheres' algorithm) that allows to perform the evaluation of the K -integrals up to 60 times faster than in a canonical way. Introduced error in total energies is somewhat larger than for RI approximation (ca. 0.5 mHartree vs. 0.1 mHartree) but a large part cancels out if energy differences are computed. The approach is especially well suited to treat large basis sets together with large number of electrons and will be particularly used in this work for CEPA calculations of the reaction barrier energies involving large paracyclophane-based ligands.

2.4.3 GEOMETRY OPTIMISATION

The Born-Oppenheimer approximation introduced in chapter 2.1.1 is the basis to define the molecular geometry in the context of fixed positions of nuclei. Up to now we have focused on the accurate description of the electronic interactions which corresponds to some configuration of nuclei. M nuclei create however their own configuration space called potential energy surface (PES) that describes how the total energy depends on the configuration of the nuclei. Any diatomic molecule has only one geometrical degree of freedom while for the description of any larger (non-linear) molecular system, $3M-6$ parameters are needed. In chemistry, we are mainly interested in some stationary points on such a multidimensional PES like local energy minima and energy maxima. The first corresponds to stable or meta-stable molecular entities that are usually observed in experimental studies. They do not necessarily have to be a global minimum. On the way from one minimum to another some saddle points are encountered. Such energy maxima are related to the transition states from the transition state theory (TST).¹³⁶⁻¹³⁹

Apart from trivial diatomics, some automatic techniques have to be applied in order to locate desired stationary points. In general, the PES of a molecule is a mathematical function and most of the methods developed for finding extrema of a given function can be utilised. For the optimisation of the minimum geometry we aim to locate a structure which corresponds to some energy minimum. Unfortunately, there is no method which will always give us the

global minimum and one has to rely either on some sampling of the PES or on chemical intuition (more often – on both). In a number of cases, like reaction intermediates, the optimisation of a local minimum is even desirable. The gradient of an energy with respect to the nuclei coordinates has to be taken in order to characterise the initial geometry and the direction of the nuclei movement. All gradient components are zero if a structure is at some stationary geometry (minimum or saddle point). The crucial point now is the algorithm which will drive the geometry optimisation process. In the TURBOMOLE package, used exclusively in this work for geometry optimisations with analytical gradients, a family of quasi-Newton-Rhpson (quasi-NR) methods are available.¹⁴⁰

Thus, it is assumed that the potential energy $V(\mathbf{x})$ around a given set of coordinates \mathbf{x}_k is quadratic and can be expanded as a Taylor series:

$$V(\mathbf{x}) \approx V(\mathbf{x}_k) + (\mathbf{x} - \mathbf{x}_k)\mathbf{V}'(\mathbf{x}_k) + \frac{1}{2}(\mathbf{x} - \mathbf{x}_k)^2\mathbf{V}''(\mathbf{x}_k) \quad (67)$$

where $\mathbf{V}'(\mathbf{x}_k)$ and $\mathbf{V}''(\mathbf{x}_k)$ are the matrices of first and second derivatives of the potential at point \mathbf{x}_k . At the geometry \mathbf{x}_0 that is a stationary point on a PES, the first derivative is zero. Therefore, the optimal geometry can be iteratively found using:

$$\mathbf{x}_0 = \mathbf{x}_k - \mathbf{V}'(\mathbf{x}_k)\mathbf{V}''^{-1}(\mathbf{x}_k) \quad (68)$$

If the second derivative and its inverse in the above equation are calculated explicitly this is equal to the true second-order Newton-Rhpson method. However, the calculation of the matrix of second derivatives (called Hessian) is relatively expensive even if an analytical formulation is available. To avoid this time-consuming step, the quasi-NR methods build up the inverse of Hessian matrix in k successive iterations so a series of matrices \mathbf{H}_k fulfils following relation:

$$\lim_{k \rightarrow \infty} \mathbf{H}_k = \mathbf{V}''^{-1} \quad (69)$$

The new position of the nuclei \mathbf{x}_{k+1} is then obtained with the gradient \mathbf{g}_k at the current position and the approximated inverse Hessian \mathbf{H}_k :

$$\mathbf{x}_{k+1} = \mathbf{x}_k - \mathbf{H}_k\mathbf{g}_k \quad (70)$$

Various schemes have been proposed for the update of \mathbf{H} at \mathbf{x}_{k+1} . Most commonly used are Broyden-Fletcher-Goldfarb-Shanno (BFGS) and Davidson-Fletcher-Powell (DFP) algorithms. The explicit expressions for \mathbf{H}_{k+1} can be found elsewhere.¹⁴¹ The matrix \mathbf{H} is usually initialized as a unity matrix \mathbf{I} but the performance of the quasi-NR methods can be significantly improved by using a better guess for the initial \mathbf{H} , e.g. by using the exact Hessian obtained at lower level of theory. While the method is only defined for positive definite \mathbf{H} , some small multiple of \mathbf{I} is added to \mathbf{H}_k in eq. (70) to assure a ‘good’ direction of search. Such ‘addition’ is restricted to the so-called trust region h , i.e. the region of validity of the truncated Taylor series (67). The threshold h is updated at each iteration.¹⁴⁰

The quasi-NR procedure was adopted by Helgaker¹⁴² to the optimisation of transition states, i.e. search of a geometry for which the Hessian matrix has exactly one negative eigenvalue while the rest are positive. The trust-region image minimisation (TRIM) method relies on the simple observation that the first order saddle point, a transition state, on the PES is an energy minimum on the inverted PES. Such an image function has the same gradient and Hessian as the primary function except for an opposite sign of the lowest eigenvalue. In principle, the minimum of this inverse is then found by means of quasi-NR methods. However, the optimisation of the TS requires a good starting Hessian and throughout this study the initial Hessian is obtained at the same level of theory as the actual optimisation process. Moreover, the starting geometry should be as close as possible to the expected TS geometry and is usually prepared by a few steps of a standard geometry optimisation with some parameters of the molecule frozen at the values close to the anticipated for the real TS. Furthermore, it is sometimes necessary to compute the exact Hessian after a few iterations of the TRIM method to assure that the procedure converges in the desired way.

Once a stationary point has been found, the eigenvalues of the exact Hessian matrix have to be calculated in order to distinguish between minima, maxima and higher-order saddle points. At the minimum geometry the Hessian will have six zero and $3M-6$ positive eigenvalues for $3M$ Cartesian coordinates of M nuclei. The transition state structure (energy maximum) corresponds to one negative eigenvalue of the Hessian matrix while the rest are positive or zero. More than one negative eigenvalue indicates a higher-order saddle point that are only of little interest in chemistry. When the obtained minimum has some negative eigenvalues or the TS has more than one of them, the distortion of the molecule along this modes usually helps to remove this unwanted artefacts. Sometimes, it is necessary to increase the numerical precision of the calculations by tightening the convergency criteria or increasing the integration grid in DFT calculations in order to get a true stationary point. Furthermore, molecular systems with very flat PES require large basis sets and calculations of very high accuracy.

2.4.4 NORMAL MODE ANALYSIS AND THERMODYNAMICAL CORRECTIONS

The Hessian matrix of the second derivatives \mathbf{V}'' can be directly converted to the force-constant matrix in mass-weighted coordinates \mathbf{F} :¹⁴¹

$$\mathbf{F} = \mathbf{M}^{-1/2} \mathbf{V}'' \mathbf{M}^{-1/2} \quad (71)$$

where \mathbf{M} is a diagonal $3M \times 3M$ matrix that contains the atomic masses.

The diagonalization of the matrix \mathbf{F} yields a set of eigenvalues λ_i (force constants) that are connected to a frequency of each normal mode ν_i by the following relation:

$$\nu_i = \frac{\sqrt{\lambda_i}}{2\pi} \quad (72)$$

With a complete set of frequencies of normal modes one can easily obtain infrared (IR) as well as Raman spectra. In the first case additional calculations of transition dipole moments are needed while in the second the polarizability derivatives have to be obtained. It should be emphasised that the effort of spectra simulation can be greatly reduced by exploration of the point group symmetry of the molecule.

Any molecule at 0 K has some non-zero energy connected to the vibrational ground state vibrations. In the harmonic approximation the zero-point energy (ZPE) is defined as

$$E_{ZPE} = \frac{1}{2} \sum_i h\nu_i \quad (73)$$

where the summation runs over all i normal modes. The E_{ZPE} correction should be always added to the electronic energy. This is especially crucial when the geometry changes dramatically, e.g. during the chemical reaction. In such case the difference in ZPE can have substantial influence on the reaction rate and other properties related to the change in energy.

The ZPE correction is calculated assuming that the total energy can be approximated as a sum of electronic and vibrational energies at the temperature of 0 K. Similarly, the total energy of the system at finite temperature can be separated into a few terms according to the rigid-rotor harmonic oscillator (RRHO) approximation.¹⁴³ In addition to electronic and vibrational contribution the translational and rotational degrees of freedom should be considered with the corresponding energy components. The total energy can be therefore written as:

$$E_{tot} = E_{elec} + E_{vib} + E_{trans} + E_{rot} \quad (74)$$

The vibrational energy E_{vib} contains the E_{ZPE} and contributions coming from the excitations to the higher oscillation levels. Equation (74) opens a way to define thermodynamic functions such as enthalpy and entropy. The bridge between properties of a single molecule and macroscopic ensemble of molecules is provided by statistical thermodynamics through the partition function q . In the framework of RRHO approximation it can be written as a product of individual partition functions:

$$q_{tot} = q_{elec} q_{vib} q_{trans} q_{rot} \quad (75)$$

Each partition function involves a summation over Boltzmann factors of all states i of the system:

$$q = \sum_i^{all\ states} e^{-\varepsilon_i/kT} \quad (76)$$

The translational and rotational partition functions are obtained by insertion of appropriate energy expressions to eq. (76) and assuming the spacing between energy levels is well below kT so the summation can be replaced by integration. Such assumption is not possible in the case of the vibrational partition function where all vibrational energy levels have to be considered. The electronic partition function involves the sum over electronic states. In most

cases the energy difference between the ground state and the first excited state is large compared to kT so the sum (76) can be truncated after the first term.

The final equations for partition functions are as follow:¹⁴⁴

$$\begin{aligned}
 q_{elec} &= g_0 e^{-\frac{\epsilon_0}{kT}} \\
 q_{vib} &= \prod_{\text{normal modes}} \frac{e^{-\frac{h\nu_i}{2kT}}}{1 - e^{-\frac{h\nu_i}{kT}}} \\
 q_{trans} &= \left(\frac{2\pi M kT}{h^2} \right) V \\
 q_{rot} &= \frac{\sqrt{\pi}}{\sigma} \left(\frac{8\pi^2 kT}{h^2} \right)^{3/2} \sqrt{I_A I_B I_C}
 \end{aligned} \tag{77}$$

In the above equations g_0 denotes the degeneracy of the spin or spatial wave function while σ is the order of the rotational subgroup in the molecular point group. M , V and I_x are molecular mass, volume of 1 mol of ideal gas and the three moments of inertia, respectively. With all components of the total partition function in hand it is easy to obtain the enthalpy and entropy of the system by simply summing up electronic, vibrational, translational and rotational contributions, each calculated by performing the differentiations in the following equations:

$$H = kT^2 \left(\frac{\partial \ln q}{\partial T} \right)_V + kTV \left(\frac{\partial \ln q}{\partial V} \right)_T ; S = kT \left(\frac{\partial \ln q}{\partial T} \right)_V + k \ln q \tag{78}$$

Calculations of H and S allow to obtain the Gibbs free energy G ($G=H - TS$). Consequently, by taking the differences of G between reactants and transition states as well as between reactants and products one can calculate reaction rates and equilibrium constants, respectively.

The quality of the data obtained – both spectroscopic and thermodynamic – is limited by the quality of the second derivatives of the energy. The frequencies obtained within the harmonic approximation are usually scaled with respect to the experimental values by some constant number, characteristic to the method used. Extensive tables of such scaling factors are available in the literature.¹⁴⁵ Moreover, a typical approach in calculations of properties of large molecules is to obtain geometry and frequencies at lower level of theory (because of the cost) and refine the electronic energy at a higher level. One relies here on the fact that geometries obtained at e.g. the DFT level with some gradient corrected functional and a small basis sets are usually already of acceptable quality. However, if high accuracy is desired then geometry optimisation and frequency analysis should be performed at highest accessible level of calculations. In some cases the harmonic approximation breaks down and anharmonicity of vibrational modes has to be taken into account by calculation of higher energy derivatives.¹⁴⁶ The situation becomes even more complicated when some of the internal rotations have small barriers and correspond to a very small frequency. While the vibrational enthalpy approaches a constant factor of RT in this case, the vibrational entropy goes towards infinity with

decreasing frequency. The free rotor model dictates the limit of RT for H_{vib} and $1/2RT$ for S_{vib} . Therefore, the total enthalpy is usually well reproduced even when free rotations are present but the total entropy and total Gibbs free energy are strongly affected by errors in low energy vibrations. However, the hindered-rotor calculations are rarely done because of their cost and complexity.¹⁴⁷

3 APPLICATIONS – A THIN LINE BETWEEN COSTS AND ACCURACY

We will now take a tour through some metallic and metalloid complexes and try to connect the electronic structure, calculated from first principles, with observed properties. The large complexes considered here place high demands on the theoretical methods which are to be applied. The key here is a balance between computational cost and the accuracy needed to answer certain questions. Therefore, in each case we will start from a formulation of aims and carefully benchmark a group of chosen methods. It will quickly become clear that some aspects are already well described at a lower level of theory whereas others require a much more sophisticated treatment. The theoretical results will be compared to experimental values if such are available. In many cases the calculations will reveal new aspects of chemical reactivity that may be tested experimentally. Furthermore, even if each of the applications constitutes a separate scientific problem, collected together they serve as a base for general conclusions that will be valuable for the selection of theoretical methods in certain applications.

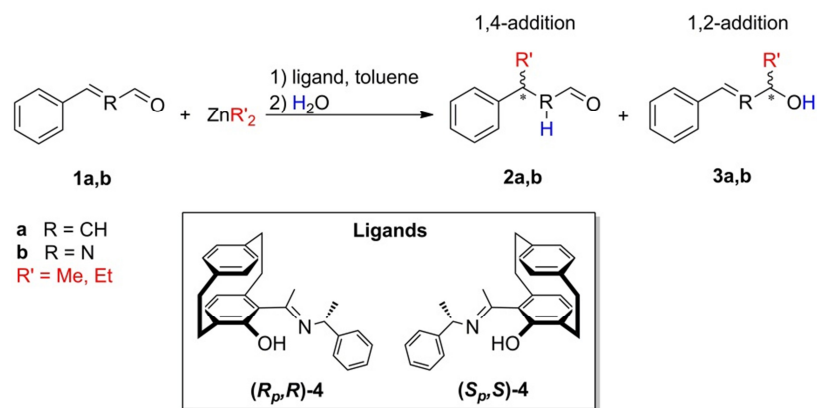
Throughout this work, all DFT and MP2 calculations were performed with Turbomole¹⁴⁸ package while the ORCA¹⁴⁹ program was used for CEPA and multireference calculations. MolDen,¹⁵⁰ VMD¹⁵¹ and Avogadro¹⁵² were utilized for visualization and drawings.

3.1 ADDITIONS OF DIALKYLZINC TO ENALS AND IMINALS CATALYSED BY PARACYCLOPHANE-BASED LIGANDS

3.1.1 INTRODUCTION

Additions of dialkylzinc to α,β -unsaturated aldehydes constitute an important class of reactions for C-C bond formation. When the reaction proceeds in the presence of a chiral catalyst, high enantiomeric excesses (*ee*) can be obtained. Aminoalcohols can be used as convenient catalysts for 1,2-additions.¹⁵³ To obtain a 1,4-product one should either use special Hoveyda-type catalysts with copper salt addition¹⁵⁴ or [2.2]paracyclophane-based *N,O*-ligands.¹⁵⁵ The second route has the key advantage that it does not involve any co-metals and therefore is more convenient. Bräse et al. examined a series of paracyclophane-containing catalysts and proved its utility, especially for addition reactions to enals¹⁵⁵ and iminals¹⁵⁶ (see Scheme 3.1.1). While in the case of iminals the 1,4-addition product was clearly the dominating one, enals showed reduced regioselectivity, i.e. significant amounts of 1,2-addition byproducts were observed. Moreover, the origin of enantioselectivity in the 1,4-addition reaction is still unclear. When the *R_p* configured paracyclophane *N,O*-ligand was used, e.g. (*R_p*,*R*)-**4**, the (*S*)-**2a** product was always obtained when reacting with cinnamaldehyde **1a** whereas the (*R*)-**2b** product was observed for *N*-formylbenzylimine **1b**.¹⁵⁵⁻¹⁵⁶ This is just because the priority of substituents on the stereogenic centre changes

upon substitution of $-\text{CH}=\text{}$ with $-\text{N}=\text{}$ groups in the 1,4-addition product. However, both substrates undergo the nucleophilic attack from the same site of the molecule and consequently the mechanisms of both reactions should be similar. The same (R_p,R) -**4** ligand catalyses the 1,2-additions in such a way, that always the *S*-configured product is obtained. Therefore it was recently proposed¹⁵⁵ that the planar chirality of the ligand is alone responsible for the stereoconfiguration of the product of both reaction pathways.



Scheme 3.1.1 Asymmetric addition reaction of dialkylzinc to α,β -unsaturated aldehydes: (i) cinnamaldehyde **1a** and (ii) *N*-formylbenzylimine **1b** catalysed by [2.2]paracyclophane-based ligands **4**. **2a,b** and **3a,b** are 1,4-addition and 1,2-addition products, respectively.

The 1,4-addition of dialkylzinc to cinnamaldehyde and *N*-formylbenzylimine as well as 1,2-addition to benzaldehyde¹⁵⁷ are efficient only when the dialkylzinc:ligand ratio is close to 2:1 or even higher. This indicates that most likely two zinc atoms are involved in the reaction of one aldehyde molecule. Moreover, it has been observed that *ee* of the product is not linearly dependent on the increasing *ee* of the ligand **4**. This is known in literature as non-linear effect (NLE) that in this case has a negative character [(-)-NLE]. A graphical illustration of this phenomena is provided in Figure 3.1.1.

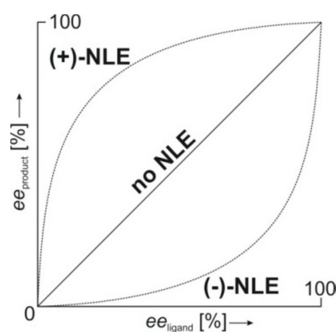


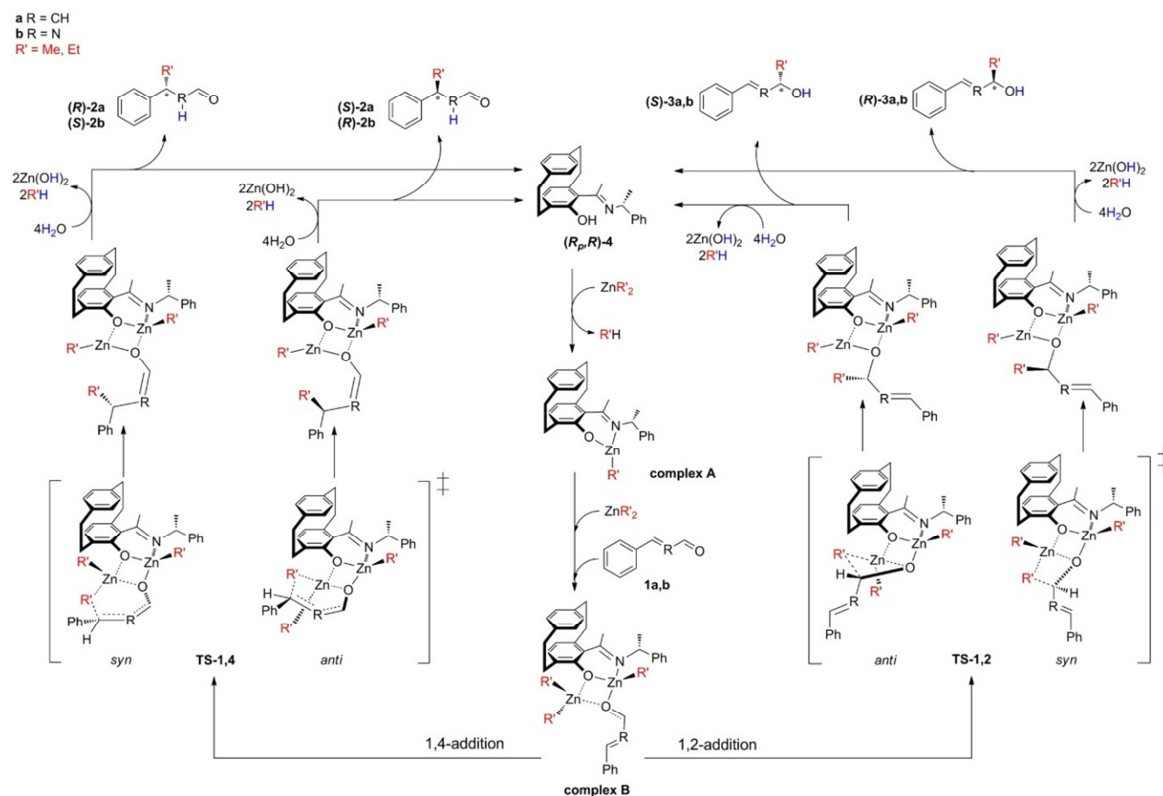
Figure 3.1.1 In most reactions purification of the chiral auxiliary (e.g. ligand **4**) leads to a linear increase of *ee* of the product. Any deviations from such linearity are called non-linear effects (NLE) and are classified as positive [(+)-NLE] and negative [(-)-NLE].

Kagan et al.^{158,159} carefully analysed the equilibria that exist in the reactions showing NLE. They argued, that the shape of curves like those presented in Figure 3.1.1 can be derived by

assuming the formation of associates between metallic systems and both possible enantiomers of the auxiliary (e.g. ligand **4**) where such polymeric structures have different thermodynamic stability constants. Indeed, the dimeric structure of the ligand **4** and the ZnCH₃ moiety have been crystalized and characterized.¹⁶⁰ The thermodynamic model predicts the (-)-NLE if the dimer is formed from the ligands of the same stereoconfiguration, i.e. the homodimers are more stable than the heterodimers. In agreement with this model, the crystal structure consists of homodimeric molecules. The qualitative explanation of this phenomenon can be provided by theoretical calculations of the relative stability of various monomeric and dimeric structures as well as by calculations of the binding energy between two monomers. The complex between ligand **4** and the ZnCH₃ (ZnCH₂CH₃) moiety will be from now on denoted as **complex A** because it is starting point in both NLE calculations and reaction path investigations.

However, the dimer of **complex A** cannot catalyse the reaction depicted in Scheme 3.1.1 because of the lack of a free coordination site. Thus, there is an agreement in literature that the reaction itself involves a monomer.^{153,157-161} Herein we propose a catalytic cycle (Scheme 3.1.2), similar for both additions. Both pathways start with the dialkylzinc coordination to the ligand (formation of **complex A**). With help of an oxygen atom from a substrate molecule the monomer can coordinate a second dialkylzinc molecule and form a binuclear system (**complex B**). Starting from this binuclear system, the preferred reaction pathway can be obtained from the heights of reaction barriers by transition state theory. Such a type of analysis was performed by Yamakawa and Noyori¹⁶² in case of the 1,2-addition of dimethylzinc to benzaldehyde in presence of an isborneol-based *N,O*-containing ligand. Their binuclear model of the active complex was successfully used to rationalize the observed enantioselectivity of the *S*-configured catalyst and the results supported that (*S*)-1-phenylethanol is the most preferred enantiomer with an activation barrier lower by about 3 kcal/mol (at the RHF/3-21G level) than the barrier leading to the *R*-configured product. Even bigger fenchone-based systems were theoretically and experimentally studied by Goldfuss *et al.*¹⁶³ Furthermore, Vázquez *et al.*¹⁶⁴ examined a large (*R*)-2-piperidino-1,1,2-triphenylethanol catalyst through QM/MM calculations. Both studies agree well with the findings of Yamakawa and Noyori. All groups suggested that the main factor affecting stereoselectivity of these 1,2-additions is the repulsion of the negatively charged alkyl groups attached to the zinc atoms. Consequently, a 6/4/4 tricyclic system (see Scheme 3.1.2) in *anti*-arrangement is formed in the transition state which reduces the overall steric repulsion and leads to the conservation of the catalysts stereoconfiguration in the product. However, it was recently shown that bulky groups attached to the ligand moiety, e.g. trimethylsilyl,¹⁶⁵ can significantly influence the stereochemistry of the reaction through steric effects. For a theoretical study it is therefore essential to include the full system because typical simplifications, such as substitutions of side groups (e.g. ethyl to methyl) not involved in the reaction, could change

these effects. Moreover, methods which can handle long range effects and the complicated electronic structure of transition states have to be used.



Scheme 3.1.2 Investigated catalytic cycle. Prior to the transfer of the alkyl group, the ligand $(R_p, R)-4$ forms a complex with two dialkylzinc molecules (alkyl = R' = methyl or ethyl) and a substrate $1a$ or $1b$. (Central column) **Complex A** refers to the ligand- ZnR' monomer and **complex B** to a binuclear zinc complex formed by reaction of **complex A** with a substrate molecule and ZnR'_2 . Both possible reaction pathways were examined, i.e. 1,2-addition (right side) and 1,4-addition (left side). The labels *syn* and *anti* stand for the configuration of the tricyclic transition states and reflect the direction from which the transferred alkyl group approaches the substrate.

Here, we demonstrate how subtle effects like weak interactions or electronic correlation, drive the reaction in a certain – not always desired – way. The first part of the work is devoted to the calculations of the various dimeric structures of **complex A** in the context of NLE. Then, the catalytic cycle presented in Scheme 3.1.2 is studied in order to explore the stereo- and regioselectivity of dialkylzinc additions to cinnamaldehyde ($1a$) and *N*-formylbenzylimine ($1b$) catalysed by the $(R_p, R)-4$ paracyclophane ligand. The results are interpreted in the context of π -conjugation of both substrates which is shown to play a crucial role for the prediction of the products. On the other hand, we use the investigated reaction for validation of different less demanding quantum-chemical methods based on density functional theory and wave function approaches. A detailed analysis of errors can serve as a benchmark and shows how exact calculations have to be for applications in homogeneous catalysis.

Furthermore, our best protocol involving LPNO-CEPA/1 calculations is employed in screening of novel ligands for the diethylzinc additions to cinnamaldehyde.

3.1.2 COMPUTATIONAL DETAILS

Geometry optimisations of all energy minima and transition states were performed at DFT level employing the gradient corrected Becke-Perdew functional BP86 in connection with a double- ζ def2-SVP basis set. In order to obtain zero-point, enthalpy and entropy corrections at 298.15 K each structure was submitted to frequency calculations at the same level of theory. The energy minima possessed only positive normal modes while transition states had exactly one imaginary frequency which was carefully checked to be the one connected with the reaction path. Because of the flexibility of the system (alkyl groups and phenyl rings) we located several local minima and corresponding transition states. Herein, only the lowest energy structures are presented.

The energy of each geometry was recalculated using the high quality, triple- ζ basis set def2-TZVP with tightened SCF convergence (10^{-7}) and enlarged grid size (m4). Additionally, single point calculations were performed with the B3LYP functional. Since neither of these functionals account for dispersion interactions we decided to augment them with the empirical corrections of Grimme (this is denoted as BP86+D and B3LYP+D, respectively). We tested both the D2 and D3 versions of the correction and found that they yield essentially the same results for the binding energies and relative stabilities of the minimum energy structures. The more recent (and much more sophisticated) D3 correction was however superior in case of transition states. For historical reasons, we used the D2 correction for the investigation of the dimer formation in context of the non-linear effects whereas the D3 version was used in the reaction paths analysis. The influence of the solvent on the reaction energetics was considered by single point calculations involving the Conductor-like Screening Model (COSMO)¹⁶⁶ with a dielectric constant of 2.38 corresponding to toluene. Moreover, each structure was submitted to SCS-MP2 calculations for the reaction barrier calculations. The frozen core approximation was applied to all non-hydrogen atoms. Because the calculations of the energy differences between various possible reaction paths are expected to be highly dependent on the electron correlation treatment, in this case we also tested the double-hybrid functional B2PLYP in which the B88 exchange functional is combined with LYP exchange and perturbation theory corrections (PT2). For the same reason, to have rigorous reference data for the benchmark of the reaction barriers we decided to perform LPNO-CEPA/1 calculations. The T_{CutPNO} parameter, which controls the truncation of PNOs, was set to 10^{-6} . To speed up the calculations, the RI approximation was applied in all cases while the RIJCOSX technique was used for exchange integrals in the HF and the subsequent CEPA calculations. In all single point calculations the def2-TZVP basis set was employed along with tight convergence criteria (*vide supra*).

3.1.3 NLE: FORMATION OF DIMERS

In order to quantitatively explain the negative non-linear effect (Figure 3.1.1) it was important to calculate the relative stability as well as the binding energies of the dimers of **complex A**. The results are summarized in Table 3.1.1, enantiomers are listed only once. We compare DFT results obtained with different exchange correlation functionals, consider the influence of van der Waals (vdW) effects by the DFT-D method and solvent effects by the COSMO method. The stereoconfiguration labels are always given for ligand **4** so the suffix '4' is omitted for clarity. For simplification only **complex A** with a ZnMe moiety is considered.

In all calculations for the monomers (**complexes A**), the S_p,R monomer was about 4 kcal/mol more stable than the S_p,S isomer. The relative energies of the dimers reflect the energy differences of the monomers, the $S_p,R/S_p,R$ dimer has the lowest and the $S_p,S/S_p,S$ dimer the highest energy. The results of the DFT calculations are comparable for different exchange correlation functionals. For the dimers, the energy differences were increased when van der Waals (vdW) interactions were considered by the DFT-D method.

An important question was, whether the catalyst is more stable in its monomeric or dimeric form. Therefore, the dimer binding energies calculated by different methods are summarized in the last part of Table 3.1.1. As long as vdW interactions were not taken into account, the energies of monomers and dimers were similar. Inclusion of solvent effects (COSMO) stabilized all monomers by 2 kcal/mol. By changing the functional to B3LYP, the dimers were slightly stabilized. When vdW interactions were considered by the DFT-D method, the dimers were strongly stabilized by about 25 kcal/mol. The strong influence of dynamic correlation was confirmed by MP2 calculations for the binding energy of the S_p,R homodimer. For this isomer the total binding energy amounts to -32.9 kcal/mol at the MP2 level.

Table 3.1.1 Relative energies of monomers and dimers of **complex A** and dimer binding energies (in kcal/mol) for various diastereomers of ZnMe·4. All values were obtained with a def2-TZVP basis set and include the ZPE corrections. The binding energies are corrected for the basis set superposition error.

<i>Relative energies of the different isomers (in kcal/mol)</i>				
monomers	BP86	BP86/COSMO	B3LYP	BP86-D
S_p,R	0.00	0.00	0.00	0.00
S_p,S	3.75	3.96	3.93	3.94
dimers	BP86	BP86/COSMO	B3LYP	BP86-D
$S_p,R/S_p,R$	0.00	0.00	0.00	0.00
$S_p,R/S_p,S$	1.72	1.55	1.62	5.44
$S_p,S/S_p,S$	3.81	3.82	3.76	9.21
$S_p,S/R_p,R$	2.80	2.66	2.78	4.13
$S_p,S/R_p,S$	1.94	1.89	1.90	3.72
$S_p,R/R_p,S$	1.23	1.19	1.22	2.33
<i>Binding energies of the dimers (in kcal/mol)</i>				
isomer	BP86	BP86/COSMO	B3LYP	BP86-D
$S_p,R/S_p,R$	2.84	4.92	0.27	-25.54
$S_p,R/S_p,S$	0.86	2.77	-1.76	-25.94
$S_p,S/S_p,S$	-0.93	0.94	-3.72	-26.24
$S_p,S/R_p,R$	-1.76	0.77	-5.32	-25.94
$S_p,S/R_p,S$	-0.39	1.96	-4.41	-25.71
$S_p,R/R_p,S$	-0.40	1.88	-4.83	-25.57

In the following, we focus our discussion on the homodimer and heterodimer formed by the S_p,R and R_p,S monomers. The calculated values show that the homodimers are around 2 kcal/mol more stable than the heterodimer. However such a stabilization is very small and prompted us to investigate which factors affect the relative stability of the dimers. To gain inside into the thermochemistry of the dimer formation the zero – point energies were obtained from the frequency calculations and are already included in the binding energies given in Table 3.1.1. The change in standard internal energy at 0K ($\Delta U^0(0) = zpe_{\text{dimer}} - \sum_{\text{monomer},i} zpe_i$) equals to 1.3 kcal/mol for the homodimer and 6.1 kcal/mol for the heterodimer. At the reaction temperature of 248 K the homodimer has an entropic stabilization of 4.2 kcal/mol compared to the heterodimer. While the reaction proceeds in a non-polar medium the greater size of the polar surface of one dimer will cause its destabilization in this solvent. Topological molecular polar surface area¹⁶⁷ (TPSA) calculations gave a value of 25 Å² for the homodimer while the value for the heterodimer amounts to 33 Å². A simple explanation of these results is that the polar center of the homodimer is better shielded. Moreover, the considered molecules contain several phenyl rings which can interact with the toluene molecules. This interaction is not included in the COSMO model, but can be estimated in the following way. According to the work of Sinnokrot and Sherrill,¹⁶⁸ the π - π sandwich interaction is in the order of -2.3 kcal/mol at an optimal distance of 3.8 Å. Both dimers can at

least interact with six toluene molecules, each phenyl ring with one solvent molecule. In contrary to the heterodimer, the homodimer possesses an extra pocket between the two phenyl rings in the side chain. The distance between them is around 7.5 Å so there is a place for at least one additional toluene ring. This extra stabilization has been estimated on the base of a small model system containing two benzene rings and a toluene molecule in the middle. A binding energy of -7.3 kcal/mol was obtained at the BP86-D level.

3.1.4 INTERACTION OF SUBSTRATE WITH COMPLEX A

In the first step of the reaction, **complex A** is formed from a dialkylzinc molecule and a paracyclophane ligand (see Scheme 3.1.2). It is obvious that at least one substrate molecule has to interact with **complex A** in the reaction. When a carbonyl oxygen is added to the Zn ion a binding pocket for the second dialkylzinc moiety is generated. Because of the experimental ratio of dialkylzinc to the number of substrate molecules being larger than two, we assume that **complex B** is formed in the next step of the reaction. A similar Zn_2O_2 unit was observed for the dimers of **complex A** (see chapter 3.1.3). Figure 3.1.2 presents binding energies of the second dialkylzinc to a system consisting of the **complex A** and a substrate molecule (enal **1a** or iminal **1b**). For all compounds and quantum-chemical methods the binuclear complex is energetically preferred. LPNO-CEPA/1 benchmark results are always between the B2PLYP+D and SCS-MP2 values. The calculated energies are relatively close to each other (12.6 kcal/mol and 13.4 kcal/mol for substrate **1a** with dimethylzinc ($ZnMe_2$) and diethylzinc ($ZnEt_2$), respectively as well as 13.5 kcal/mol and 15.0 kcal/mol for iminal **1b** with $ZnMe_2$ and $ZnEt_2$, respectively). As expected, neither pure nor hybrid density functionals approach these results. Augmentation with dispersion corrections improves the calculated binding energies significantly but they are still overshoot by about 30% in comparison to the LPNO-CEPA/1 reference. Also the double hybrid B2PLYP functional does not account for all long-range interactions and therefore the D3 correction seems to be mandatory (the obtained energies are about 20% higher than the reference). It is worth noting that addition of empirical dispersion terms reduces the dependence of the computed binding energies on the density functional compared to uncorrected DFT results. Simulation of solvation with the COSMO model has minor influence on the binding energies. The minor increase (0.5 – 0.8 kcal/mol) of the binding energies can be addressed to shielding of the polar core of the complex by the second dialkylzinc molecule.

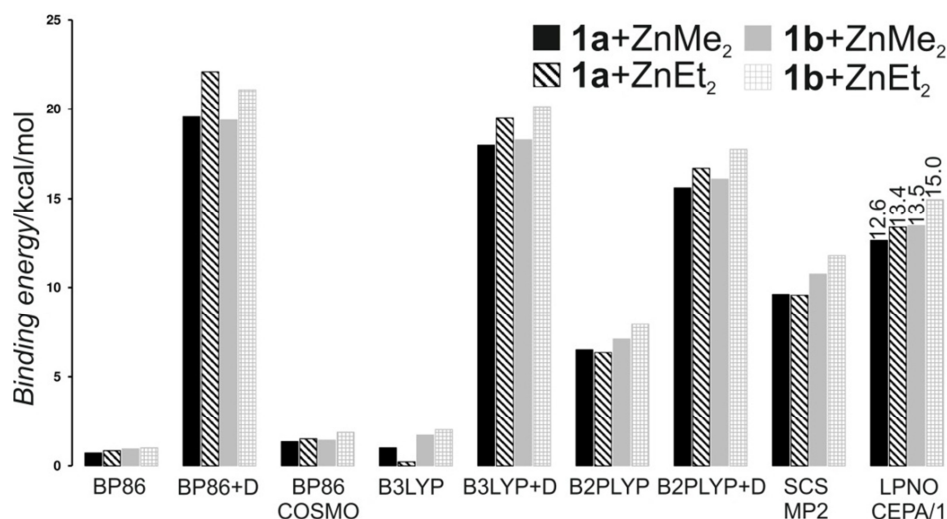


Figure 3.1.2 Comparison of binding energies (counter-poise and zero-point energy corrected) of the second dialkylzinc molecule ($\text{ZnR}'_2 = \text{ZnMe}_2, \text{ZnEt}_2$) to the ligand- ZnR' -substrate complex (abbreviated in legend to the substrate number **1a** or **1b**) calculated at different levels of theory. LPNO-CEPA/1 values are given explicitly.

The structures of the binuclear complexes are shown in Figure 3.1.3. Most bond distances – for example the Zn-C bonds and $\text{Zn}^1\text{-O}^4$, $\text{Zn}^1\text{-O}^2$, $\text{Zn}^3\text{-O}^4$, $\text{Zn}^1\text{-N}$ bonds – are more or less the same in all four systems. Only the $\text{Zn}^3\text{-O}^2$ bond varies significantly. It is elongated by about 0.6 Å, when the substrate is changed from cinnamaldehyde **1a** to *N*-formylbenzylimine **1b**. Moreover, the torsion angle θ , $\text{O}^2\text{-C}^8\text{-N}^9\text{-C}^{10}$, is close to 64° for substrate **1b**. This is not the case for **1a** where the angle θ , $\text{O}^2\text{-C}^8\text{-C}^9\text{-C}^{10}$, is more or less planar ($\sim 3^\circ$). Such a deformation from planarity indicates that the rotation around the $\text{C}^8\text{-N}^9$ single bond is less strained in comparison to the $\text{C}^8\text{-C}^9$ bond. *N*-methyleneformamide – a smaller analogue of **1b** – is a known example of a compound which even if expected to be planar is in fact bent and adopts a gauche conformation ($\sim 60^\circ$).¹⁶⁹⁻¹⁷² This is due to two major forces determining the structure of the compound – conjugation, which is highest for the planar conformation, and lone pairs repulsion (N and O), which is smallest in the perpendicular arrangement.¹⁷¹

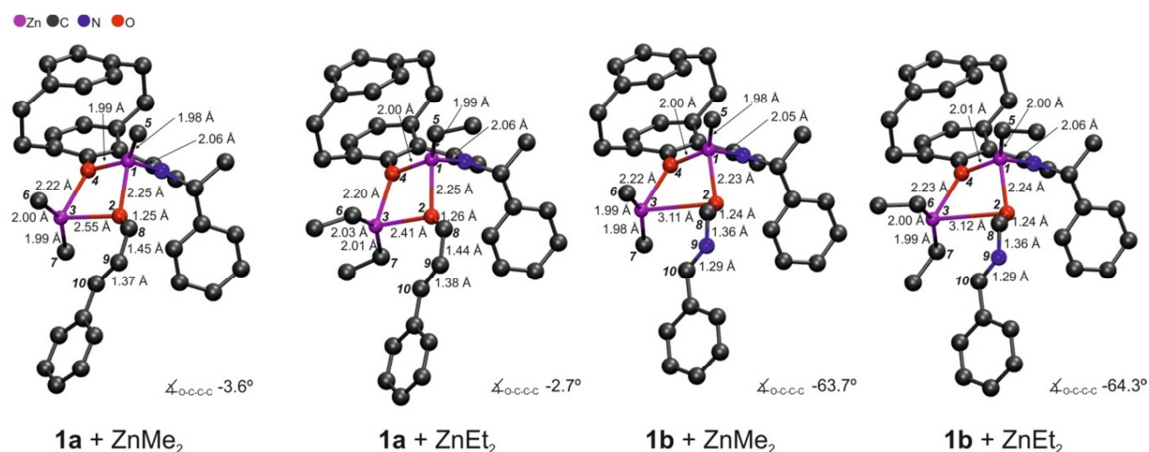


Figure 3.1.3 Comparison of geometries of the binuclear **complexes B** (compare with Scheme 3.1.2). For each structure, selected bond lengths are given along with atom numeration used in text. At the bottom of each structure, the torsion angle θ , O²-C⁸-C⁹-C¹⁰, is listed. Hydrogen atoms are omitted for clarity.

3.1.5 DELOCALIZATION ENERGY OF SUBSTRATES AND TRANSITION STATES

For the detailed analysis of the conformational flexibility, we performed a relaxed potential energy surface scan at BP86/def2-SVP level along θ for both substrates and present the results in Figure 3.1.4. As expected, cinnamaldehyde **1a** prefers a planar conformation. The *trans* ($\theta = 180^\circ$) conformer is 1 kcal/mol more stable than *cis*. The rotation barrier between these conformers has a relatively high value of 11.4 kcal/mol. Interestingly, this was not the case for *N*-formylbenzylimine **1b** where the minimum along the examined path is located at $\theta = 46^\circ$ (*gauche*) and both *cis* and *trans* isomers are about 1 kcal/mol higher in energy with rotation barriers lower than 2 kcal/mol. As for *N*-methyleneformamide, the rotation around the C-N bond is much less constrained in comparison to the C-C bond in **1a** and, in consequence, the delocalization energy of **1b** is much smaller than in case of **1a**. All 1,4-addition barriers are lower for *N*-formylbenzylimine by at least 3 kcal/mol (see Figure 3.1.5). This can again be attributed to the higher structural flexibility of the transition state for 1,4-addition with respect to θ , which is in most cases more than two times larger in both *syn* and *anti* conformation of **1b** in comparison to **1a** (see Table 3.1.2). At the same time the change of the substrate from **1a** to **1b** increases the activation barriers of 1,2-additions by 1 – 3 kcal/mol.

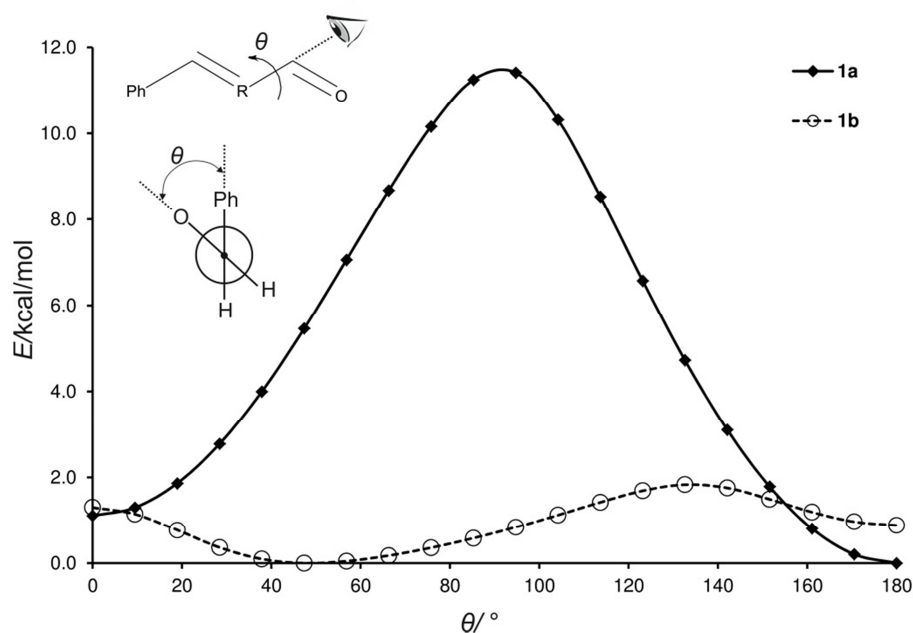


Figure 3.1.4 Change in energy (BP86/def2-SVP) upon rotation around the torsion angle θ (defined graphically) in substrates **1a** and **1b**. For fixed values of θ the rest of the molecule was allowed to relax.

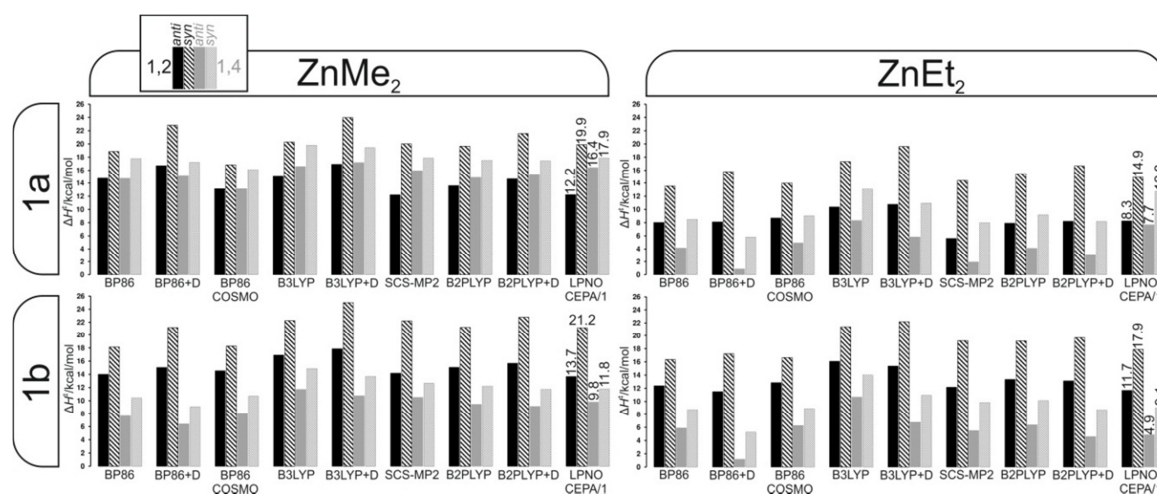


Figure 3.1.5 Activation enthalpy (ΔH^\ddagger) of the alkyl group transfer in asymmetric addition reactions of dialkylzinc to α,β -unsaturated aldehydes **1a** and **1b** calculated at various levels of theory. Black – 1,2-addition, grey – 1,4-addition. LPNO-CEPA/1 values are given explicitly.

Table 3.1.2 Structural parameters of the calculated transition states of 1,2- and 1,4-addition reactions of dialkylzinc ($R'=Me, Et$ for $ZnMe_2$ and $ZnEt_2$, respectively) to the substrates **1a** ($R=CH$) and **1b** ($R=N$). θ is the torsion angle between atoms 2, 8, 9 and 10 while α is the Bürgi-Dunitz angle between the transferred carbon atom (6 or 7), the acceptor carbon atom (8 or 10) and the distal atom (2 or 9) of the substrate. Bond lengths are given in angstroms (Å) and angles in degrees (°).

R	1,2				1,4				1,2				1,4			
	<i>anti</i>		<i>syn</i>		<i>anti</i>		<i>syn</i>		<i>anti</i>		<i>syn</i>		<i>anti</i>		<i>syn</i>	
R'	Me	Et	Me	Et												
Zn^1-O^2	2.13	2.14	2.15	2.15	2.12	2.14	2.13	2.13	2.17	2.17	2.20	2.20	2.17	2.17	2.20	2.20
Zn^1-O^4	2.06	2.06	2.05	2.06	2.07	2.06	2.06	2.06	2.03	2.04	2.02	2.03	2.04	2.04	2.03	2.03
Zn^3-O^2	2.25	2.22	2.28	2.26	2.20	2.16	2.23	2.20	2.10	2.09	2.14	2.12	2.08	2.09	2.11	2.11
Zn^3-O^4	2.05	2.06	2.05	2.06	2.05	2.06	2.05	2.06	2.13	2.12	2.15	2.14	2.13	2.14	2.13	2.16
Zn^1-C^5	1.98	1.99	1.98	1.99	1.98	1.99	1.98	1.99	1.98	1.99	1.97	1.99	1.97	1.99	1.97	1.99
Zn^3-C^6	2.21	2.24	2.18	2.16	1.97	1.99	1.98	1.99	2.19	2.28	2.14	2.20	2.00	2.01	2.00	2.01
Zn^3-C^7	1.97	1.99	1.98	1.99	2.20	2.24	2.17	2.23	1.99	2.00	1.99	2.01	2.21	2.24	2.17	2.21
C^6-C^8	2.29	2.37	2.29	2.37	–	–	–	–	–	–	–	–	–	–	–	–
C^7-C^8	–	–	–	–	2.31	2.31	2.33	2.38	–	–	–	–	–	–	–	–
C^6-C^{10}	–	–	–	–	–	–	–	–	2.41	2.44	2.47	2.51	–	–	–	–
C^7-C^{10}	–	–	–	–	–	–	–	–	–	–	–	–	2.37	2.43	2.39	2.48
C^8-O^2	1.31	1.31	1.30	1.31	1.31	1.32	1.30	1.31	1.30	1.31	1.29	1.29	1.30	1.30	1.29	1.29
C^8-R^9	1.47	1.47	1.40	1.40	1.47	1.47	1.40	1.40	1.39	1.39	1.32	1.32	1.39	1.39	1.32	1.32
R^9-C^{10}	1.36	1.36	1.30	1.30	1.36	1.36	1.30	1.30	1.42	1.42	1.35	1.35	1.43	1.42	1.35	1.36
θ	2.4	0.5	8.4	7.7	0.4	5.0	-4.0	-0.9	3.5	2.1	10.5	8.6	-6.1	-5.2	-12.6	-12.1
α	114.2	115.9	115.1	116.6	117.2	119.1	117.5	119.9	105.4	101.9	104.8	103.3	109.0	105.6	109.0	105.2

Further geometrical changes which accompany the change from substrate **1a** to **1b** are summarised in Table 3.1.2. In all transition states the Zn-C bond to the transferred alkyl group is slightly shorter for **1b**, e.g. 2.28 Å for cinnamaldehyde and 2.20 Å for *N*-formylbenzylimine in the 1,4-*anti*-addition. Moreover, the new forming C-C bond is not influenced at all upon changes of the substrate in 1,2-additions and is only slightly elongated (0.02 – 0.06 Å) for 1,4-additions.

In all transition states the former $C^8=O^2$ double bond is elongated to 1.30 Å (from 1.24 Å). In case of 1,4-additions the middle bonds of the substrates, C^8-C^9 and C^8-N^9 , are 0.05 Å shorter indicating the formation of a new C=C or C=N double bond in the product. The bonds between zinc atoms and the carbon atoms from those alkyl chains which are inactive in the reaction are not influenced by the reagent **1a** or **1b**. In the transition states the new C...C bond is up to 0.09 Å longer in case of $ZnEt_2$. The Bürgi-Dunitz angle α for 1,2-additions varies from 114° to 120° being significantly higher than the expected value of 107°.^{173,174} While α is mainly determined by $n \rightarrow \pi^*$ interaction,¹⁷⁴ the shape of the antibonding π^* orbitals of the carbonyl group will be strongly affected by conjugation of the C=N double bond and

repulsion with the nitrogen lone pair. As can be extracted from Figure 3.1.5 the reactions which involve diethylzinc have lower energy barriers. The Mulliken charges on the hypercoordinated carbon atom are more negative for methyl (-0.6) than for ethyl (-0.3) substituents. The differences in the reaction barriers are in line with a better stabilization of the negative charge through induction effects when the transferred alkyl group is bigger or more branched.

For the detailed analysis of the factors influencing the relative barrier heights in the examined reactions we performed the activation strain analysis.^{175,176} We decomposed the activation energy ΔE^\ddagger of the transition state (TS) into the interaction energy ΔE_{int} between substrate (**1a** or **1b**) and the remaining part of the **complex B**,ⁱ the strain energy $\Delta E_{\text{strain}}^\ddagger$ describing the deformation energy of both parts of **complex B** in order to adopt the TS geometries, and finally the interaction energy between these deformed fragments in the transition state $\Delta E_{\text{int}}^\ddagger$ (see eqn (79) and Figure 3.1.6):

$$\Delta E^\ddagger = \Delta E_{\text{int}} + \Delta E_{\text{strain}}^\ddagger + \Delta E_{\text{int}}^\ddagger \quad (79)$$

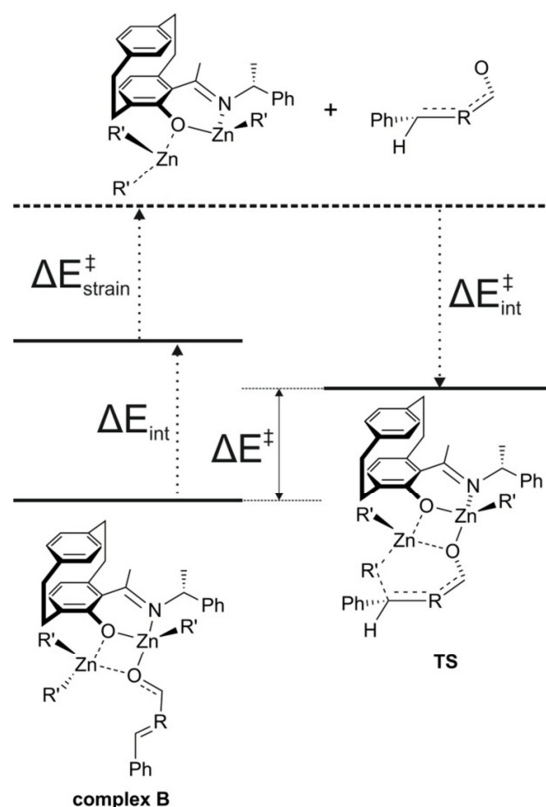


Figure 3.1.6 Schematic presentation of the performed activation strain analysis.

The results of the strain analysis are summarised in Table 3.1.3. As expected, ΔE_{int} remains rather constant and is in the order of 22 kcal/mol. The activation strain energy is significantly larger for *syn*-additions than for *anti*-additions (up to 11 kcal/mol). This is caused by the

ⁱ Both fragments were calculated at the structure they have in **complex B**.

relatively strained tricyclic system formed in the transition state, which prefers *anti*-arrangement (see Figure 3.1.7). Interestingly, the differences in strain energies are less pronounced in case of 1,4-additions compared to 1,2-additions. We concluded that in order to avoid the *syn*-conformation in the 1,4-addition bulkier ligands are necessary. This is caused by the long distance between the C atom accepting the alkyl group and the stereo-inducing group. For 1,2-additions the change of the substrate has only little effect on the strain energy, whereas substitution of **1a** with **1b** decreases it by as much as 10 kcal/mol for 1,4-additions. This further confirms higher flexibility of the *N*-formylbenzylimine. Moreover, better stabilisation of the negative charge by an ethyl group is reflected in the interaction energies of the deformed fragments in the TS. The absolute value of $\Delta E_{\text{int}}^{\ddagger}$ was at least 4 kcal/mol higher for the larger alkyl substituent.

Table 3.1.3 Interaction energies between substrate (**1a** or **1b**) and the remaining part of the respective **complex B** (ΔE_{int}), activation strain energies ($\Delta E_{\text{strain}}^{\ddagger}$), interaction energies of the deformed fragments at the TS geometry ($\Delta E_{\text{int}}^{\ddagger}$) and total activation energy ΔE^{\ddagger} . All values are in kcal/mol.

Addition	R	R'	Isomer	ΔE_{int}	$\Delta E_{\text{strain}}^{\ddagger}$	$\Delta E_{\text{int}}^{\ddagger}$	ΔE^{\ddagger}
1,2	CH	Me	anti (S)	21.6	29.6	-38.2	13.0
			syn (R)		40.0	-41.0	20.5
		Et	anti (S)	28.1	-42.1	8.9	
			syn (R)	40.8	-48.7	15.1	
	N	Me	anti (S)	22.2	26.8	-34.1	14.9
			syn (R)		36.7	-36.4	22.5
		Et	anti (S)	28.0	-38.2	12.4	
			syn (R)	40.8	-42.4	19.8	
1,4	CH	Me	anti (S)	22.9	40.8	-45.2	17.2
			syn (R)		44.9	-47.7	18.8
		Et	anti (R)	42.8	-50.1	8.6	
			syn (S)	44.0	-53.3	13.7	
	N	Me	anti (S)	22.7	31.9	-42.9	11.1
			syn (R)		38.4	-47.9	12.7
		Et	anti (R)	35.1	-52.2	5.6	
			syn (S)	41.2	-54.1	9.8	

3.1.6 STEREOSELECTIVITY

Yamakawa and Noyori¹⁶² suggested that the tricyclic system in the 1,2-transition state prefers *anti*-arrangement because of less steric hindrance in comparison to the *syn*-conformer. Our calculations fully support these findings and broaden this idea to 1,4-transition states for which also *anti*-stereochemistry gives the lower-energy conformer (see Figure 3.1.7). The differences between activation enthalpies of *syn*- and *anti*-conformers ($\Delta\Delta H_{\text{syn-anti}}^{\ddagger} = \Delta H_{\text{syn}}^{\ddagger} - \Delta H_{\text{anti}}^{\ddagger}$) calculated at various levels of theory are summarized in Table 3.1.4. It is worth noting that all tested methods correctly predict the stereochemistry of both 1,2- and 1,4-addition reactions. As for any other quantum chemical method we cannot expect the LPNO-CEPA/1 results to be exact. However, it was the most sophisticated method used in this study

and we defined the mean absolute error (MAE) and maximum error (MAX) as deviations with respect to the LPNO-CEPA/1 reference values. The differences are highest for the BP86 functional (1.2 and 3.5 kcal/mol, respectively) but are significantly reduced by dispersion corrections (0.1 and 1.5 kcal/mol, respectively). The results obtained at B3LYP and B2PLYP level are less influenced by dispersion corrections. SCS-MP2 yields results comparable to B3LYP (MAE 0.7 kcal/mol and MAX 2.2 kcal/mol).

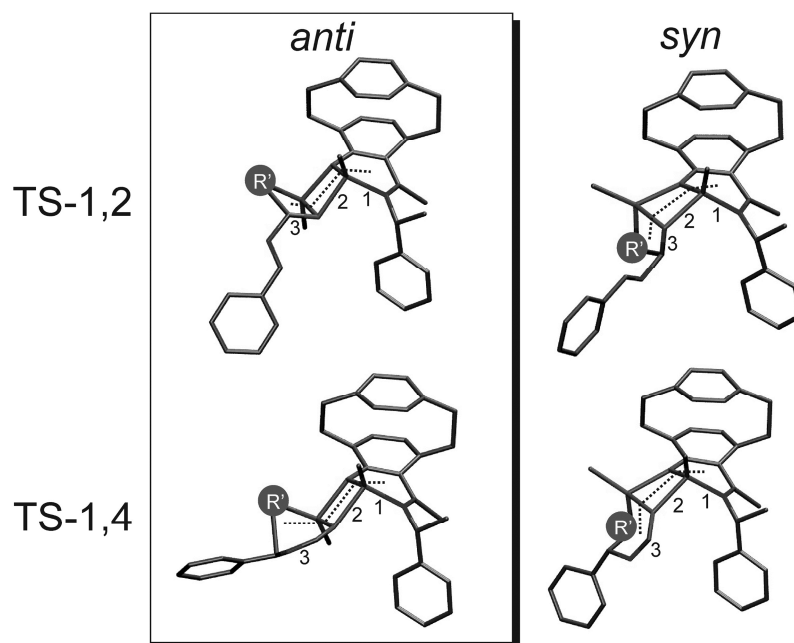


Figure 3.1.7 Comparison of *syn*- and *anti*-arrangement of the three rings (1, 2, 3) formed in all examined transition states. Because of smaller steric repulsion the *anti*-conformation is always preferred.

Table 3.1.4 Differences between activation enthalpies of *syn*- and *anti*-conformers of 1,2- and 1,4-addition reactions $\Delta\Delta H_{syn-anti}^\ddagger$ of $ZnMe_2$ ($R'=Me$) and $ZnEt_2$ ($R'=Et$) to 1a ($R=CH$) and 1b ($R=N$). MAE – mean absolute error, MAX – maximum absolute error calculated with respect to LPNO-CEPA/1 reference. All values are given in kcal/mol.

Addition	R	R'	BP86	BP86+D	B3LYP	B3LYP+D	SCS-MP2	B2PLYP	B2PLYP+D	LPNO-CEPA/1
1,2	C	Me	4.1	6.1	5.3	7.1	7.8	6.1	7.0	7.7
	H	Et	5.5	7.7	7.0	8.9	8.8	7.6	8.5	6.6
	N	Me	4.1	6.1	5.4	7.2	8.0	6.2	7.1	7.5
		Et	4.0	5.7	5.3	6.8	7.1	5.9	6.5	6.2
1,4	C	Me	3.1	2.2	3.2	2.3	2.0	2.7	2.2	1.5
	H	Et	4.3	5.0	4.8	5.1	6.1	5.1	5.2	5.1
	N	Me	2.8	2.7	3.2	2.9	2.1	2.8	2.6	2.0
		Et	2.9	4.1	3.4	4.2	4.4	3.8	4.1	4.2
MAE			1.2	0.1	0.4	0.5	0.7	0.1	0.3	–
MAX			3.5	1.5	2.4	2.2	2.2	1.6	1.8	–

3.1.7 REGIOSELECTIVITY

Different trends are observed for the regioselectivity, which is measured by $\Delta\Delta H^\ddagger_{1,2-1,4}$ ($\Delta\Delta H^\ddagger_{1,2-1,4} = \Delta H^\ddagger_{1,2} - \Delta H^\ddagger_{1,4}$) and summarised in Table 3.1.5. The lowest MAE is observed for SCS-MP2 (0.8 kcal/mol). Second was B3LYP with a value of 1.0 kcal/mol. Interestingly, the double hybrid functional B2PLYP and the gradient-corrected BP86 functional yield similar MAE (2.0 and 2.4 kcal/mol, respectively). Surprisingly, addition of dispersion corrections deteriorates the situation. For BP86+D an MAE of 5.2 kcal/mol was observed, 2.8 kcal/mol higher than for the pure functional. Furthermore, only the pure B3LYP functional gives a value lower than 3 kcal/mol for MAX (2.6 kcal/mol). Inclusion of dispersion corrections increases MAX by 1.7 kcal/mol. For B2PLYP+D the MAE is 1.5 kcal/mol higher than for pure B2PLYP. For ZnMe_2 additions to **1a** neither BP86 nor BP86+D properly predicts the 1,2-product to be more stable than the 1,4-product. The origin of such high errors is connected to the differences in dynamic correlation energy in the 1,2- and 1,4-transition states. While 1,2-addition leaves the double bond (C=C or C=N) untouched the 1,4-addition forces formation of a new double bond (compare the bond lengths between atoms 8 and 9 in Table 1). More precisely we can track this difference by analysis of the CEPA-wave functions of the transition states. The biggest contribution corresponds to a $n \rightarrow \pi^*$ excitation. The weights of this excitation are 0.07 and 0.13 for 1,2- and 1,4-*anti*-addition of ZnEt_2 to **1a**, respectively. Furthermore, we calculated the difference of energies of the *anti*-conformers of the 1,2- and 1,4- addition of ZnMe_2 to **1a** at a multireference CASSCF/NEVPT2 level with active space of two electrons on two orbitals (largest amplitude in LPNO-CEPA/1 calculations). Obtained value of -2.45 kcal/mol agrees well with single-reference LPNO-CEPA/1 result (-2.61 kcal/mol). The discrepancies between non-correlated methods and correlated ones were previously also reported for much smaller, copper and lithium catalysed additions by Dorgio and Morokuma.¹⁷⁷ The reliability of the LPNO-CEPA/1 model is confirmed by comparison with experiment.¹⁵⁵ The experimental ratio of yields of the 1,4- and 1,2-*anti*-products (*S*-1,4 and *S*-1,2, respectively) of ZnEt_2 additions to **1a** is 2.2:1 while the computed one is 2.7:1. The agreement is excellent (though ΔH^\ddagger values were used in the Eyring equation and no solvent effects were included) and not accessible with other methods which predict the exclusive formation of 1,4-*anti*-product (*S*-1,4).

Table 3.1.5 Differences between activation enthalpies of the lowest energy 1,2-*anti*- and 1,4-*anti*-paths ($\Delta\Delta H_{1,2-1,4}^\ddagger$). Positive value indicates that the 1,4-path is preferred (lower in energy). Abbreviations as in Table 3.1.4. All values are given in kcal/mol.

R	R'	BP86	BP86+D	B3LYP	B3LYP+D	SCS-MP2	B2PLYP	B2PLYP+D	LPNO-CEPA/1
CH	Me	0.0	1.6	-1.6	-0.3	-3.7	-1.2	-0.6	-4.2
	Et	3.9	7.3	2.0	4.9	3.7	3.8	5.2	0.6
N	Me	6.4	8.6	5.2	7.1	3.6	5.6	6.5	3.9
	Et	6.5	10.3	5.4	8.6	6.7	7.0	8.5	6.8
MAE		2.4	5.2	1.0	3.3	0.8	2.0	3.1	–
MAX		4.2	6.7	2.6	4.3	3.1	3.2	4.6	–

3.1.8 THERMODYNAMIC VS. KINETIC CONTROL

As shown in Table 3.1.6, the transfer of the alkyl group from the Zn moiety to the substrate molecule in **complex B** is highly exothermic (about -40 kcal/mol). We have to admit that solvent effects which are not included in our calculations should lower the exothermicity of the reaction. In the products the coordination of one zinc centre changes from four-fold tetrahedral surrounding to a planar three-fold coordination. The latter should be destabilised by the non polar solvent. However, for **complex B** and the transition states the arrangement of the substituents is very similar and solvent effects should cancel. Furthermore, $\Delta\Delta H$ should not be affected because the solvent effect are similar for the different reactions. In case of 1,4-addition, the use of **1b** increases the energy span of the reactions by about 2 kcal/mol (the reactions are slightly more exothermic). For 1,2-additions ΔH is less dependent on the stereochemistry of the process while for 1,4-additions the formation of the *syn*-product is more exothermic by 3 – 5 kcal/mol in comparison to the *anti*-product. The reason is that the repulsion of the phenyl rings from the substrate and the side chain of the ligand is smaller in the *syn*-product. This suggests that the enantioselectivity of the reaction is different for kinetic (*anti*-product) and thermodynamic control (*syn*-product).

For the combination of **1b** with dimethylzinc *ee* of the major 1,4-product is in the experiment in the order of 60%.¹⁵⁶ Considering exclusively kinetic control through the barrier heights $\Delta\Delta H_{syn-anti}^\ddagger$ (2.0 kcal/mol) we obtained *ee* equal to 94%. The difference can be caused either by the influence of the thermodynamic control ($\Delta\Delta H_{syn-anti} = -3.6$ kcal/mol, *syn*-product more stable), or by small errors in the barrier heights which strongly influence *ee* through the exponent in the Eyring equation.

Table 3.1.6 The change in enthalpy (ΔH) at LPNO-CEPA/1 level of theory for the transfer of the alkyl group from the Zn moiety to the substrate molecule in **complex B**.

Addition	R	R'	Isomer	ΔH [kcal/mol]
1,2	CH	Me	anti (S)	-35.5
			syn (R)	-35.9
		Et	anti (S)	-40.9
			syn (R)	-41.0
	N	Me	anti (S)	-34.7
			syn (R)	-35.1
		Et	anti (S)	-39.0
			syn (R)	-40.3
1,4	CH	Me	anti (S)	-35.4
			syn (R)	-38.8
		Et	anti (R)	-42.3
			syn (S)	-44.6
	N	Me	anti (S)	-37.7
			syn (R)	-41.3
		Et	anti (R)	-42.3
			syn (S)	-47.7

3.1.9 SCREENING OF NEW LIGANDS

The LPNO-CEPA/1 calculations provide energies that are in quantitative agreement with the experimental findings. The next step of the calculations should therefore be a rational design of new catalysts for the tested reaction. It is still a challenge to effectively obtain a high amount of the 1,4-product **2a** in the reaction of cinnamaldehyde **1a** with diethylzinc. The best ligand for this reaction reported up to now is the analogue of ligand **4** where the phenyl ring in the side chain is exchanged with the more bulky cyclohexyl group. The reaction yields a mixture of compounds: 1,4-product (~60%), a number of side-products (~35%) and a small amount of 1,2-product. This observation suggests that 1,4-additions require larger groups attached to the ligand in order to suppress the 1,2-addition path. Moreover, excellent enantiomeric excesses (>99%) are in line with our findings that larger ligands will favour *anti* additions. However, there is still need for better catalyst that will increase the yield of 1,4-product, reduce the amount of by-products as well as will have similar high *ee*. The question of side-reactions is rather out of scope of this theoretical calculations but decreasing the 1,4-reaction barrier along with high stereo- and regioselectivity can be addressed by *in silico* testing a set of new ligands.

We decided to investigate the group of ligands shown in Figure 3.1.8. They differ from the one previously used by substitution of the C=N containing side chain (compare with Scheme 3.1.1) with more rigid pyrazole groups. The substituents attached to the β -nitrogen atom of pyrazole were systematically varied yielding the ligands **5-11**.

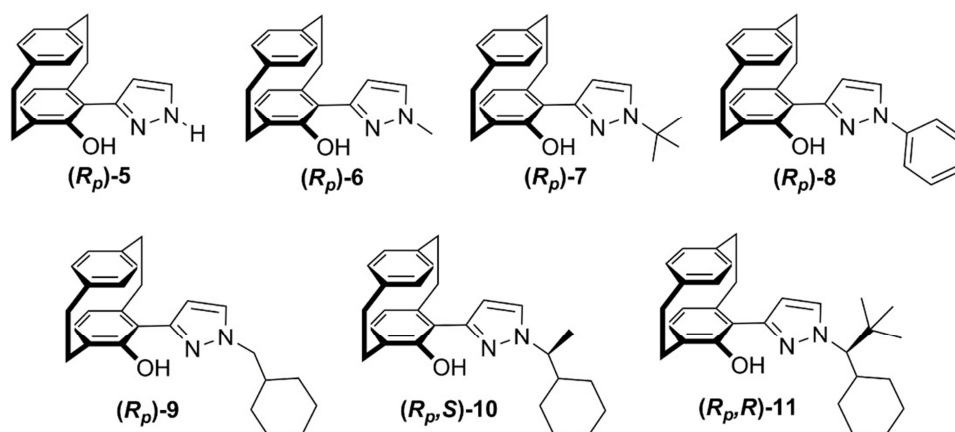


Figure 3.1.8 The ligands **5-11**, that were chosen for *in silico* tests for activity in diethylzinc additions to cinnamaldehyde **1a**.

In order to test the selectivity of the ligands **5-11** in the addition of diethylzinc to cinnamaldehyde **1a**, we proceeded in the same way as for the reference ligand **4**. Thus, in each case we optimised **complex B** i.e. a complex of the ligand, a ZnEt_2 and a substrate molecule. In the next step, *syn*- and *anti*-transition state structures for 1,2- and 1,4-additions were obtained and finally, geometry optimisations were carried out for the corresponding products. Each structure was then submitted to LPNO-CEPA/1 calculations. The activation enthalpies for 1,2- and 1,4-additions leading to products **3a** and **2a**, respectively, are collected in Table 3.1.7.

The absolute activation enthalpies for 1,4-*anti*-additions with all tested ligands are lower than those calculated for the reference structure **4** (7.7 kcal/mol). Increasing bulkiness of the side chain through introduction of a cyclohexyl group via a methylene linker (ligands **9-11**) was gradually increasing the stereoselectivity of the 1,4-addition but the regioselectivity was significantly deteriorated. This is caused by the proximity of the transferred ethyl group and the side chain in the 1,2-transition state. The lowest barrier was observed in case of ligand **11** (1.0 kcal/mol), i.e. the ligand with the highest sterical hindrance. However, the same activation enthalpy is predicted for 1,2-*syn*-addition with this ligand so high stereoselectivity is not combined with high regioselectivity. Interestingly, also for ligands **6** and **7** the *syn* configuration of the transition state was preferred over the *anti*-conformation in the 1,2-addition most probably due to the more rigid nature of the pyrazole side ring. The most promising ligand from the tested set is **7** where a bulky *tert*-butyl group is attached to the β -nitrogen atom of pyrazole. $\Delta\Delta H^\ddagger_{\text{syn-anti}}$ for the 1,4-addition is here 2.6 kcal/mol while $\Delta\Delta H^\ddagger_{1,2-1,4}$ is predicted to be 1.0 kcal/mol. Therefore, the *ee* of **2a** should be close to 100% while according to transition state theory the ratio of **2a** to **3a** will be close to 6:1.

Table 3.1.7 The activation enthalpies (ΔH^\ddagger) of diethylzinc additions to cinnamaldehyde **1a** with various ligands (see Figure 3.1.8) calculated at LPNO-CEPA/1 level.

Ligand	Addition	ΔH^\ddagger [kcal/mol]	
4	1,2	anti (S)	8.3
		syn (R)	17.9
	1,4	anti (R)	7.7
		syn (S)	12.8
5	1,2	anti (S)	7.9
		syn (R)	8.4
	1,4	anti (R)	5.9
		syn (S)	6.5
6	1,2	anti (S)	6.1
		syn (R)	5.9
	1,4	anti (R)	4.2
		syn (S)	5.3
7	1,2	anti (S)	6.3
		syn (R)	4.5
	1,4	anti (R)	3.5
		syn (S)	6.1
8	1,2	anti (S)	10.6
		syn (R)	10.2
	1,4	anti (R)	7.6
		syn (S)	7.9
9	1,2	anti (S)	4.8
		syn (R)	4.7
	1,4	anti (R)	4.1
		syn (S)	7.0
10	1,2	anti (S)	5.0
		syn (R)	8.1
	1,4	anti (R)	4.6
		syn (S)	9.1
11	1,2	anti (S)	1.9
		syn (R)	1.0
	1,4	anti (R)	1.0
		syn (S)	7.3

3.1.10 CONCLUSIONS

The calculations confirm the experimental finding that the catalyst is mainly in its dimeric form. However, in solution, the stabilization of the dimers will be less pronounced, because of dispersion interactions of the monomer with the solvent molecules which can fill the space occupied by the second molecule in the dimer. The homodimers were found to be more stable than the heterodimers and are favoured mainly by entropy contributions and solvent interactions. Thus, the calculations provide the explanation of the experimentally observed negative non-linear effect.

The high yields of the additions of the dialkylzinc reagents to *N*-formylbenzylimine **1b** can be traced back to lower π -conjugation and therefore higher flexibility in comparison to the reaction with cinnamaldehyde **1a**. Moreover, the better yields for the addition of ethyl compared to methyl can be addressed to the intuitive rule that the negative charge on the transferred group is better stabilized by more bulky/more branched alkyl substituents. In consequence the reaction barriers are significantly lower in this case.

The regioselectivity of the examined reactions is influenced by two effects. The 1,2-addition results in a product which partially conserves the π -conjugation in the side chain of the product. For the 1,4-addition the loss of this type of stabilisation is balanced by higher correlation energy, due to stronger interaction of the transferred alkyl group with the electron-rich phenyl ring. This stabilises the respective transition states. The stereoselectivity of the reaction is dominated by the long range interactions between groups which are not directly involved in the reaction. Particularly the *anti*-conformation of the tricyclic system in the transition states is preferred and leads to the observed stereochemistry of the products.

Furthermore, we analysed which methods can be used in further studies of similar systems. The examined density functionals perform well for binding energies and stereoselectivities when augmented with dispersion corrections. Prediction of regioselectivity is a more demanding task and correlated wave-function based methods like LPNO-CEPA/1 are recommended. For larger systems, systematic studies at this level will be too time consuming. In such cases, DFT results should at least be validated by MP2 calculations.

The computational setup was used in *in silico* screening of novel ligands that contain substituted pyrazole rings as side-chain. We found a system, in absence of side-reactions, should outperform other ligands for 1,4-additions of diethylzinc to cinnamaldehyde. This striking result is left for experimental verification.

3.2 CHARACTERISATION OF UNUSUAL BONDS IN SOME GERMANIUM AND TIN CLUSTERS

3.2.1 INTRODUCTION

The zinc-based systems discussed in the previous chapter have closed shell character. In the transition states of the investigated reactions one bond was elongated (Zn-C) while at the same time a second bond was formed (C-C). Such situations can be properly described with single reference methods. However, there is a number of examples in chemistry where one or more bonds are enormously elongated with no compensation of other bond lengths. The particular examples here are metalloid cluster compounds of the general formula M_nR_m ($m > n$, M – metal or semi-metal, R – ligand) that are ideal model systems for studies of element formation from oxidized species on atomic scale.^{178,179} They can be synthesized by various methods.¹⁸⁰ One of the most promising is a synthetic strategy proposed by Schnepf and co-workers for the preparation of germanium¹⁸¹ and tin¹⁸² clusters via a disproportionation reaction of metastable subvalent halides. In this method, metalloid clusters are intermediate products and are stabilised by exchange of the halide anions with bulky electron-donating ligands.

These systems often possess atoms with low coordination numbers and show an increased reactivity as well as unusual electronic properties. A rhombic motif (Figure 3.2.1a) with a general formula of M_4R_6 has been recently found in two systems (see Figure 3.2.1b,c): $Ge_{14}[Si(SiMe_3)_3]_5Li_3(THF)_6$ **12**¹⁸³ and $Sn_4Si[Si(SiMe_3)_3]_4(SiMe_3)_2$ **13**.¹⁸⁴ In both cases the two opposite atoms of the ring system are only threefold coordinated. For these two atoms, a X-ray structure analysis shows a distance which is significantly longer than a single bond, but short enough to suggest that an interaction exists. Its nature is supposed to be similar to the one observed for bridgehead atoms of [1.1.1]propellanes. The CASSCF studies of Breher et al.¹⁸⁵ on a newly synthesized Ge_5Mes_6 (Mes – mesityl) as well as on its silicon and tin analogues revealed a biradicaloid character of the M...M interaction, i.e. the bonding orbital between the two atoms has an occupation number significantly lower than 2 (1.9) while an occupation of 0.1 was observed for the corresponding antibonding orbital.

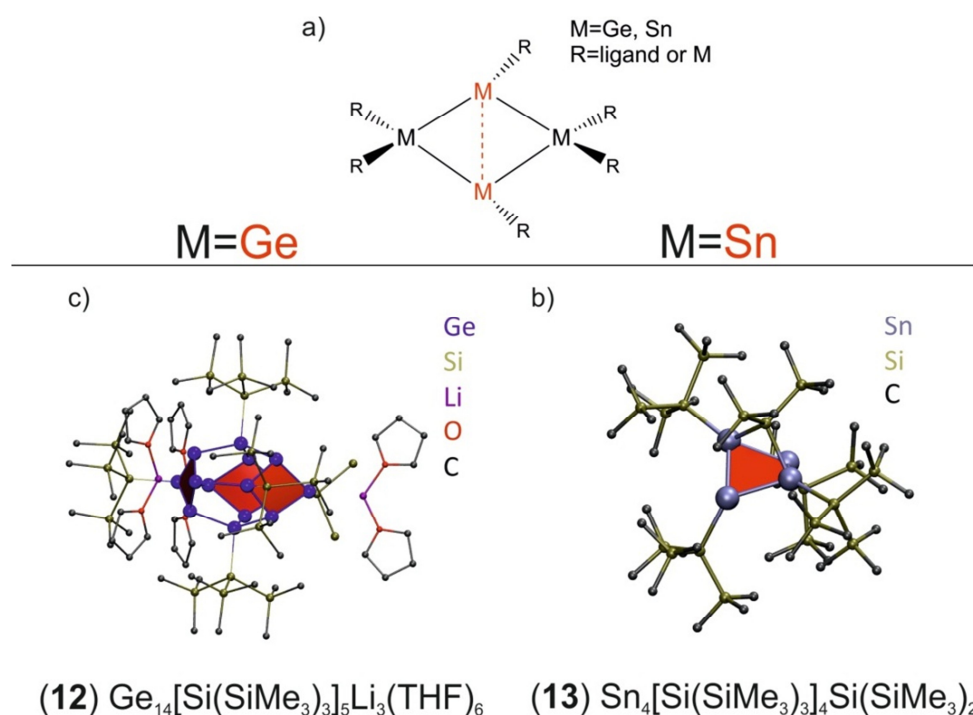


Figure 3.2.1 (a) Schematic representation of the M_4R_6 motif found in the two studied molecules: (b) $\text{Ge}_{14}[\text{Si}(\text{SiMe}_3)_3]_5\text{Li}_3(\text{THF})_6$ **12** and (c) $\text{Sn}_4\text{Si}[\text{Si}(\text{SiMe}_3)_3]_4(\text{SiMe}_3)_2$ **13**. The rhombic motifs were highlighted with red color. Hydrogen atoms are omitted for clarity.

In structure **2** only one Sn_4 entity can be found while compound **12** possesses three Ge_4 rings. The experimental distances between the undercoordinated atoms are 2.84 Å and 3.82 Å for **12** and **13**, respectively. The sums of the covalent radii are 2.42 Å for two germanium atoms and 2.80 Å for two tins.¹⁸⁶ Thus, the elongations of the bonds are similar to those observed in germanium¹⁸⁵ and tin¹⁸⁷ [1.1.1]propellanes. Despite of these similarities, the arrangement of metalloid atoms in the M_4R_6 entity of **12** and **13** is different from the one which was observed in a M_5R_5 subunit of propellanes. The ligands that are used for stabilization will probably have much larger influence on the electronic structure of the Sn_4 entity in **13** where each bridgehead atom forms two homoatomic bonds as well as a bond to a ligand molecule. Moreover, the highly strained Ge_4 rings in **12** are unique from the chemical point of view. This motivated us to study the unusual electronic structure of **12** and **13** in greater detail.

The fundamental question is whether the $\text{M}\dots\text{M}$ interaction has the expected biradicaloid character. Experimentally, they are both EPR silent which indicates a singlet ground state. However, both compounds show some reactivity patterns that are characteristic for radical compounds. The X-ray data further suggests a bond elongation in $\text{M}\dots\text{M}$ interaction. Moreover, **12** can be an unusual example of a multiradicaloid compound because of the three basic subunits along with six ‘naked’ atoms present in the molecule. Additionally, the strength of the biradicaloid interaction is still unknown. It would be very valuable to learn how to control the degree of the radical character of a molecule by changing its substituents and consequently the geometrical parameters, i.e. the strength of the $\text{M}\dots\text{M}$ interaction. However,

molecules **12** and **13** have prohibitively large sizes for high-level computations and most calculations have to be performed for simplified models. The challenge of this approach is that one has to find the smallest system that already reflects all important features of a parent molecule. This model can then be used in a ‘bottom-up’ strategy for the design of new chemical compounds with unusual properties and reactivity.

3.2.2 COMPUTATIONAL DETAILS

All geometry optimisations were performed at DFT level employing the BP86 functional. Depending on the system size either the def2-SV(P) or the def2-TZVP basis set was applied. The corresponding def2-ecp effective core potential¹⁸⁸ was used for tin atoms. Energy minima were confirmed by vibrational frequency calculations and possessed only positive modes. The starting orbitals for the CASSCF calculations were obtained from natural orbitals of a ground state MP2 computations and the selection of the active space was based on the occupation numbers of the MP2 natural orbitals. The basis set for the MP2 computations depended on the system size (*vide supra*), while in all CASSCF calculations the def2-TZVP basis set was used.

3.2.3 GERMANIUM CLUSTER

The structure of the germanium cluster **12** was first optimised at the BP86/def2-SV(P) level. The obtained geometry was in good agreement with X-ray data so there was no need for further refinement. In these DFT calculations, a close shell singlet ground state was observed. As has already been discussed, the molecule has to be simplified for the CASSCF treatment. For further calculations, the THF molecules in **12** were substituted by water molecules while the bulky Si(SiMe₃) groups were represented by SiH₃. In the resulting Ge₁₄(SiH₃)₅Li₃(H₂O)₆ cluster **12a** (see Figure 3.2.2) only the position of the hydrogen atoms was reoptimised, whereas the geometry of the Ge₁₄ kernel was conserved.

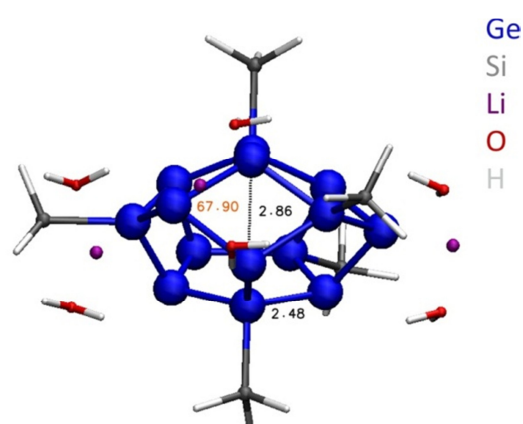


Figure 3.2.2 Optimised molecular structure of the model compound Ge₁₄(SiH₃)₅Li₃(H₂O)₆ **12a**. The length of a representative Ge-Ge single bond as well as an interatomic distance between the undercoordinated bridgehead atoms are highlighted in black (Å). The Ge-Ge-Ge acute angle within the rhombic motif is given in orange (°).

Structure **12a** was submitted to a MP2/def2-SV(P) calculation and the resulting four natural orbitals with occupation numbers 1.8 – 1.9 as well as seven natural orbitals with occupation numbers of 0.05 and 0.1 electrons were considered in the active space of the state specific (singlet) CASSCF(8,11) calculations. However, after a few optimization steps, it became obvious that an active space of six orbitals is sufficiently accurate. The other orbitals were either doubly occupied or empty. Thus, the final CASSCF calculations were performed in a (6,6) active space.

Figure 3.2.3 shows the six orbitals ($2a_1, 2e$),ⁱ together with their orbital energies ε and occupation numbers n . These orbitals are linear combinations of those six sp^3 hybrid orbitals of the six undercoordinated germanium atoms, which are not involved in the three classical single bonds. The three strongly occupied orbitals are the symmetry adapted linear combinations of the bonding orbitals, while the three weakly occupied orbitals are the corresponding antibonding orbitals. The occupation of the three bonding orbitals is significantly smaller than 2, while the antibonding orbitals show an increase in occupation number. This observation clearly indicates a weakening of the bonds between bridgehead germanium atoms, in accord with a radicaloid character. As suggested earlier by the geometric structure, the bonding is indeed comparable to the weak bonding between the ‘naked’ atoms in the M_5R_5 propellanes.¹⁸⁵ Next, we calculated the relative energy of the three lowest triplet states for **12a** using a state average CASSCF, employing the six partly filled orbitals obtained from the singlet state in the active space. The lowest triplet state is found to be doubly degenerate and 2.11 eV higher in energy than the singlet ground state. The next triplet state is 88.9 meV higher in energy, indicating that a coupling of the three Ge-Ge bonds with biradicaloid character is present in **12**. Thus, from an orbital point of view, **12** can be described as a singlet hexaradicaloid compound, which is an extension of the biradicaloid character onto a larger cluster compound.

ⁱThe structure has virtually C_3 symmetry but the calculations were performed without symmetry constrains. However, the orbital labels are adopted from the C_3 point group.

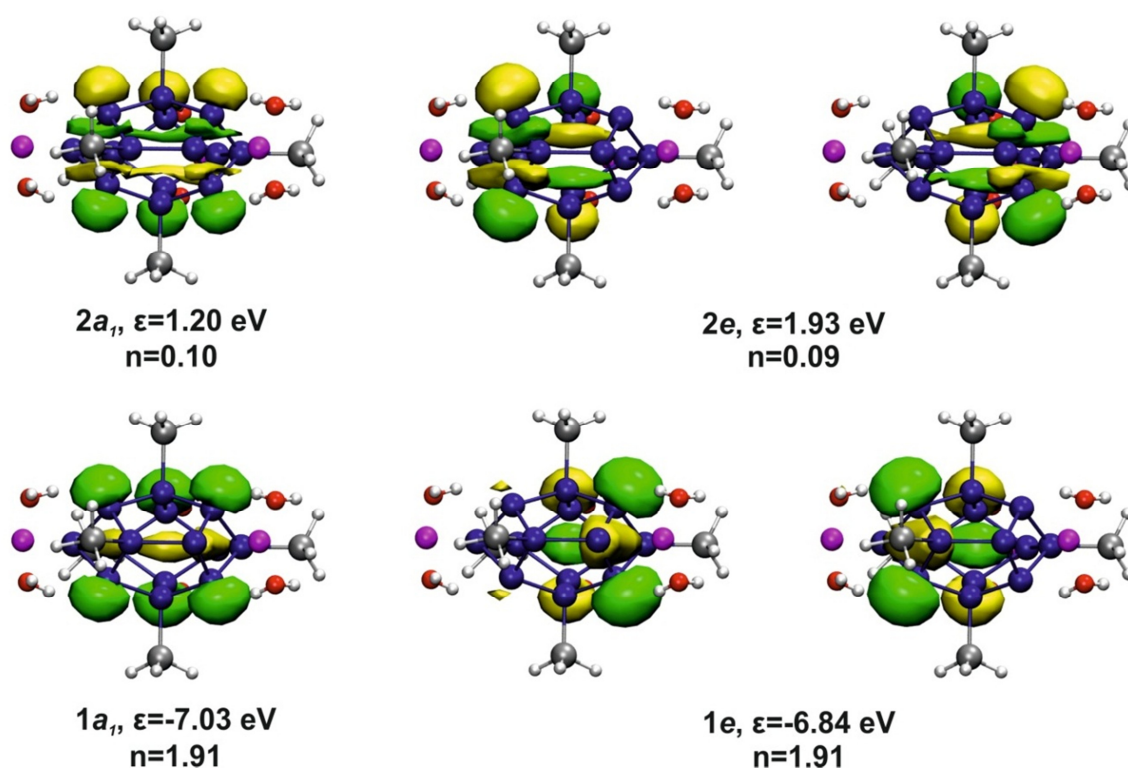


Figure 3.2.3 Active orbitals of the CASSCF calculations for the singlet ground state of **12a**, with occupation numbers, n , and energies, ϵ , of the respective orbitals. The numbering of orbital numbers $1a_1$, $1e$, $2a_1$, and $2e$ takes only the orbitals of the active space into account.

Beside the biradicaloid character of the bridgehead Ge...Ge interaction the question about the bond strength of this bond still remains. To get a deeper insight we constructed two model systems to obtain an estimate for the interaction between two undercoordinated Ge atoms in Ge_4R_6 entities.

The first model system is Ge_2H_6 with a tetrahedral surrounding at the Ge atoms and a typical Ge-Ge single bond. Figure 3.2.4 shows the potential energy curves obtained in a state average CASSCF calculation for the lowest singlet and triplet states as a function of the Ge-Ge distance. The minimum of the curve is located at a typical Ge single bond distance of 2.5 Å with a binding energy of 2.41 eV. For the Ge-Ge distance of 2.84 Å as in the Ge...Ge interatomic distance in **12a**, the binding energy is reduced to about 2 eV and the singlet triplet splitting accounts to 4.2 eV, being much higher than the value of 2.1 eV, calculated for **12a**. Furthermore, the occupation numbers of the active orbitals for the ground state singlet are still two and zero for the bonding and antibonding orbital, respectively. This result shows that the elongation of the bond alone is not responsible for the radicaloid character of the Ge centres.

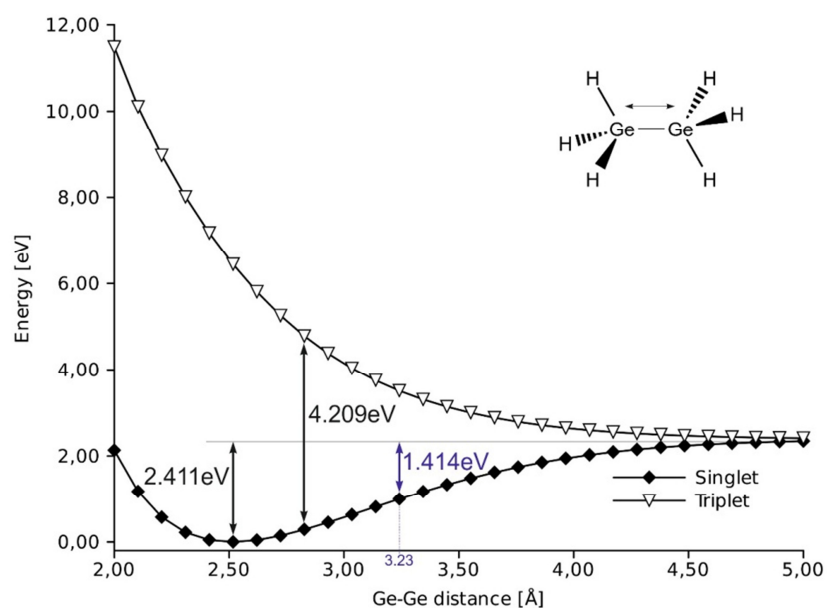


Figure 3.2.4 CASSCF calculations on the singlet (◆) and triplet (▽) potential curves of a Ge-Ge single bond of Ge_2H_6 .

As the major difference between the Ge_4R_6 entity and the simple model system (Ge_2H_6) for the Ge...Ge interaction is the arrangement of the additional bonding partners, we set up a second model explicitly taking into account the Ge_4 ring structure (see Figure 3.2.5). The calculations for this model compound yield now a singlet-triplet energy difference of 1.7 eV at a Ge-Ge distance of 2.88 Å. At the minimum structure of Ge_4H_6 , the calculated occupation numbers are 1.87 for the bonding and 0.12 for the antibonding orbital, respectively. These values are in good agreement with those obtained for the Ge_{14} cluster **12a** (compare with Figure 3.2.3). For the Ge_2H_6 model, a similar singlet-triplet gap like at this minimum was not observed until a distance of 3.5 Å. Moreover, the single Ge-Ge bond strength at the distance of 3.23 Å is reduced by 60% (see the values in blue in Figure 3.2.4).

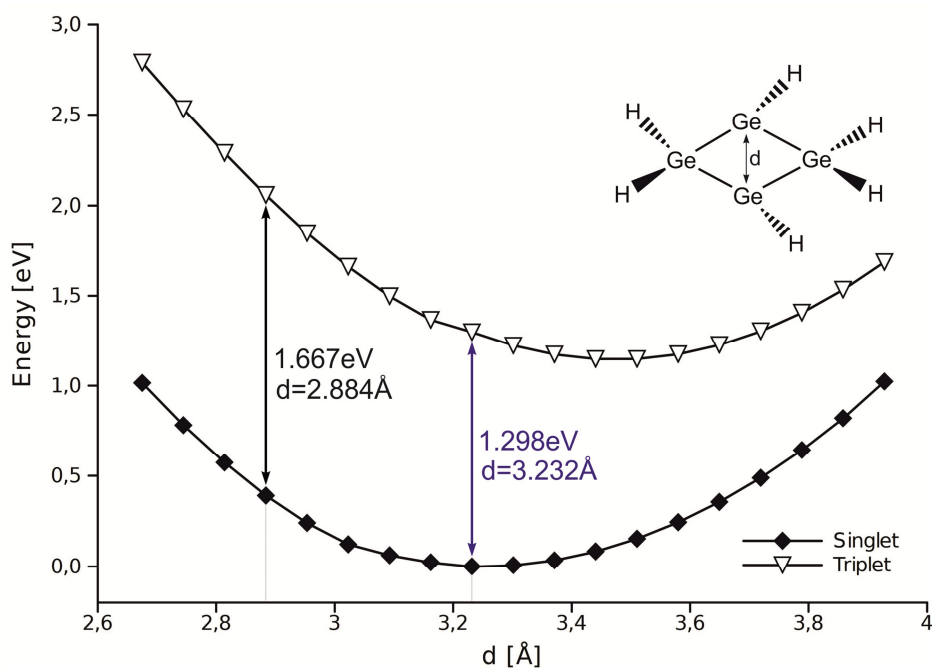


Figure 3.2.5 CASSCF calculations on the singlet (◆) and triplet (∇) potential curves of a Ge four-membered ring (Ge_4H_6) with the same local structure as in **12a**.

The weak bond in the ring system is caused by the orientation of the atomic orbitals which are available for the diagonal Ge-Ge bond (Ge connected by d in Figure 3.2.5) and are similar to those involved in the Ge...Ge interaction in **12**. Due to the arrangement of the other three bonds formed by the germanium centres, the remaining electrons at each Ge are located in orbitals which point to the outside of the ring and the interaction will be much weaker than for a classical Ge-Ge bond of the same length (2.86 Å). Such a dependency between bonding pattern and arrangement of the ligands is also seen in the first example of bond length isomerism in bicyclobutanes,¹⁸⁹ i.e. the other substituents have a vital influence on the bonding between two bridgehead germanium atoms. As we will shortly see, the tin cluster **13** is perfect base for the analysis of such an influence.

3.2.4 TIN CLUSTER

The butterfly arrangement of the tin atoms in $\text{Sn}_4\text{Si}[\text{Si}(\text{SiMe}_3)_3]_4(\text{SiMe}_3)_2$ **13** along with the long distance of 3.82 Å between threefold coordinated bridgehead Sn atoms strongly suggest a biradicaloid character of this molecule. We optimized the structure of **13** at BP86/def2-SV(P) level and obtained the MP2/def2-SV(P) natural orbitals. The (2,2) active space that was used in all CASSCF calculations consisted of those two valence orbitals of the threefold coordinated Sn atoms that did not take part in the two-center two-electron (2c2e) bonds (natural orbitals occupations of 1.8 and 0.2). Finally, the two orbitals in the active space had occupations of 1.7 and 0.3 electrons in the singlet state calculations. The same active space yielded a triplet state 0.67 eV above the singlet state. Thus, the strong biradicaloid character is present in this molecule. The radicaloid bond is elongated by about 35% in comparison to the

sum of vdW radii of the involved atoms while it was only 15% longer in the case of molecule **12**. This is certainly caused by the bulky ligands attached to the butterfly-like Sn₄ ring. We have already seen in the previous section (3.2.3) that the biradicaloid character is determined by both bond elongation and orientation of ligands. In order to further investigate the latter dependency we performed calculations on the model system (SiH₃)₄Sn₄SiH₂ **13a** (where every SiMe₃ group in **2** is substituted by a hydrogen atom).

In this model compound, the Sn-Sn-Si angle α (Figure 3.2.6) was systematically varied from 88° through 213°, while all other structural parameters were simultaneously optimized at the BP86/def2-TZVP level. Such an one-dimensional cut of the potential energy surface $E(\alpha)$ of model compound **13a** was obtained for singlet, triplet and broken symmetry (BS) states (Figure 3.2.7).

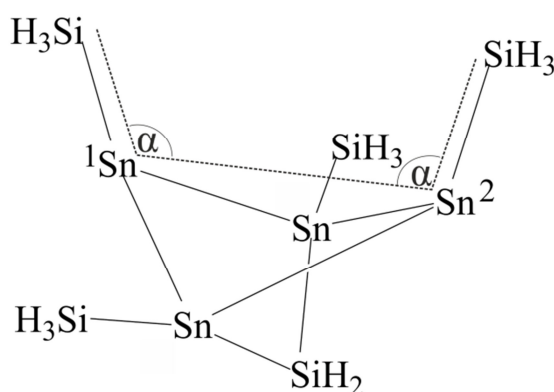


Figure 3.2.6 Model compound (SiH₃)₄Sn₄SiH₂ **13a** used in potential energy surface scans [$E(\alpha)$].

In the range between 88° and 185° the DFT singlet state is clearly the lowest in energy. The broken symmetry state converged here to closed shell singlet (HOMO natural orbital occupation number of 2). At α about 135° and 185° some discontinuities in the singlet/BS potential energy surfaces are present. Inspection of the distance between Sn¹ and Sn² (see Figure 3.2.6) clearly indicates that at this points sharp transitions between long (~4.0 Å) and short (~3.0 Å) distances occurs. For α values larger than 185° the singlet structure, even if lower in energy, was unnaturally distorted because of the long Sn¹-Sn² bond. The broken symmetry geometry does not show this behavior and follows the triplet surface. This is also clear from the BS HOMO natural orbital occupation number that is close to 1.3. In order to further investigate this sharp transitions we performed the state specific singlet and triplet CASSCF calculations on the BS structures. As for the large system **13**, the active space of two electrons on two orbitals (2,2) was chosen and the orbital selection was performed on the basis of MP2/def2-TZVP natural orbitals.

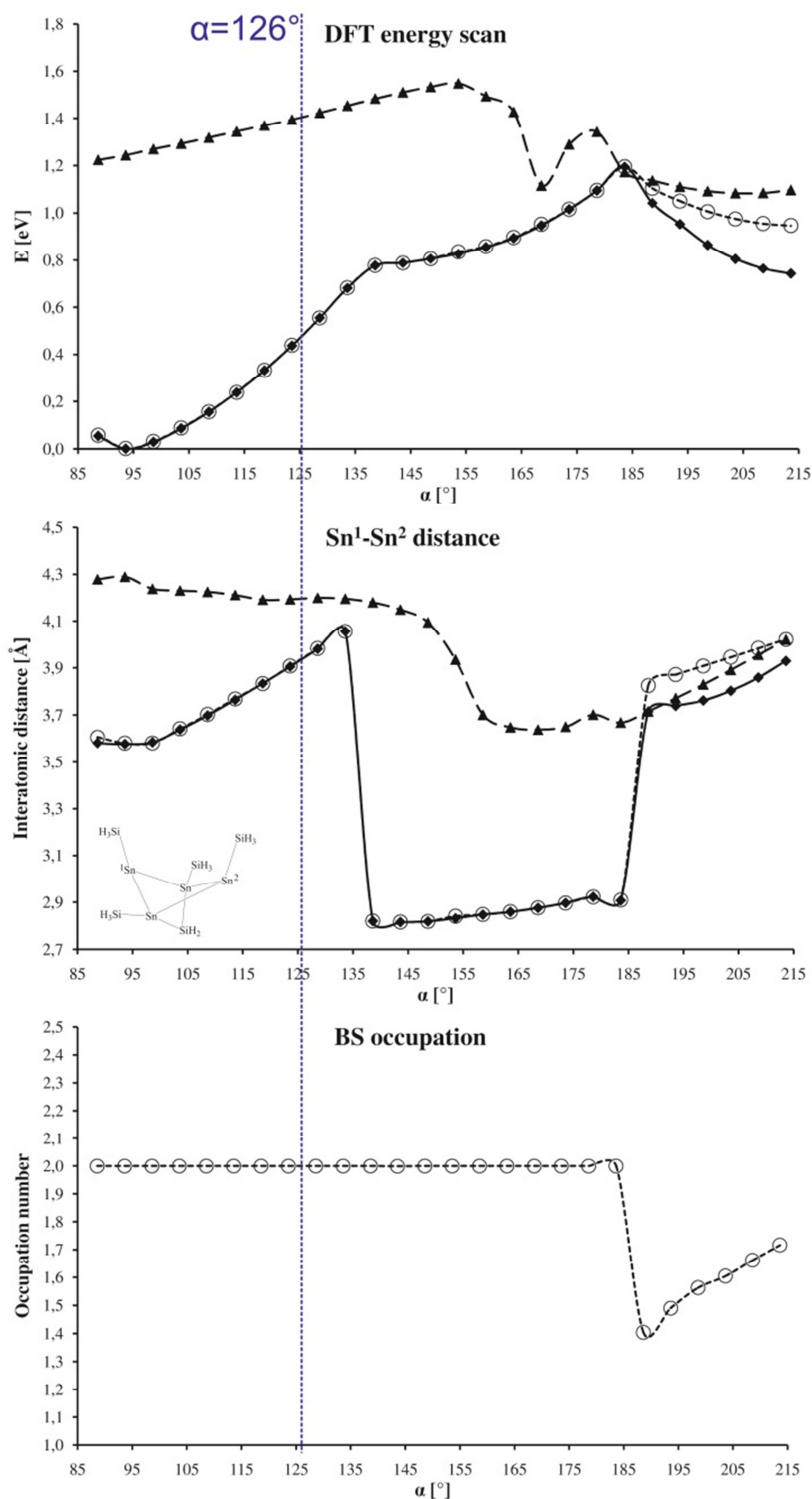


Figure 3.2.7 Behaviour of the energy, Sn...Sn distance and broken symmetry (BS) occupation for the model compound $\text{Sn}_4(\text{SiH}_3)_4\text{SiH}_2$ **2a** as a function of the Sn-Sn-Si angle α for singlet (◆), triplet (▲) and BS (○) states. The dotted blue line at $\alpha = 126^\circ$ indicates the experimental value for **13**.

The occupation numbers, n_1 and n_2 , and orbital energies, ε_1 and ε_2 , of the natural orbitals from the CASSCF(2,2) calculation for the singlet ground state provide information on the character

of the bond between the threefold coordinated Sn centers. Three different regions (I-III) are identified in Figure 3.2.8, divided by sharp, first order-like transitions around 135° and 185°. The experimental value for **13** (126°) is close to the transition between regions I and II.

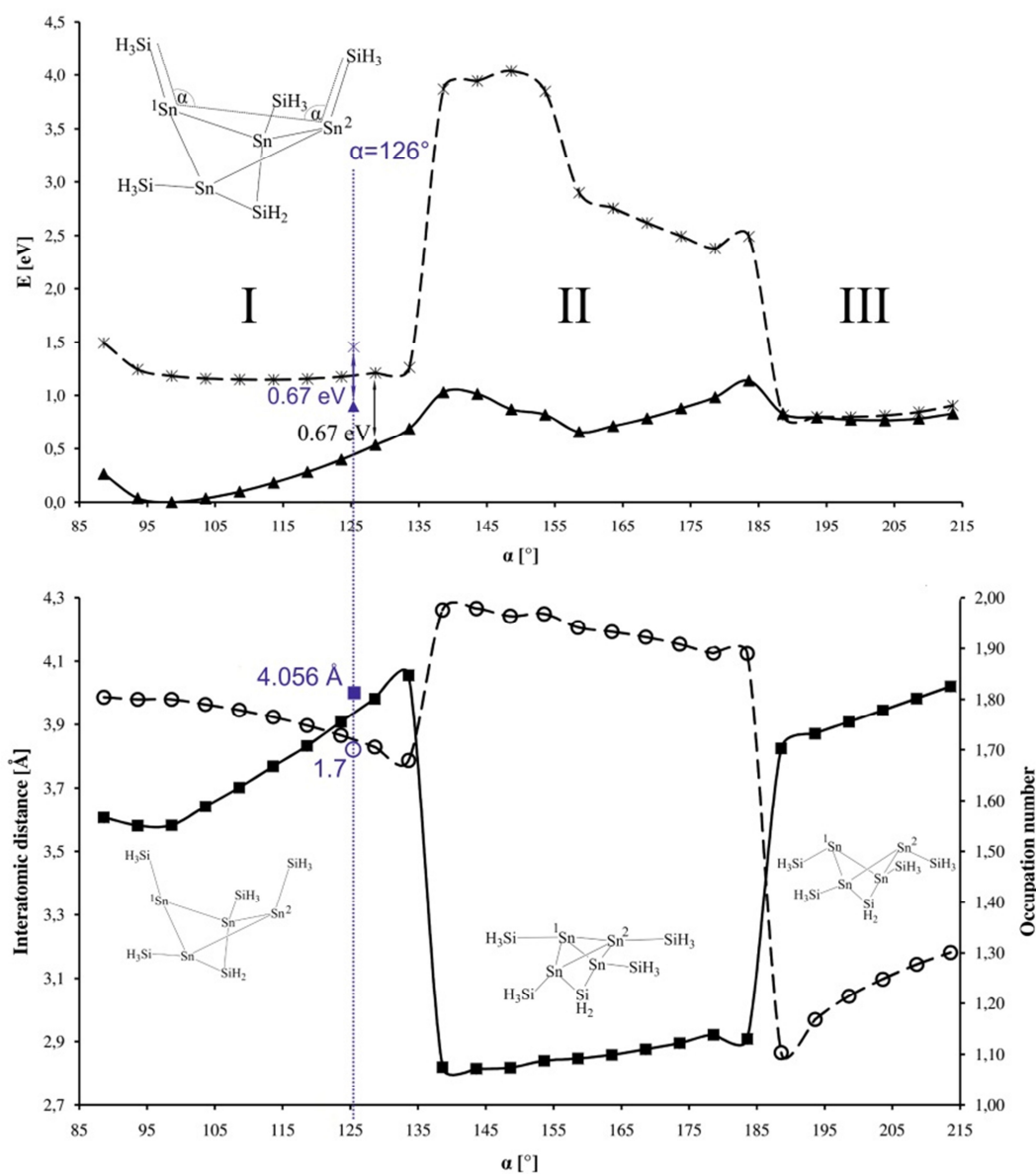


Figure 3.2.8 Top: Calculated energies of the model molecule $\text{Sn}_4(\text{SiH}_3)_4\text{SiH}_2$ **13a** in its singlet (\blacktriangle) and triplet ($*$) state as a function of the Sn-Sn-Si angle α . Bottom: Angular dependence of the tin-tin bond distance between Sn^1 and Sn^2 (\blacksquare) and the occupation number n_1 obtained from the CASSCF calculation of the singlet state (\circ) (the structure of **13a** in the different regions I, II and III is also shown). For comparison the values for **13** are given as a dotted line.

As already noted from DFT calculations, the geometrical parameters are very different in the three regions illustrated in Figure 3.2.8. Further details are provided by CASSCF calculations and these three regions can be described as follows:

(I): A typical singlet biradicaloid system is observed for angles smaller than 135° . That is, the occupation number of the bonding orbital n_1 is between 1.7 and 1.8, a value that is significantly reduced compared to the case of a $2c2e$ bond ($n_1=2$). Additionally, a singlet-triplet gap between 0.6 eV and 1.2 eV and a $\text{Sn}^1\text{-Sn}^2$ distance longer than 3.50 \AA are obtained from the calculations. The active orbitals are formed by sp^3 -like hybrids which point away from each other (Figure 3.2.9(i)). The bonding situation is thus comparable to other biradicaloid systems.^{183,185} Interestingly, the biradicaloid character increases with an increasing angle α , i.e. when the arrangement at the tin atom becomes increasingly planar. The active orbitals exhibit more and more p -character during this process.

(II): The arrangement at the tin atoms becomes pyramidal once again with an increase in the angle α . Consequently, the active orbitals regain sp^3 character and become facial (Figure 3.2.9 (ii)). The Sn-Sn distance is between 2.80 and 3.00 \AA – typical for a single bond – and the occupation number n_1 is equal to 2.0. Additionally, the singlet-triplet gap is larger than 2 eV, confirming the presence of a classical Sn-Sn single bond.

(III): For angles greater than 185° , the active orbitals are oriented parallel to each other (Figure 3.2.9 (iii)), leading to a weaker interaction. The Sn-Sn distance is increased to values larger than 3.70 \AA . The electronic structure is typical for a biradical, i.e. the singlet-triplet gap is close to zero (around 0.01-0.1 eV) and both active orbitals are nearly singly occupied.

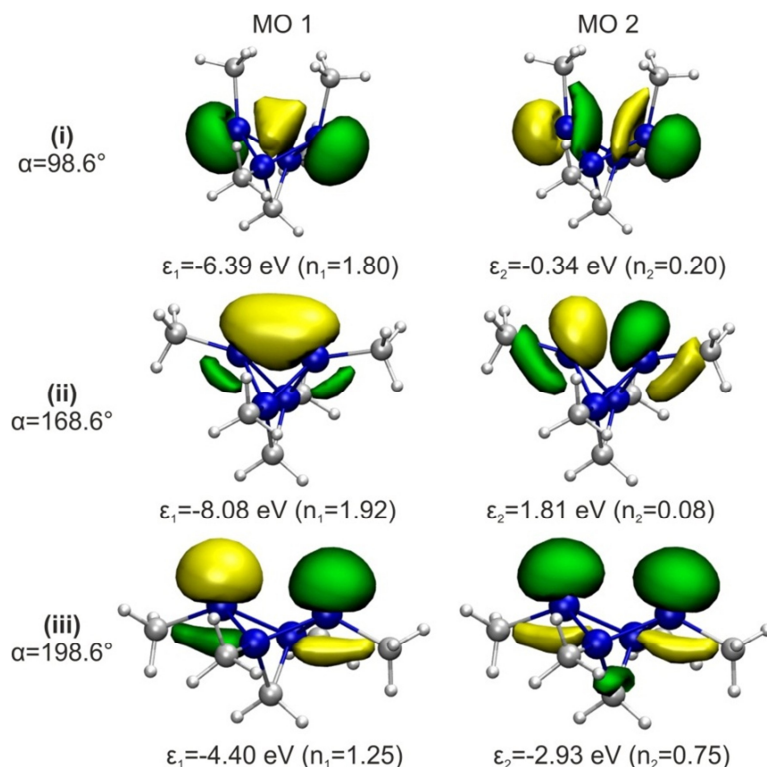


Figure 3.2.9 Natural orbitals of the CASSCF calculations for **13a** for three different angles α which are representative for the regions I, II, and III. ϵ_1 and ϵ_2 are the orbital energies and n_1 and n_2 the occupation numbers of the natural orbitals, respectively. Color code: tin – blue, silicon – grey, hydrogen – white.

These results clearly show that the orientation of the ligand directly affects the bonding between the two tin atoms with coordination number three. Similar results were recently obtained for a bicyclic [2.2.0] germanium compound.¹⁹⁰ These calculations, however, did not investigate the transitions between the regions depicted in Figure 3.2.8. Furthermore, the calculations presented herein show that the transitions between regions I (singlet biradicaloid), II (2c2e bond), and III (triplet) are quite abrupt. That is, small changes can lead to drastic changes in bonding and, thus, in chemical behavior. Because the Sn-Sn-Si angle α inside **13** (126°) is close to the critical angle of 135° between regions I and II, the polyhedral cluster **13** provides an ideal model system for further investigations on this general topic.

3.2.5 CONCLUSIONS

Both synthesised molecules, $\text{Ge}_{14}[\text{Si}(\text{SiMe}_3)_3]_5\text{Li}_3(\text{THF})_6$ **12** as well as $\text{Sn}_4\text{Si}[\text{Si}(\text{SiMe}_3)_3]_4(\text{SiMe}_3)_2$ **13**, are members of the growing family of radicaloid species. In the first one, three biradicaloid M_4R_6 entities are combined into one hexaradicaloid molecule possessing a singlet ground state. The tin cluster **13** was shown to be close to the first-order like transition between a singlet biradicaloid and a classical system with 2c2e bond. It was clearly shown that the Ge...Ge biradicaloid interaction has only 60% of energy of a single Ge-Ge bond strength. Furthermore, the bonding situation between undercoordinated atoms of a M_4R_6 ring system depends not only on the bond elongation but also on the orientation of the ligands. This unexpected result is of general interest, for example, in biocatalytic processes where enzymes are in a so-called entatic state.¹⁹¹ Whether the electronic ground state changes drastically with small changes in the ligand in biocatalytic systems still remains an open question.

The computed multiradicaloid character was in both cases confirmed by the reactivity similar to the true multiradical systems while the singlet ground state agrees with EPR data. The latter was also observed at the DFT level but the proper handling of the unusual bond elongation and resulting radicaloid character clearly requires multireference treatment. With this respect, CASSCF was shown to provide data in very good agreement with the experimental findings.

3.3 NICKEL DIMER AND TRIMER: NEUTRAL AND ANIONIC STATES

3.3.1 INTRODUCTION

In the gas phase experiments, negatively charged nickel clusters of different sizes can be formed and solvated by alcohol molecules. For these complexes, neither the structure nor the electronic states are known but in mass-selected IR spectra the O-H frequencies can be obtained. The relation between the vibration observed and the electronic structure can be established by accurate quantum chemical calculations. These experiments were recently successfully carried out for small anions of cobalt clusters.^{192,193} It was shown that the BLYP functional properly reproduced the bond lengths of both Co_2 and Co_2^- obtained with the CASPT2 method. Wang *et al.*¹⁹⁴ performed detailed Generalized Van Vleck Perturbation Theory (GVVPT2) calculations on the cobalt dimer and underlined the need of a consistent correlation treatment with *ab initio* methods in this case. In comparison to cobalt, the nickel atom contains one more electron in the $3d$ orbital. Thus, the correlation effects are expected to be even larger than in the case of cobalt atom. Not surprisingly, the near degeneracy of the 3D ground state of the nickel atom with the 3F state is a challenge for theoretical methods.¹⁹⁵ Therefore, it seems useful to test a set of DFT functionals against high-level multireference methods in calculations concerning small nickel-containing systems.

In the previous chapter we clearly saw the importance of multireference treatments in systems with elongated bonds. In case of transition metal dimers the latter problem is even more severe because of their open shell character. The d -orbital near-degeneracies have to be taken into account what usually makes the single determinant-based methods a very poor choice. However, for larger systems like the cobalt complexes discussed in the next chapter DFT is the method of choice because of the computational costs. Nevertheless, in most cases it is still possible to perform single point calculations with the CASSCF wave function. Unfortunately, for quantitative results the active space which would be needed in case of $3d$ transition metal complexes should involve all d (preferably $3d$ and $4d$ to take care on the $d-d'$ correlation effects), $4s$, and $4p$ orbitals of the metal centre as well as some orbitals of the ligands. Even such an extremely large active space still does not cover all correlation effects. Therefore, as CASSCF becomes quickly intractable, small active spaces based on chemical intuition are preferred. In order to account for the rest of correlation energy, perturbation theory or some types of CI are usually employed. The first was widely tested for relatively large molecules (especially at the CASPT2 level) while CI-based methods have been applied over the years to small systems with great success (see for example ref. 116). However, CASPT2 suffers from the intruder state problems while MRCI-type methods are very expensive and only approximately size consistent. The NEVPT2 version of the multireference perturbation theory is intruder state free and size consistent. It was shown that it provides excellent results in the case of transition metal compounds even in complicated cases, like the ground states of Cr_2 ¹⁰⁴ and Fe_2 ¹⁹⁶ as well as in calculations of zero-field splitting parameters in large manganese

complexes.¹⁹⁷ The calculations concerning the chromium dimer and Mn-containing systems were performed in the framework of strongly contracted NEVTP2 (SC-NEVPT2), while the iron dimer was treated at the more rigorous partially contracted level (PC-NEVPT2).

In this chapter we will apply the SC-NEVPT2 approach to the nickel dimer and confirm its applicability to molecules with extremely complicated electronic structures. Furthermore, it will be used in calculations of the ground state properties of Ni_2^- as well as in potential energy explorations for Ni_3 and Ni_3^- . The properties of these neutral and negatively charged clusters are still a subject of discussion and highly correlated calculations can provide additional data. Ni_2 was considered in numerous correlated calculations and the most recent bond length (2.23 Å) obtained from CASPT2 calculations¹⁹⁸ is still not fully consistent with the experimental values (2.20¹⁹⁹ or 2.16 Å²⁰⁰ depending on the experiment). On the contrary, the CASPT2 vibration frequency is in good agreement with experimental data^{201,202} (calculated 294 cm^{-1} vs. experimental 260-300 cm^{-1}). The ground state has been found to be 0_g^+ both experimentally and theoretically and originates from coupling between the nearly degenerate $^1\Sigma_g^+$ and $^3\Sigma_g^-$ states. Interestingly, this finding is consistent with the ground state predicted by ligand-field theory.²⁰³ In case of DFT, depending on the functional used actually any number can be produced, fitting either to experiment or to theory (see Table 3.3.2).²⁰⁴⁻²⁰⁸ The dimeric and trimeric anions of nickel can be generated in the experimental set-up in form of complexes with one or more ethanol molecules. By comparison of the measured stretching frequencies of the O-H bond of the alcohol with calculated values at various cluster geometries and spin states one can conclude on the most probable geometry of the experimentally observed compounds. Thus, we will benchmark a set of DFT functionals for the structure of the nickel dimer. Then, the selected method will be used for the computations of the ground state structures of both aforementioned anionic nickel clusters. In a next step, such negatively charged systems will be solvated with one or two ethanol molecules and the stretching vibrations of the O-H bonds will be evaluated at optimised geometries.

3.3.2 COMPUTATIONAL DETAILS

The active spaces for the CASSCF calculations were always carefully selected on the basis of high spin ROHF orbitals. The CASSCF-based computations concerning the Ni_2 molecule were performed in D_{2h} symmetry while in case of its negative ion and the trimers C_1 symmetry was employed. The potential energy surface scans of the dimers were carried out between 2.0 and 2.5 Å with a step size of 0.05 Å. The corresponding bond length and spectroscopic parameters were then obtained from numerical fit. In MRACPF calculations two consequent truncation schemes were applied. The determinants from the reference multideterminant wave function having coefficients lower than T_{pre} were neglected. The resulting functions consisting of the most important determinants were used only for the generation of excited single and double determinants. The interaction with the reference wave

function was approximated with a MP2-like procedure and weak perturbors (small value of the T_{sel} parameter) were not considered.ⁱ Various combinations were tested and $T_{pre} = T_{sel} = 10^{-8}$ was found to be good compromise between computational demand and accuracy. However, these computations were still rather expensive with about 2 million of determinants and over 3 million CFSs. Further details of all multireference calculations are given in text. The NEVPT2 geometry optimisations of the nickel trimers were performed with numerical gradients obtained with an increment of 0.005 Bohr. If not stated otherwise the def2-QZVPP basis set was used.

The DFT calculations were performed with a series of popular functionals without symmetry restrictions. The list includes GGAs (BP86, BLYP), the meta-GGA TPSS, the hybrid functional B3LYP and meta-hybrid TPSSh. The first three were already successfully applied to large metallic clusters^{8,192} whereas both hybrids have a different amounts of HF exchange (20% and 10%, respectively) and are expected to perform better with respect to spin energetics. Relativistic corrections were not included in this calculations. The integration grid was of size 4 while the SCF convergency criteria were tightened to 10^{-7} . The convergency of the gradients was set to 10^{-4} . The scaling factor for the O-H stretching frequency at TPSSh/def2-QZVPP level of 0.971 was obtained by fitting the theoretically obtained value for the ethanol molecule in vacuum (3802 cm^{-1}) to the experimental gas phase frequency²⁰⁹ (3690 cm^{-1} ; diluted ethanol vapours at low pressure).

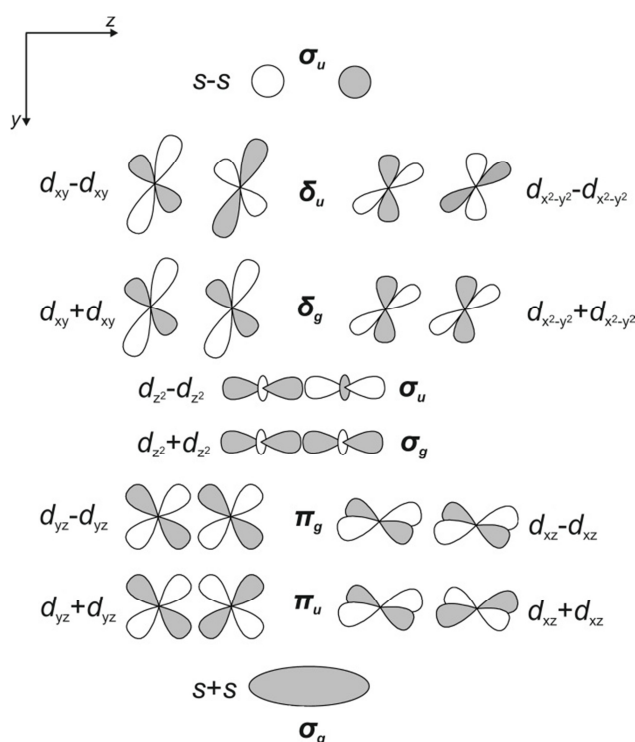
3.3.3 NEUTRAL AND ANIONIC STATES OF THE NICKEL DIMER

As already mentioned in the Introduction the nickel dimer has a complicated electronic structure and there is still an on-going debate about the bond length in this molecule. High-level *ab initio* calculations predict too long interatomic distance in comparison to experiment (0.03^{199} up to 0.07 \AA^{200} depending on the experimental set-up) but the calculated vibrational frequency was in range of the experimental error bars (as derived from both photoelectron spectroscopy²⁰¹ and Raman spectra²⁰²). In mass-selected IR spectroscopy, Ni_2^- can be potentially observed as a complex with a number of alcohol molecules. However, the experimental bond distance of this anion was derived from its neutral precursor and was reported to be $2.26 \pm 0.02\text{ \AA}$, i.e. 0.1 \AA longer than in Ni_2 . If we take the discrepancy between experiment and theory for the neutral specie into account, no clear reference is available. Thus, we chose to firstly perform a scan along the Ni-Ni bond in the neutral dimer for six $\delta\delta$ states that have been previously reported to be the lowest in energy and nearly degenerate.¹⁹⁸ The states included in the averaging were $^1\Sigma_g^+$, $^1\Sigma_u^-$, $^1\Gamma_g$, $^3\Sigma_u^+$, $^3\Sigma_g^-$, $^3\Gamma_u$. The active space in the CASSCF calculations consisted of four δd orbitals ($d_{xy}+d_{xy}$, $d_{xy}-d_{xy}$, $d_{x^2-y^2}+d_{x^2-y^2}$, $d_{x^2-y^2}-d_{x^2-y^2}$; see Scheme 3.3.1)ⁱⁱ and two $4s$ orbitals. This led to an active space of 8 electrons on 6

ⁱFor further details see: F. Neese, *J. Chem. Phys.* 2003, **119**, 9428.

ⁱⁱThe molecule was oriented along z axis.

orbitals (8,6). Such a set-up corresponds to that chosen in the CASSCF/CASPT2 calculations of Pou-Américo et al.¹⁹⁸ MRACPF calculations were performed on the top of the reference in order to take electron correlation into account. The $1s2s2p$ electrons were kept frozen while the eight $3s3p$ electrons of each Ni atom were included in the correlation treatment. Because of convergence issues with the (8,6) reference CASSCF active space, the reference list in MRACPF calculations was generated from a CAS(10,7) where an additional doubly occupied d_{z^2} orbital was included in the active space. For relativistic corrections the DKH Hamiltonian at second order (DKH2) was used.



Scheme 3.3.1 Diagram of the molecular orbitals of the nickel dimer. For each combination a symmetry label is given ($D_{\infty h}$). Both combinations of $4s$ orbitals along with four δ orbitals were chosen to enter the active space in the CASSCF calculations.

The NEVPT2 method was then compared with the rigorous reference as well as with previously reported *ab initio* data. The comparison of these numbers can be found in Table 3.3.1. All presented methods predict a longer bond distance for all states in contrast to the experimental value of 2.20 (assigned as $\Omega=4$)¹⁹⁹ or 2.16 (most probably $\Omega=0$).²⁰⁰ The vibrational frequency for all states at MRACPF+DKH level is between 283 cm^{-1} and 310 cm^{-1} (ω_e for $^1\Sigma_u^-$ and $^3\Gamma_u$, respectively). The corresponding bond lengths were found in a very narrow range of 2.21-2.23 Å. The NEVPT2(8,6)+DKH values are systematically 0.01 Å shorter than MRACPF data while the frequencies are overestimated by about 15 cm^{-1} . Moreover, the NEVPT2(10,7)+DKH calculations yielded essentially the same result confirming a proper choice of the CASSCF active space. The CASPT2(8,6) calculations

overshoot the bond lengths by 0.01 – 0.03 Å but perform better for frequencies. The internally contracted ACPF study of Bauschlicher²¹⁰ did not include relativistic corrections. Furthermore, the 3s and 3p electrons were kept frozen in contrary to our and the CASPT2 studies, and also relatively small basis set was employed. As a consequence, even with a very large active space [(20,12)] the results are not satisfactory. Moreover, it is important to include the 3s3p electrons in the correlation treatment. Exclusion of the relativistic corrections (at any level) rather systematically yields too long bonds (about 0.03 Å).

Both CASPT2 and ICACPF methods predict the $^1\Gamma_g$ state as the ground state. Our MRACPF calculations show $^3\Sigma_g^-$ as ground state and $^1\Gamma_g$ only 0.013 eV higher in energy. The other states are up to 0.077 eV higher in energy at this level of theory. The NEVPT2 calculations agree with the CASPT2 ground state but the next state is predicted to have $^3\Sigma_g^-$ symmetry instead of $^1\Sigma_g^+$, which is virtually degenerated with the ground state. However, ligand field theory²⁰³ as well as the most recent experiment²⁰⁰ predict the ground state to be described as $\Omega=0$, which can only arise by mixing $^1\Sigma_g^+$ with $^3\Sigma_g^- (0_g^+)$ or $^1\Sigma_u^-$ with $^3\Sigma_u^+ (0_u^-)$. It is rather obvious that the ordering of states in the ground state of the nickel dimer obtained at any level of theory will be strongly affected by spin-orbit interactions. Thus, at the molecular separation of 2.22 Å we performed NEVPT2(8,6)+DKH calculations with inclusion of spin-orbit interactions. Consistently with the CASPT2 results, the ground state was clearly 0_g^+ with 0_u^- lying 74 cm^{-1} above. The calculated coupling matrix element was equal to 1725 cm^{-1} , somewhat larger than the one calculated with CASPT2 (1206 cm^{-1}) and. In any case, the bond between the two nickel atoms in a neutral dimer has rather mainly 4s-4s character with very little *d-d* involvement.

Table 3.3.1 Comparison of the calculated equilibrium bond lengths (r_e) and the vibrational frequencies (ω_e) of the six lowest-lying electronic states of Ni₂ at different levels of theory. For each method the values for the lowest state of the given method are underlined. The basis sets used here include the def2-QZVPP [11s6p5d3f2g] basis for non-relativistic calculations and its partially decontracted version in DKH calculations [14s10p5d3f2g].

Method		This work					Literature	
		MRACPF	MRACPF +DKH	NEVPT2	NEPVT2 +DKH	NEVPT2 +DKH	ICACPF ^b	CASPT2 +RC ^c
Active space	State	(10,7)	(10,7)	(8,6)	(8,6)	(10,7)	(20,12)	(8,6)
Property ^a								
¹ Σ _g ⁺	r_e [Å]	2.25	2.22	2.25	2.21	2.21	--	2.23
	ω_e [cm ⁻¹]	267	285	277	303	305	--	294
¹ Σ _u ⁻	r_e [Å]	2.26	2.23	2.25	2.22	2.21	2.30	2.24
	ω_e [cm ⁻¹]	270	283	275	303	304	256	297
¹ Γ _g	r_e [Å]	2.25	2.22	<u>2.25</u>	<u>2.21</u>	<u>2.21</u>	<u>2.29</u>	<u>2.23</u>
	ω_e [cm ⁻¹]	267	286	<u>277</u>	<u>303</u>	<u>305</u>	<u>253</u>	<u>293</u>
³ Σ _u ⁺	r_e [Å]	2.26	2.23	2.25	2.22	2.21	2.30	2.24
	ω_e [cm ⁻¹]	270	290	275	303	304	255	297
³ Σ _g ⁻	r_e [Å]	<u>2.26</u>	<u>2.23</u>	2.25	2.22	2.21	2.29	2.23
	ω_e [cm ⁻¹]	<u>270</u>	<u>290</u>	275	303	303	253	294
³ Γ _u	r_e [Å]	2.24	2.21	2.25	2.21	2.21	2.30	2.24
	ω_e [cm ⁻¹]	269	310	277	303	305	256	297

^arecent experimental studies suggest $r_e = 2.16 \text{ \AA}^{200}$ and $\omega_e = 259 \text{ cm}^{-1}^{202}$

^bsee Ref. 210 for details. [8s4p3d2f] basis set.

^csee Ref. 198 for details. [6s5p4d3f2g] basis set; RC- relativistic corrections (mass velocity and one-electron Darwin terms)

The DFT calculations are not expected to reproduce exactly the multireference results (at least not for the right reason). However, a careful benchmark should allow the selection of one functional that closely follows the picture drawn from MR calculations. Thus, we decided to test a set of popular DFT functionals in order to establish a base for further much larger calculations on solvated nickel clusters. The main criterion here was the bond length. We restricted ourselves to investigate only singlet, triplet and broken symmetry singlet states.

The singlet state in all DFT calculations had ¹Σ_g⁺ symmetry. It was possible to converge to both δδ and σσ states. However, the converged result for the first state having a hole at the d_{xy}-d_{xy} orbital was only accounted within the restricted formalism. The second state with a hole at d_{z2}-d_{z2} orbital was obtained both with the restricted and unrestricted approach. The triplet state had ³Σ_u⁺ symmetry with the unpaired electrons residing on d_{z2}+d_{z2} and d_{z2}-d_{z2} orbitals, i.e. had σσ character. The δδ triplet could not be converged in the SCF procedure. Such problems are probably caused by multiple states lying extremely close in energy. The broken symmetry solution was obtained from the σσ triplet state. Recent DFT studies showed ππ or δδ states to be the lowest in energy depending on the functional used.²⁰⁴⁻²⁰⁸ However, these calculations utilized much smaller basis sets and were still not consistent with *ab initio*

data. We were able to converge them with rather high spin contamination with the def2-TZVP basis set but subsequent projection of orbitals into larger basis set let us to convergence problems. Thus, no further effort was made to obtain other electronic states. The reference non-relativistic NEVPT2 data for the states higher in energy than the $\delta\delta$ configurations were obtained with full valence CAS i.e. consisting of all d and both $4s$ orbitals. This NEVPT2(20,12) calculations were used in a potential surface scan of 25 singlets and 25 triplets. As expected, the results for $\delta\delta$ states were the same as those obtained previously with the smaller (8,6) active space. The $\sigma\sigma$ $^1\Sigma_g^+$ state was calculated to be 0.32 eV higher in energy than the $\delta\delta$ ground state of the same symmetry while the $\sigma\sigma$ state of $^3\Sigma_u^+$ symmetry was found to have 0.50 eV higher energy than $\delta\delta$ $^3\Sigma_u^+$ state. Both $\sigma\sigma$ configurations have longer bond distances than the ground state of the nickel dimer (2.29 Å and 2.40 Å for $^1\Sigma_g^+$ and $^3\Sigma_u^+$ states, respectively).

All tested DFT functionals underestimate the bond lengths of $\sigma\sigma$ states while too long bonds were obtained for the $\delta\delta$ $^1\Sigma_g^+$ electronic configuration (see Table 3.3.2). The $\sigma\sigma$ triplet was the lowest in energy for BP86, BLYP and TPSS functionals. In case of hybrid functionals, the broken symmetry (BS) solution was the lowest in energy and the $^3\Sigma_u^+$ state was lying about 0.03 eV above. Moreover, the BS bond length calculated with the TPSSh functional is the same as the ground state, non-relativistic NEVPT2 value for the nickel dimer. This result can be understood by the fact that d electrons of the nickel atoms are very weakly coupled which was also observed in the multireference calculations. Interestingly, the vibrational frequency obtained with the TPSSh functional (289 cm^{-1}) was very close to the reference value (277 cm^{-1} at the NEVPT2 level). Therefore, the TPSSh functional with the BS approach was consequently chosen for further studies of the anion of the nickel dimer as well as its complexes with the ethanol molecule. This is also the method of choice for DFT studies of neutral and anionic forms of the nickel trimer. Nevertheless, the convergence problems as well as the existence of the low energy broken symmetry solution clearly reflect the fact that the nickel dimer constitutes a limiting case for a single reference treatment at DFT level.

Table 3.3.2 Equilibrium bond distances (r_e) for selected states of Ni_2^- calculated with various functionals. For each method the values for the lowest state of the given method are underlined. Recently reported DFT data are marked in italic and are assumed to be the ground state for a given method. The vibrational frequency for the BS state calculated with the TPSSh functional is given in bold. The NEVPT2(20,12) reference data are listed for comparison.

State	r_e [Å]					
	BP86	BLYP	TPSS	B3LYP	TPSSh	NEVPT2
$^1\Sigma_g^+$ ($\sigma\sigma$) ^a	2.06	2.09	2.06	2.05	2.04	2.29
$^1\Sigma_g^+$ ($\delta\delta$) ^a	--	--	--	2.30 ^c	--	<u>2.25</u>
$^1\Sigma_g^+$ ($\delta\delta$) ^b	2.43	2.51	2.41	2.32	2.33	--
$^1\Sigma_g^+$ ($\pi\pi$) ^a	2.11 ^c	2.13 ^c	--	--	--	2.26
$^3\Sigma_u^+$ ($\sigma\sigma$) ^a	<u>2.30</u>	<u>2.33</u>	<u>2.31</u>	2.39	2.34	2.40
$^3\Sigma_u^+$ ($\delta\delta$) ^a	--	--	--	2.30 ^e	--	2.25
$^3\Sigma_g^-$ ($\pi\pi$) ^a	2.10 ^d	2.13 ^d	--	2.08 ^e	--	2.26
BS ^a	2.16	2.16	2.18	<u>2.30</u> (2.29) ^f	2.25 [289 cm⁻¹]	--

^aunrestricted formalism

^brestricted formalism

^cFrom Ref. 204.

^dFrom Ref. 206.

^eFrom Ref. 205.

^fValue in bracket is from Ref. 207 and corresponds to the BS state obtained from triplet $\pi\pi$ state.

The only experimental estimate for the bond length of Ni_2^- is given by Lineberger *et al.*²⁰¹ They concluded that this anion has a $\delta\delta$ configuration and on the base of previous experimental studies of the neutral compound the bond length of 2.26 Å was proposed (elongation of about 0.1 Å upon electron attachment). The corresponding vibrational frequency was estimated to be 210 ± 25 cm⁻¹. Such a weakening of the bond was assigned to the fact that the electron is attached to the σ^* orbital of the neutral molecule. Recent DFT results employing various GGA functionals showed the distance between the nickel atoms to be between 2.17 and 2.21 Å for the ground state quartet state of $^4\Sigma_u^-$ symmetry. Such a short bond together with a too large vibrational frequency of about 280 cm⁻¹ clearly indicates that higher level calculations have to be performed for more reliable estimations. Similar to Gutsev and Bauschlicher²⁰⁶ we assumed here the empirical “ ± 1 rule” so that the ground state multiplicity of an ion differs by ± 1 from the neutral counterpart. Thus, we performed CASSCF calculations followed by the NEVPT2 treatment with a (9,6) active space averaging over the $^2\Sigma_u^+$, $^2\Sigma_g^-$, $^2\Gamma_u$, $^4\Sigma_g^+$, $^4\Sigma_u^-$, $^4\Gamma_g$ states. The data can be found in Table 3.3.3.

Table 3.3.3 Comparison of the calculated equilibrium bond lengths (r_e) and vibrational frequencies (ω_e) for the six lowest-lying electronic states of Ni_2^- at CASSCF/NEVPT2 level with a (9,6) active space with (indicated with +DKH suffix) and without the DKH Hamiltonian. For both methods the values for the lowest state of the given method are underlined. The basis sets used here include def2-QZVPP [11s6p5d3f2g] for non-relativistic calculations and its partially decontracted version in DKH calculations [14s10p5d3f2g].

State	Property	NEVPT2	NEVPT2+DKH
$^2\Sigma_g^-$	r_e [Å]	2.32	2.30
	ω_e [cm $^{-1}$]	222	243
$^2\Sigma_u^+$	r_e [Å]	2.32	2.31
	ω_e [cm $^{-1}$]	225	244
$^2\Gamma_u$	r_e [Å]	2.32	2.30
	ω_e [cm $^{-1}$]	220	243
$^4\Sigma_g^+$	r_e [Å]	2.32	2.30
	ω_e [cm $^{-1}$]	220	242
$^4\Sigma_u^-$	r_e [Å]	<u>2.33</u>	<u>2.31</u>
	ω_e [cm $^{-1}$]	<u>222</u>	<u>241</u>
$^4\Gamma_g$	r_e [Å]	2.33	2.31
	ω_e [cm $^{-1}$]	222	241

Similarly to the neutral nickel dimer, the anion shows a high density of $\delta\delta$ states and all of them were found in a narrow energy window of 0.03 eV. The ground state in both relativistic and non-relativistic NEVPT2 calculations had $^4\Sigma_u^-$ symmetry. The next states were of $^4\Sigma_g^+$ and $^4\Gamma_g$ symmetry and were found with energies about 50 cm $^{-1}$ higher than the ground state to be nearly degenerate. Relativistic bond compression was less pronounced than in the neutral dimer and all calculations with the DKH Hamiltonian gave bond lengths 0.02 Å shorter than the non-relativistic ones with the corresponding vibrational frequency about 20 cm $^{-1}$ larger. The best relativistic estimate for the interatomic distance and vibrational frequency of the ground state of Ni_2^- is therefore 2.31 Å and 241 cm $^{-1}$, respectively. The calculated frequency is expected to be slightly too high because in case of the neutral dimer a systematic overestimation in comparison to MRACPF were observed. Thus, the bond elongation of 0.1 Å and the vibrational frequency compare well with the experimental findings of Lineberger *et al.*²⁰¹ For the sake of completeness we performed additional NEVPT2+DKH calculations involving spin-orbit coupling. The ground state was identified to be a $\Omega=5/2$ state as derived from the $^4\Gamma_g$ state. The next state having $\Omega=3/2$ was an equal mixture of the $^4\Sigma_u^-$ and the $^2\Sigma_u^+$ states. It was found 259 cm $^{-1}$ above the ground state.

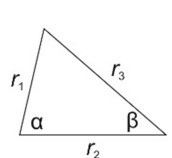
In the DFT calculations we assumed that the additional electron is located on the σ^* orbital as it was concluded from the multireference calculations. For the TPSSh BS state with such an

excess electron the calculated bond length was 2.34 Å what is in excellent agreement with the ground state, non-relativistic NEVPT2 calculations. It is therefore clear that the TPSSh functional is able to give quantitatively correct results for the nickel dimers and will probably also work fine for larger clusters.

3.3.4 NEUTRAL AND ANIONIC STATES OF THE NICKEL TRIMER

The neutral nickel trimer has most probably C_{2v} symmetry. The comparison of the structural parameters obtained in recent experimental and theoretical studies can be found in Table 3.3.4. The analysis of the Raman spectrum in solid argon together with calculation of the expected isotopic fine structure for various geometries led Moskovits and DiLella²¹¹ to the conclusion that the angle in the Ni_3 molecule is between 90° and 100° . The DFT-assisted IR experiments of Davlyatshin *et al*²¹² suggest an acute angle for this structure and a triplet ground state. Up to now, only DFT based calculations were reported for the nickel trimer. Recently, a near-equilateral triangular structure with bonds of 2.22 Å and 2.23 Å was obtained for the triplet ground state with the gradient-corrected PW86 functional.²¹³ Similar (near) equilateral structures were previously considered by many groups and the interested reader is referred to the comprehensive work of Papas and Schaefer.²¹⁴ Calvayrac²¹⁵ was the first to report a structure more consistent with the experimental Ni-Ni-Ni angle. The value calculated with the generalized LSD approach was 105° for the septet state but the bond lengths were rather unphysically too short (shorter than 2 Å). Subsequent calculations of Derosa and co-workers²¹⁶ performed with the hybrid B3PW91 functional gave a quintet state with a C_{2v} structure with an angle of 67.5° , two bonds of 2.35 Å, and one of 2.61 Å.

Table 3.3.4 Comparison of the recent experimental and theoretical structural parameters of the ground state of the Ni_3 molecule. At the bottom of the table the multiplicity of the state is given. The interatomic distances (r_1, r_2, r_3) and angles (α, β) are defined graphically.



	Exp.	PW86 ²¹³	BP86 ²¹⁴	LSD ²¹⁵	B3PW91 ²¹⁶	NEVPT2 ^c	TPSSh ^c
α	$\sim 60^\circ$ ^a	60°	60.0°	41°	68°	57°	57°
β	90° - 100° ^b $\sim 60^\circ$ ^a	59°		100°	56°	66°	66°
r_1	--	2.25 Å	2.23 Å	2.90 Å	2.61 Å	2.52 Å	2.43 Å
r_2	--	2.28 Å	2.23 Å	1.68 Å	2.35 Å	2.30 Å	2.23 Å
r_3	--	2.28 Å	2.23 Å	1.97 Å	2.35 Å	2.30 Å	2.23 Å
$2S+1$	3^a	3	3	7	5	5	5

^aB3LYP simulation of the IR transitions from Ref. 212.

^bBased on the expected isotopic fine structure of the Raman bands for various geometries. From Ref. 211.

^cThis work.

To the best of our knowledge, no experimental structure is known for Ni_3^- . With the gradient-corrected BPW91 functional Weber and Jena²¹⁷ obtained an equilateral triangular form (bond lengths of 2.25 Å) only 0.03 eV above the linear ground state with a shorter bond lengths of 2.20 Å. Furthermore, the complicated photoelectron spectrum of Ni_3^- was addressed to the co-

existence of two isomers with very similar energy.²¹⁸ Interestingly, simple VWN calculations on Ni_3^- yielded a isosceles triangular form while the PW86 functional showed a nearly-linear minimum with an angle of 165° .²¹³ In all calculations the ground state was predicted to have three unpaired electrons, i.e. to be a quartet state.

Table 3.3.5 Comparison of the recent theoretical sets of structural parameters of the ground state of the Ni_3 molecule. At the bottom of the table the multiplicity of the state is given. At the TPSSh level the linear and the triangular isomers were nearly degenerate and data for both structures are presented. The definitions of the interatomic distances (r_1 , r_2 , r_3) and the angles (α , β) can be found in Table 3.3.4.

	BPW91 ²¹⁷	VWN ²¹³	PW86 ²¹³	NEVPT2 ^a	TPSSh linear ^a	TPSSh triangle ^a
α	180°	60°	165.0°	180°	180°	57°
β	0°	59°	8°	0°	0°	66°
r_1	2.20 Å	2.15 Å	2.25 Å	2.34 Å	2.32 Å	2.32 Å
r_2	2.20 Å	2.17 Å	2.25 Å	2.34 Å	2.32 Å	2.28 Å
r_3	--	2.17 Å	--	--	--	2.28 Å
2S+1	4	4	4	6	6	6

^aThis work.

In order to investigate both, the neutral and the anionic states of the nickel trimer, at the NEVPT2 level one has to carefully select an appropriate active space. In our opinion the most systematic way is to start with a full valence CAS for Ni_3 , i.e. 30 electrons on 18 orbitals (all 3d and 4s orbitals in the active space). We decided to perform this rather demanding calculation with a smaller def2-TZVPP basis set which will also be applicable in potential energy surface scans as well as in geometry optimisations. We noted, that the bond lengths of all previously calculated states of Ni_2^- at NEVPT2 level with the def2-TZVPP basis set were only 0.01 – 0.02 Å longer than with the def2-QZVPP basis. The ordering of states is the same in both calculations. Thus, the triple- ζ basis set with an additional set of polarization functions seems to be a good compromise between cost and accuracy for the NEVPT2 calculations on Ni_3 and Ni_3^- . For the starting geometry both bond lengths were set to 2.25 Å and the angle between them was 100° . The CASSCF wave function was optimised simultaneously for one singlet, one triplet and one quintet spin state. The active space was systematically reduced by elimination of doubly occupied orbitals and the final active space for the Ni_3 calculations was of (6,6) size. The active space for the anion calculation was obtained from the neutral one by addition of one electron [CAS(7,6)]. The averaging procedure included in this case one doublet, one quartet and one sextet spin state. The NEVPT2 results are compared to the TPSSh values obtained with the structures optimised with this functional. Because DFT calculations are by far simpler than multireference computations, the def2-QZVPP basis set was employed here.

The orbitals that entered the active space are presented in Figure 3.3.1. Interestingly, the selection procedure yielded three orbitals being linear combinations of $3d$ orbitals (41, 43, 44) as well as three orbitals having s character (40, 42, 45). In potential energy surface scans (see Figure 3.3.2) the bond lengths r_1 and r_2 were varied between 2.2 Å and 2.5 Å and the Ni-Ni-Ni angle α changed from 60° (triangular form) to 180° (linear isomer). For all combinations of bond lengths the optimal angle was almost 60°. All calculated electronic states were very close in energy with a quintet ground state, a triplet lying about 0.05 eV above and a singlet about 0.14 eV higher in energy. For $\alpha > 100^\circ$ the potential energy surface is flat. The lowest energy was obtained for a structure with an isosceles triangle, with a bond lengths of 2.30 Å for the legs, and 2.50 Å for the base ($\alpha \approx 60^\circ$). This geometry was selected for a geometry optimisation of the quintet state with numerical gradients. The ground state structure was very close to the starting arrangement of the atoms. Thus, the NEVPT2 calculations confirm the experimental acute-angle C_{2v} structure and predict the linear isomer to be about 0.40 eV higher in energy. The structures optimised with the TPSSh functional essentially preserve all features obtained with the multireference calculations. This result is expected because the quintet is essentially a single reference case (95% of one configuration with unpaired electrons on orbitals 41-44) in contrast to the singlet and triplet states. With the TPSSh functional an isosceles triangular geometry was also found to be the most stable with two bonds of 2.23 Å and one 2.43 Å that are slightly shorter than those obtained at the NEVPT2 level.ⁱ The angle between the legs was 66°. The linear isomer had two equal bonds of 2.28 Å and was 0.41 eV higher in energy than the ground state. Therefore, the agreement between *ab initio* and DFT numbers is considered as satisfactory. The NBO analysis of both isomers shows that the molecule consists of nickel atoms of slightly different configurations. For the linear geometry two atoms were of $3d^{8.7}4s^{1.4}$ configuration and one of $3d^{8.6}4s^{1.2}$. The difference was more pronounced for the triangular structure where these atoms possessed $3d^{8.8}4s^{1.2}$ and $3d^{9.1}4s^{0.6}$ configurations, respectively. This reflects the differences in the degree of s - d hybridization in both structures.

ⁱThe bond lengths obtained at the NEVPT2 level with def2-QZVPP should be slightly shorter than those obtained with smaller def2-TZVPP basis set.

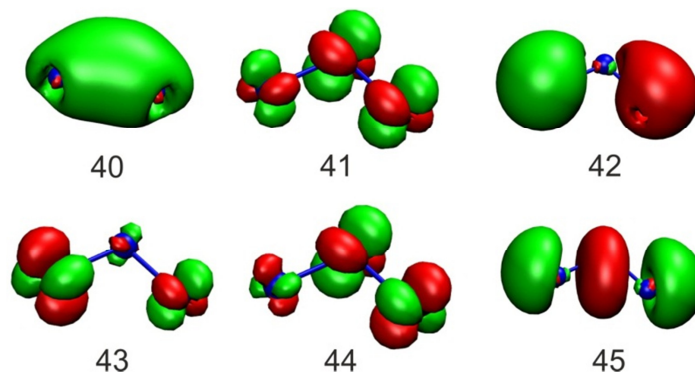


Figure 3.3.1 The six orbitals which formed the active space in the multireference calculations for Ni_3 and its anion.

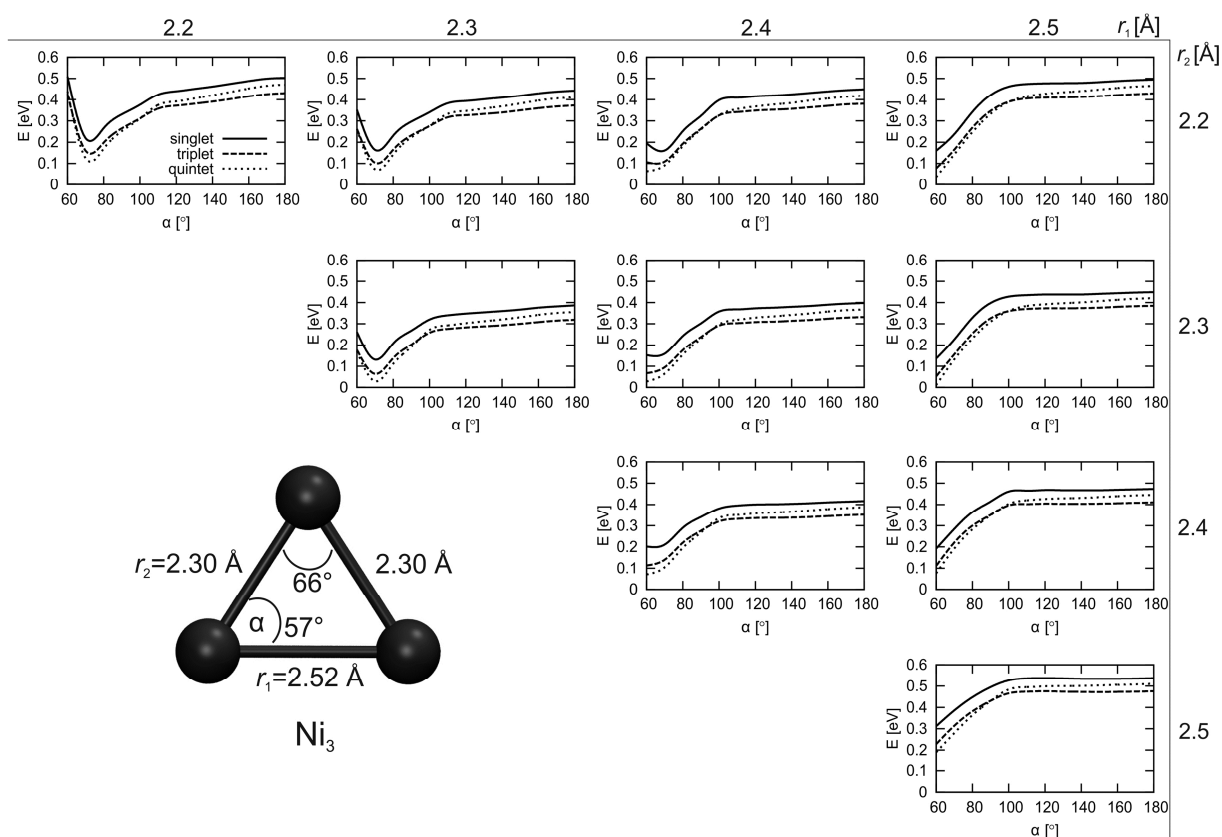


Figure 3.3.2 The ground state quintet geometry of Ni_3 as well as the dependency of the relative energy on the interatomic distances r_1 , r_2 and the angle α (defined graphically). The energy of the ground state was set to 0 eV. The calculations were performed at the CASSCF(6,6)/NEVPT2 level with the def2-TZVPP basis set. The interatomic distances were varied between 2.2 and 2.5 Å with a step size of 0.1 Å while α was changed from 60° up to 180° with 10° steps at each combination of r_1 and r_2 .

A similar analysis of the potential energy surface was performed in case of Ni_3^- and the obtained data is presented in Figure 3.3.3. At any nuclei configuration, the doublet state is virtually degenerate with the quartet state. Moreover, at any interatomic distances the linear structure is favoured. The optimised quartet geometry is linear with equal bond lengths of

2.34 Å. It is noteworthy that the sextet state that is derived from a quintet state of the neutral molecule is nearly degenerate with a doublet and quartet state at about triangular geometry while it rises in energy when the atoms align a linear structure. In the sextet state, the last orbital in the active space labelled as 45 is occupied in contrary to the neutral molecule. Its energy is smaller for α close to 60° because of the overlap between the two outer parts of the same phase (see Figure 3.3.1) as well as by higher hybridization with some d orbitals. The wave function of the quartet state consists to 97% of a configuration with three unpaired electrons residing on three linear combinations of $3d$ orbitals. Thus, the excess electron is attached to the orbital having mostly s character (42). This observation is consistent with the explanation of the similarities of photoelectron spectra between small nickel, copper and palladium anion clusters provided by Ganteför and Eberhardt.²¹⁹ They argued that the excess electron will prefer the more delocalized σ^* orbital over the strongly localized $3d$ because of the strong Coulombic repulsion with the other nine electrons occupying the $3d$ orbitals.

Treatment of the quartet state of the linear isomer at the DFT level (TPSSh) should be straightforward because of the almost single reference character of this state. However, it possesses significant multireference character when the geometry changes to the triangular form. Indeed, the calculations on the triangular isomer converged to a state with significant spin contamination (expected 3.75, found 4.64). At this geometry a single reference sextet state was found in the NEVPT2 calculations. Due to the fact that it was very close in energy with the singlet state, we decided to optimise the triangular isomer on the sextet potential energy surface. Interestingly, the linear and triangular arrangements of nickel atoms were found very close in energy at the TPSSh level. The sextet isosceles triangular structure (the legs of 2.28 Å and the base of 2.32 Å) was the ground state in this calculations. The linear quartet state was only 0.01 eV higher in energy. In this case, the bond lengths were only slightly shorter in comparison to NEVPT2 and were equal to 2.32 Å. Interestingly, at a linear geometry two nickel atoms of $3d^{8.9}4s^{1.5}$ and one of $3d^{9.0}4s^{1.0}$ natural configurations were found while in the triangular isomer all atoms had $3d^{8.9}4s^{1.4}$ configuration. Thus, in the linear anion the middle atom is best described as $3d^9 4s^1$. For the sake of comparison we optimised both isomers also with the GGA functional, BLYP, that was previously used in similar studies on cobalt clusters.¹⁹² The linear structure was found to be the lowest in energy (with bond lengths of 2.27 Å) while the equilateral triangular quintet (2.32 Å) was 0.13 eV higher in energy. Because the considered structures differ not only in the geometry but also in the spin state, the relative energies of both geometries are highly dependent on the functional. The meta-hybrid TPSSh favours a triangular structure with higher multiplicity but the linear isomer has nearly the same energy. In contrary, the gradient-corrected BLYP functional predicts the geometry with the lower multiplicity (linear quartet) to be more stable. However, the TPSSh optimised structures are closer to the results obtained with multireference methods. Therefore, TPSSh will be used in the optimisations of the solvated cluster anions. This also

allows us to be consistent with the dimer calculations where this meta-hybrid functional was clearly the best from the tested set.

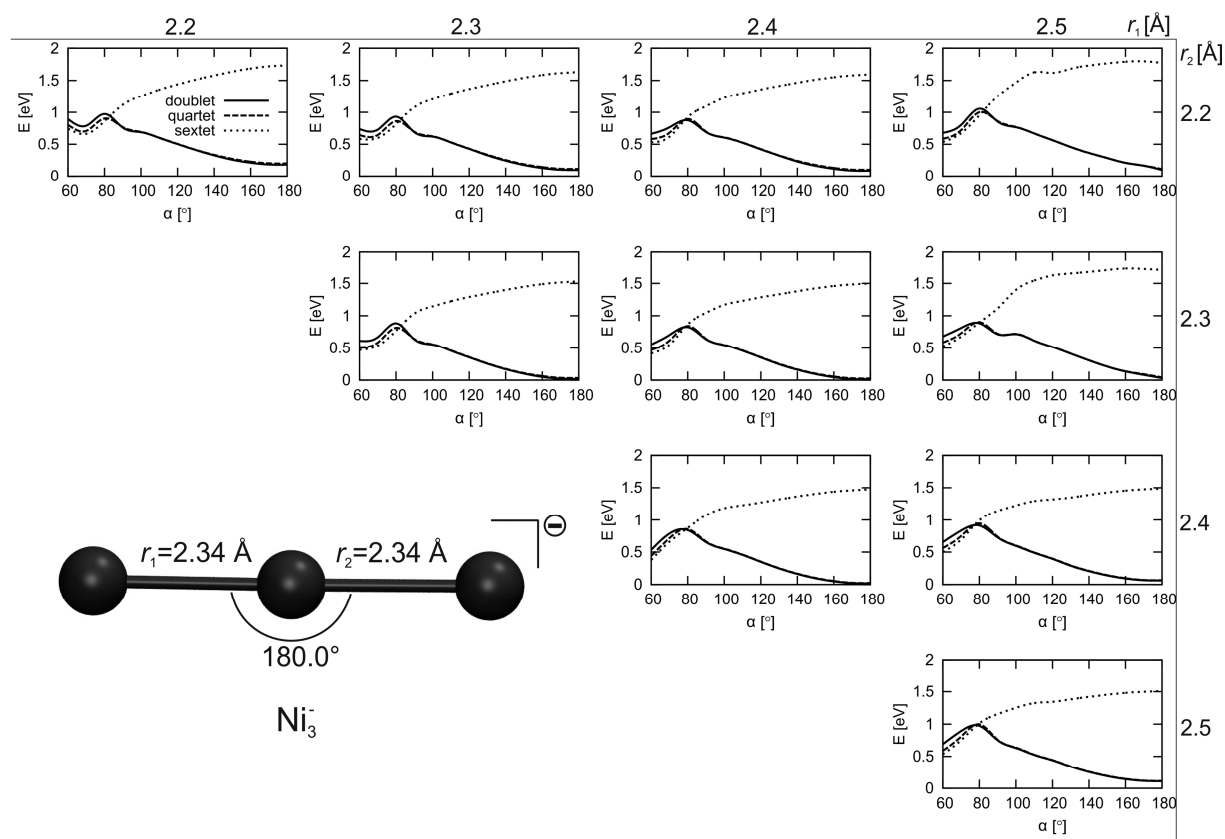


Figure 3.3.3 The geometry of the quartet state of Ni_3^- as well as the dependency of the energy on the interatomic distances r_1 , r_2 and the angle α (defined graphically). The calculations were performed at the CASSCF(7,6)/NEVPT2 level with the def2-TZVPP basis set. The interatomic distances were varied between 2.2 and 2.5 Å with a step size of 0.1 Å while α was changed from 60° up to 180° with 10° steps at each combination of r_1 and r_2 .

3.3.5 SOLVATED NICKEL CLUSTERS

In the following the structure of the Ni_2^- and Ni_3^- complexes with one or two alcohol molecules will be determined. Such small negatively charged nickel clusters solvated by ethanol molecules will be experimentally investigated by mass-selected IR spectroscopy and one of the aims of these calculations is to compare the calculated O-H stretching frequencies with the measured spectra. In case of the dimer complexes with one or two ethanol molecules (denoted as (2,1) and (2,2), respectively) we started from a neutral high spin complex ($S=1$) with Ni...Ni interatomic distance of 2.25 Å to assure convergence to the desired electronic state. A subsequent spin-flip procedure led to the BS state. The converged orbitals from the BS calculations were used as starting point for the anion geometry optimisation. An important question in the case of the nickel trimer anion was whether it has a linear or a triangular

structure. Because it is possible that the ground state geometry changes upon solvation, we decided to optimise both possible atom arrangements and the obtained structures were labelled as (3,1)L and (3,2)L for a linear complex with one and two alcohol molecules, respectively, as well as (3,1)T and (3,2)T in case of the triangular isomer. The linear form was assumed to have a quartet state while the triangular isomer was optimised on the sextet potential energy surface.

The structures of the solvated anionic nickel clusters along with the vibrational frequencies of the O-H stretching modes are presented in Figure 3.3.4. The dimer has essentially the same Ni-Ni bond length as the free anionic clusters (only 0.01 Å longer). The (scaled) stretching O-H frequency was calculated to be 3290 cm⁻¹ which is somewhat larger than the value of 3214 cm⁻¹ observed experimentally for the analogous cobalt cluster.¹⁹² In the case of cobalt the calculated O-H bond distance (BLYP/6-311+G(d)) was 1.00 Å with corresponding computational frequency of 3247 cm⁻¹. The Co...H distance was found to be equal for both cobalt atoms (2.59 Å) while in our case the ethanol molecule is shifted in the direction of one nickel atom. One of the Ni...H interatomic distances is therefore shorter (2.49 Å) and the second is much longer (2.99 Å). The structure was obtained in a series of optimisation-frequency calculation-distortion sequences because of a multiple saddle points problem (position of the alcohol molecule, rotation around the C-C bond). We note however, that the monitored stretching frequency was only slightly affected (± 3 cm⁻¹) by the position of the alcohol molecule, i.e. the O-H bond length was always the same. This suggests that the corresponding part of the potential energy surface is here very flat and the main factor which influences the red shift of the frequency is the coulombic attraction of the hydrogen atom of the alcohol group by the negatively charged nickel dimer. Adding another ethanol molecule does not alter the Ni-Ni distance. The frequencies for both alcohol molecules are blue-shifted in comparison to (2,1) (3299 cm⁻¹ and 3311 cm⁻¹).

Adding another nickel atom to (2,1) can lead to the structures (3,1)L or (3,1)T. The optimised structures had no imaginary frequencies so both were (local) minima on the potential energy surfaces. The frequencies were slightly red-shifted in comparison to the (2,1) system and were found to be 3281 cm⁻¹ and 3278 cm⁻¹, respectively. As expected, the triangular form was found to be the lowest in energy. The stabilisation was a bit more pronounced than for the isolated cluster and equal to 0.14 eV. However, this probably an artefact of the functional and GGA functionals will most probably yield an opposite trend. The final distinction between both isomers will be eventually possible by measuring complexes with two alcohol molecules as it was done in case of cobalt clusters. The difference in O-H frequencies of both solvated ethanol entities is 15 cm⁻¹ for (3,2)L whereas it increases up to 87 cm⁻¹ in case of (3,2)T. The variation is large enough to make a clear assignment. Moreover, in agreement with NEVPT2 calculations of the Ni₃⁻ PES, the bond distances of both isomers will be quite flexible. This can best be seen when going from structure (3,1)T to (3,2)T where variations of the bond

lengths of $\pm 0.01 \text{ \AA}$ inside the Ni triangle are observed just upon addition of one alcohol molecule.

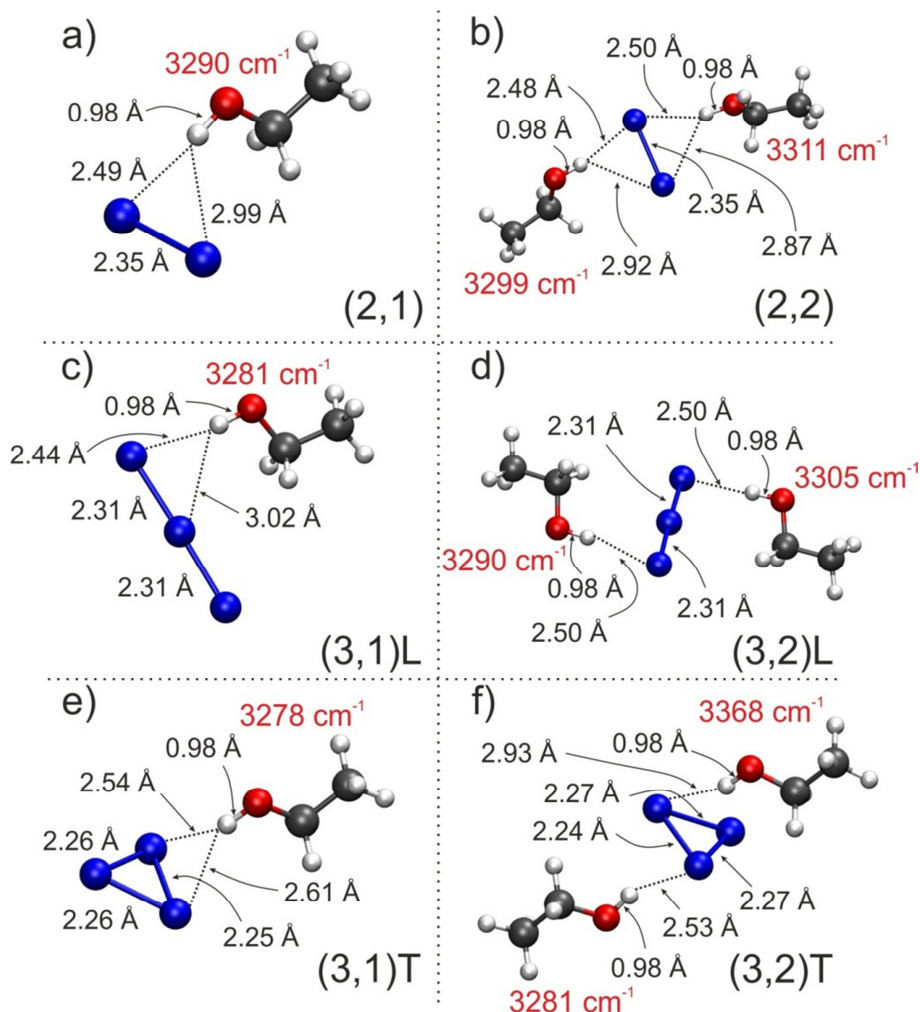


Figure 3.3.4 Negatively charged anion of the nickel dimer (a, b) and the nickel trimer (c-f) solvated with one (a, c, e) or two ethanol molecules (b, d, f). The most important interatomic distances are given in black. The calculated vibration frequencies of the O-H bonds are given in red next to each alcohol molecule. The structures were optimised at the TPSSh/def2-QZVPP level. For the frequencies a scaling factor of 0.971 was applied. The ethanol gas-phase frequency is 3690 cm^{-1} .²⁰⁹

3.3.6 CONCLUSIONS

We have evaluated the properties of small neutral and anionic nickel clusters at the NEVPT2 level. First, the method was validated with high-level MRACPF calculations on the Ni_2 molecule. The calculated bond lengths for various $\delta\delta$ states agreed within 0.01 \AA while frequencies were only about 10 cm^{-1} higher. The ground state of this molecule is predicted to be 0_g^+ which arises from mixing of $^1\Sigma_g^+$ and $^3\Sigma_g^-$ states. The ground state bond length is predicted to be $2.21 \pm 0.01 \text{ \AA}$ ($^1\Sigma_g^+$) which is in moderate agreement with the experimental estimate ($2.16 - 2.20 \text{ \AA}$). However, the calculated vibrational frequency of $303 \pm 10 \text{ cm}^{-1}$ is

within the error bars of the experimental measurements (260 – 300 cm^{-1}). Moreover, it was found that the TPSSh functional is able to reproduce the non-relativistic ground state bond length of 2.25 Å if a broken symmetry state obtained from the $^3\Sigma_u^+$ electronic state is applied. The gradient-corrected functionals predicted too short bonds probably because of an overestimation of the electron pairing effect which can be corrected by incorporation of exact HF exchange in the functional (10% in case of TPSSh). The negatively charged dimer has an excess electron attached to the σ^* orbital that weakens the bond between the two nickel atoms and leads to a substantial bond elongation of 0.1 Å. The ground state was identified to be a $\Omega=5/2$ state as derived from the $^4\Gamma_g$ state. The bond length and vibrational frequency were calculated to be 2.31 Å and 241 cm^{-1} , respectively.

The neutral nickel trimer has an isosceles triangular form. In this structure, the bond lengths are equal to 2.30 Å for the legs with an angle between them being 66° and a length of the base is 2.52 Å. Although, this molecule has a quintet ground state, states with multiplicity 1 and 3 were found to be very close in energy. The linear isomer was 0.4 eV higher in energy. The same was found at DFT level with the TPSSh functional and this striking result is addressed to the single reference character of this molecule at both geometries. The situation is far more complicated in the Ni_3^- molecule where the quartet ground state has a linear structure with the bond lengths equal to 2.34 Å at NEVPT2 level and is nearly a single reference case but the triangular form being higher in energy by about 0.5 eV has a multireference wave function. We found the sextet state of the triangular isomer to have almost a single determinant wave function. Thus, the DFT optimisation of the triangular form was carried out on the sextet potential energy surface. As expected, the TPSSh functional provided geometries close to the multireference structures but slightly overestimated the stability of the triangular high spin isomer. Thus, at this level both geometries were nearly equal in energy. The functionals without exact HF exchange such as BLYP were expected to give an opposite trend. Indeed, the linear form at the lower multiplicity was about 0.13 eV more stable than the triangular sextet isomer. However, the bond lengths differed much more from the NEVPT2 values than in case of the TPSSh functional. Thus, no clear preference is given to any of the tested functionals. We used TPSSh because of consistency with the dimer calculations.

Despite the fact that it is impossible to judge which of the isomers of Ni_3^- is the ground state at the DFT level, we decided to obtain the geometries of these complexes with one and two ethanol molecules at TPSSh level. At each geometry the frequency of the O-H stretching mode was evaluated and compared with available experimental data for the cobalt complexes. A similar red shift was observed for this vibration upon coordination to the cluster. Moreover, it was found that by measuring O-H stretching frequencies of the Ni_3^- solvated with two alcohol molecules one can distinguish between the linear and the triangular isomer. In the first case the difference between the two measured frequencies should be small (about 15 cm^{-1}) while in the latter it should be much larger (about 90 cm^{-1}).

3.4 MOLECULAR OXYGEN ACTIVATION BY β -DIKETONATE COBALT COMPLEXES

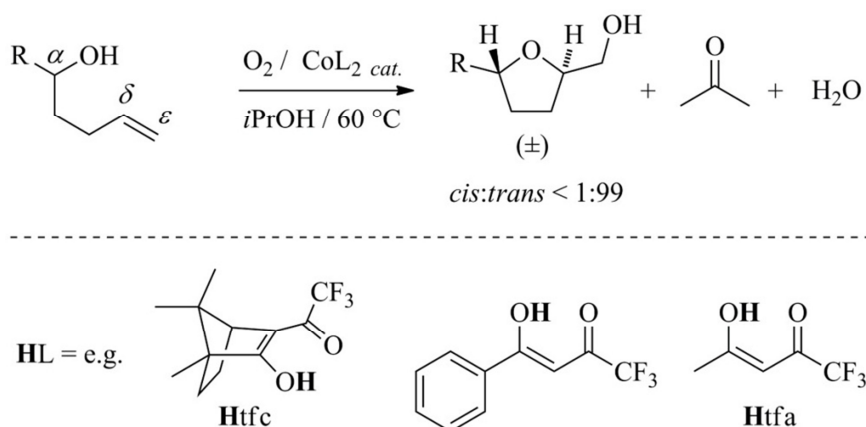
3.4.1 INTRODUCTION

Molecular oxygen is available in seemingly unlimited quantities from the Earth's atmosphere, which makes it an attractive oxidant for sustainable hydrocarbon oxyfunctionalization.^{220,221} Oxidative hydrocarbon transformation using molecular oxygen as terminal oxidant (aerobic oxidation) is strongly exothermic but proceeds at ambient temperature comparatively slow.²²² The inertness of the oxygen molecule with respect to many substrates arises from its triplet electronic ground state, leading to notable activation barriers in reactions with singlet molecules.²²³

A common strategy to lower activation barriers in aerobic oxidations of singlet molecules is to change the electronic state of the dioxygen molecule, for example, via photosensitisation into a singlet state, or via addition to a paramagnetic compound into a doublet state.²²⁴ Short lifetimes in solution and the significant energy input needed for changing the electronic state so far precluded a wider spread application of singlet dioxygen for synthetic scale oxidative transformations. The standard procedure to activate dioxygen in synthesis is binding to a paramagnetic transition metal compound, such as an iron(II) porphyrin complex, for example, in cytochrome P450, or a cobalt(II) chelate.²²⁵

The unique affinity of molecular oxygen toward cobalt(II) compounds was discovered by Werner and Mylius in 1898.²²⁶ Thermochemistry, kinetics, and the mechanism of the dioxygen binding to cobalt(II) Schiff base complexes, and the chemical nature of adducts formed from the reaction were studied experimentally²²⁷⁻²³⁰ and theoretically.²³¹⁻²³³ In synthesis, however, the transition metal catalyst not only binds and thus activates the oxygen molecule but also mediates selective breaking of the oxygen-oxygen bond in the presence of a co-reductant to achieve substrate oxygenation and to form one molecule of water as a by-product (Scheme 3.4.1).²³⁴

Today, the most versatile reagents to catalyse aerobic oxidations in synthesis are cobalt(II) diketonate-complexes, such as bis[trifluoroacetylacetonato(-1)]cobalt(II) $[\text{Co}(\text{tfa})_2]$.^{234,235,236} This complex is able to catalyse the oxidation of alkenols into functionalized tetrahydrofurans (Scheme 3.4.1). The oxidative cyclization thereby occurs with remarkable stereoselectivity and leaves a substituted tetrahydrofurylmethyl radical as reactive intermediate. The cyclized radical can be trapped, for example with bromine atom donors or an alkene, to furnish valuable building blocks for organic synthesis.^{237,238} In solutions of isopropanol, that is without added trapping reagent, the aerobic alkenol oxidation furnishes tetrahydrofuryl methanols (Scheme 3.4.1).



Scheme 3.4.1 Aerobic oxidation of δ,ϵ -unsaturated alcohols (bishomoallylic alcohols). R = e.g. *tert*-butyl or phenyl (top) and structure formulae of 1,3-diketones HL (drawn in the enol form) that are used as auxiliaries for cobalt(II) catalysts CoL_2 in synthesis (hydrogen atoms that are removed as protons upon coordination of HL to cobalt(II) are drawn in bold).

From synthesis, $\text{Co}(\text{tfa})_2$ is obtained as a solvated complex having ethanol and water attached to the cobalt atom. We therefore concluded that one alcohol molecule, that is the alkenol substrate (Figure 3.4.1), and one oxygen molecule bind to cobalt in the active catalyst, leading to a coordination number of six at the metal centre. If we now imagine an exchange of one oxygen by a nitrogen atom in each tfa ligand we will get a Schiff-base type ligand. For such a system we know from experiment that dioxygen adducts to cobalt Schiff bases complexes usually exist in the superoxocobalt(III) form $([\text{Co}^{3+}]-\text{O}_2^-)^{228,229,239}$ with a dioxygen molecule bound in an end-on manner.^{239,240} Strašák and Kaválek²²⁹ examined furthermore bridging of cobalt(III) centres by one peroxo O_2^{2-} ligand. Using electron paramagnetic resonance spectroscopy, Hoffman and co-workers²³⁹ were able to show, that the cobalt-oxygen complexes containing Schiff-base ligands are in a low spin form ($S=1/2$) with an unpaired electron located on the oxygen moiety. This statement has further been supported by cyclic voltammetry studies of Tamagaki et al.²²⁸ on a cobalt complex with imidazolyl-containing ligands and by Bakac and Espenson²⁴¹ through ESR studies on macrocyclic cobalt-oxygen complexes. Nevertheless, the macrocyclic complexes have been reported as peroxo species.²⁴²

The Schiff base complexes of cobalt were subject of single point ab initio Hartree-Fock studies (1976)²³² as well as recent DFT calculations (1999)²³¹ carried out with fully optimized structures. In agreement with the experiment, both studies show that the $[\text{Co}]-\text{O}_2$ complex has a doublet spin state and formally can be described as a superoxocobalt(III) compound. For different ligands the counterpoise-corrected binding energy of the oxygen molecule was estimated to be in the order of 12 kcal/mol. It was pointed out that the cobalt complex without oxygen molecule is in doublet spin state with a quartet state 1.3 kcal/mol above.

Dibasic Schiff-base ligands form 1:1 complexes with Co^{2+} ions. The same was observed for porphyrins which were in the center of interest of a work of Newton and Hall.²⁴³ With an ab

initio generalized molecular orbital (GMO) method followed by configuration interaction (CI) calculations the authors compared the bonding situation between the cobalt atom and an oxygen and identified $[\text{Co}^{3+}]\text{-O}_2^-$ as the best description among the proposed structures. The Co-O bond (oriented in z-direction) was formed by the cobalt $3d_{z^2}$ orbital and one of π^* orbitals of the oxygen molecule. The $3d_{yz}$ and both π orbitals at dioxygen remained nearly unchanged, which will be important in investigations outlined below. A change in the electronic nature of ligands, in most instances, modifies the geometry of the transition metal complex and the electronic structure at the central ion.

Although it is known that solutions of trifluoroacetylcamphor-derived cobalt(II) complex $[\text{Co}(\text{tfc})_2]$ in isopropanol rapidly take up dioxygen, details of dioxygen binding and utilization in oxidations catalyzed by cobalt(II) diketonate-complexes are unknown.²³⁶ To improve characteristics of cobalt(II) catalysts and thus to extend the scope of the cobalt method toward a general method for carbon-oxygen bond formation from alcohols and alkenes, we investigated the mechanism of dioxygen binding to a cobalt(II) complex $\text{Co}(\text{tfa})_2$ by computational analysis, and addressed the following questions.

- Is the ground state of $\text{Co}(\text{tfa})_2$ a high spin or a low spin state?
- How does oxygen bind to $\text{Co}(\text{tfa})_2$?
- Does the dioxygen binding change the spin state of $\text{Co}(\text{tfa})_2$?

3.4.2 COMPUTATIONAL DETAILS

Geometry optimizations as well as frequency calculations for all studied geometries were performed at the DFT level, employing the BP86 functional in connection with the double- ζ quality def2-SV(P) basis set. Each energy minimum was confirmed by frequency analysis. Moreover, the energy of each geometry was recalculated using the high quality, triple- ζ basis set def2-TZVP and an integration grid enlarged from m3 to m4. Because we were mainly interested in relative spin-state energetics of the calculated cobalt-oxygen compound which is known to be functional-sensitive, we compared the BP86/def2-TZVP results with single-point calculations utilizing B3LYP and TPSSH^{244,245} functionals. Again a def2-TZVP basis and an integration grid size m4 was applied. Such a choice of functionals allows us to compare results with increasing Hartree-Fock exchange contribution: 0% for BP86, 10% for TPSSH and 20% for B3LYP. To speed up the calculations we took advantage of the resolution of identity (RI) approximation.

Finally, we performed CASSCF calculations on selected structures in connection with a def2-TZVP basis set and additional polarization functions on cobalt (def2-TZVPP). Since Radoń et al.²⁴⁶ showed the importance of inclusion of dynamic correlation in calculations involving similar cobalt chelates, we decided to submit the CASSCF wave functions into the strongly-contracted NEVPT2 calculations. This approach was successful in case of nickel clusters and

similar accuracy is expected for other 3d transition metals. Details of this multireference calculations are given in the following sections.

3.4.3 MODEL

After O₂-uptake the Co centre of the transition metal complex is coordinated by two tfa-ligands and one O₂-molecule. As it was indicated in the introduction, the model for studying oxygen binding to Co(tfa)₂ should have one alcohol molecule bound to cobalt in order to mimic conditions relevant for oxidation catalysis. We used water and ethanol for this purposes. Geometry optimizations were performed using different configurations of the transition metal complex to obtain the most stable isomer, which is the *cis*-configured structure shown in Figure 3.4.1. We therefore used the *cis*-isomer of Co(tfa)₂(H₂O)(O₂) in all subsequent calculations. As no significant changes in relative energies of the isomers were observed upon substitution of H₂O with EtOH, we decided to use the aqua complex in all calculations described in the following.

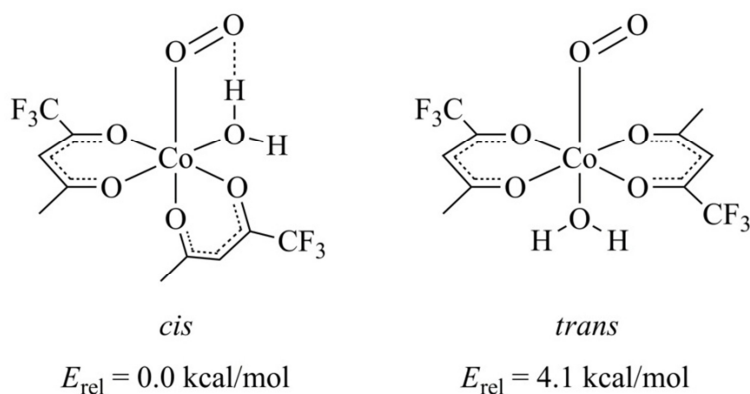


Figure 3.4.1 Structures of *cis/trans*-isomers of Co(tfa)₂(H₂O)(O₂) showing a hydrogen bond between coordinated O₂ and water (dashed single bond).

3.4.4 THE GROUND STATE OF THE ADDUCT

In order to obtain the electronic ground state of Co(tfa)₂(H₂O)(O₂), we optimized the geometry of the system for different spin states at the DFT level. At long Co··O₂ distances Co²⁺, as a d⁷ system, can either be in high spin configuration, S_{Co}=3/2, or in low spin configuration S_{Co}=1/2. The spin of the complex can couple with the spin of the O₂ molecule (³Π or ¹Δ state) to different total spins. An overview of possible spin states at long distances is given in Table 3.4.1. At the DFT level five different electronic configurations of the long distance system were used as a starting point in the geometry optimization of the adduct:

I. Sextet state, which results from coupling of high spin Co^{↑↑↑} with triplet O₂.ⁱ

ⁱCo^{↑↑↑} and Co^{↓↓↓} represents the high spin state of the catalyst where the unpaired electrons have α or β spins, respectively. Co[↑] and Co[↓] represent the low spin state where the unpaired electron has α or β spin, respectively. The unpaired electrons at the oxygen molecule have always α spin.

II. Broken symmetry^{247,248} doublet state: high spin $\text{Co}^{\downarrow\downarrow}$ with triplet O_2 ($^3\Pi$), the spin of the unpaired Co-orbitals obtained for the sextet state were flipped to β spin.

III. Quartet state: low spin Co^\uparrow with triplet O_2 ($^3\Pi$).

IV. Doublet state: low spin Co^\uparrow with singlet O_2 ($^1\Delta$).

V. Broken symmetry doublet: low spin Co^\downarrow with triplet O_2 ($^3\Pi$). The starting orbitals were obtained by spin flip of the unpaired electron on Co from calculation III.

Table 3.4.1 Possible spin states of $\text{Co}(\text{tfa})_2(\text{H}_2\text{O})(\text{O}_2)$ at long cobalt-oxygen distance defined by spin state of cobalt (S_{Co}), oxygen molecule (S_{O_2}) and the total spin of the system (S_{tot}). Spin states in bold are discussed in text as I-V.

S_{Co}	S_{O_2}	S_{tot}
3/2	1	5/2^I , 3/2, 1/2^{II}
1/2	1	3/2^{III} , 1/2^V
3/2	0	3/2
1/2	0	1/2^{IV}

In Table 3.4.2 the results of the geometry optimizations are summarised. The numbers I-V refer to electronic configurations described above. While the total spin of the system is kept fixed during the optimization process, the electronic structure can change. The resulting electronic configuration is classified by the spin density of Co and O atoms and the charge on the cobalt centre. All examined functionals indicate that the ground state of the $\text{Co}(\text{tfa})_2(\text{H}_2\text{O})(\text{O}_2)$ system is a doublet state with one unpaired electron symmetrically distributed on the oxygen moiety and a spin density of zero on the cobalt atom (see Figure 3.4.2). The oxygen-oxygen bond is elongated upon activation from an initial equilibrium distance of 1.216 Å to 1.294 Å. According to Bryantsev et al.²⁴⁹ a bond length of about 1.30 Å in combination with a vibrational frequency of $\sim 1150 \text{ cm}^{-1}$ shows a superoxo mode of dioxygen binding (O_2^-). While the bond length of $\text{Co}(\text{tfa})_2(\text{H}_2\text{O})(\text{O}_2)$ is in this range, the vibrational frequency is significantly higher (1214 cm^{-1}), presumably due to hydrogen bonding between the bound dioxygen and the aqua-ligand (O...H distance is 1.620 Å).

From an NBO analysis of $\text{Co}(\text{tfa})_2(\text{H}_2\text{O})(\text{O}_2)$ which showed a charge of +1.2 at cobalt we concluded that the oxidation state of the metal is still +II. The total spin density on the bound dioxygen molecule on the other hand agrees with superoxo-complex formation. This suggests that the system can be formally described, either like a Schiff-base- or a porphyrin-complex, as $\text{Co}^{\text{III}}\leftarrow\text{O}_2^-$ with a dative oxygen-to-cobalt bond or may be viewed as $\text{Co}^{\text{II}}\text{-O}_2^0$ if the composition of the σ -bond between the cobalt and oxygen atom orbital is a combination with nearly equal contributions of Co and O_2 orbitals.^{243,250}

Table 3.4.2 Selected data for the geometries of $\text{Co}(\text{tfa})_2(\text{H}_2\text{O})(\text{O}_2)$ obtained for different spin-states. The states (I-V) are explained in text. The oxygen atoms count is given in Fig. 2. The electronic structures of resulting geometries are classified by spin densities (sd) on cobalt and oxygen as well as by charge (ch) on the cobalt atom. The spin density for oxygen is given only for one atom because its distribution is symmetrical. All energies are in kcal/mol.

Spin	E^{BP86}	E^{B3LYP}	E^{TPSSH}	Co-O1 [Å]	O1-O2 [Å]	sd(Co)	sd(O)	ch(Co)
I	24.5	4.0	15.4	2.308	1.252	2.7	0.8	1.5
II	16.0	7.3	19.0	1.924	1.267	-1.9	0.7	1.4
III	18.1	4.0	18.0	1.935	1.269	1.5	0.6	1.4
IV, V	0.0	0.0	0.0	1.900	1.294	0.0	0.5	1.2

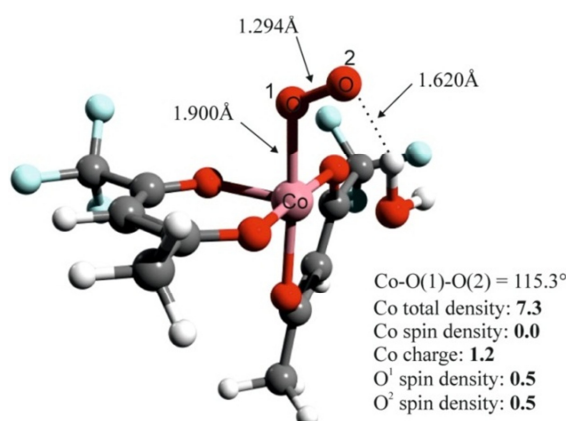
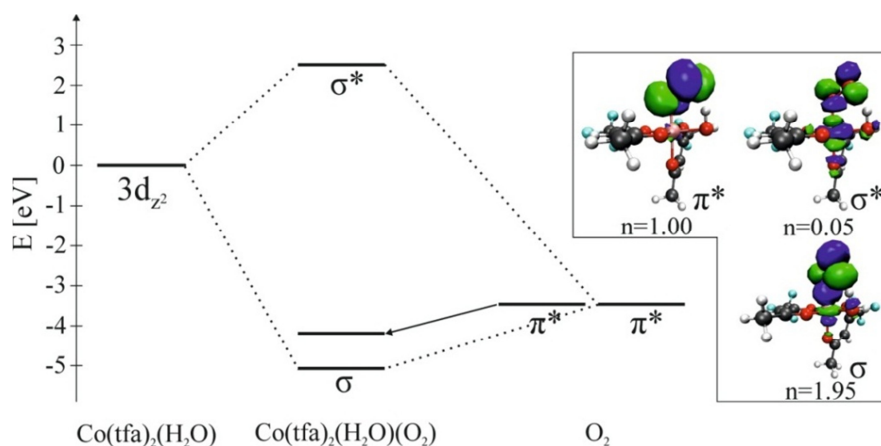


Figure 3.4.2 Geometry of the low spin $\text{Co}(\text{tfa})_2(\text{H}_2\text{O})(\text{O}_2)$ catalyst with the most important interatomic distances and results from the NBO analysis.

We undertook NEVPT2 calculations to distinguish between these two electronic configurations of the cobalt-dioxygen entity. The NEVPT2 calculations were based on a state averaged CASSCF (SA-CASSCF) wave function and the ground state DFT-optimized structure (Figure 3.4.2). Starting orbitals for the SA-CASSCF calculations were obtained from localized ROHF (restricted open shell Hartree Fock) orbitals resulting from high spin, sextet calculations. Five d orbitals of the cobalt atom and two π^* orbitals of the oxygen molecule were chosen to enter the active space with nine electrons what led to a (9,7) active space. The results confirm that the studied system prefers a low spin configuration (see comparison in Table 3.4.3). From the initial five d orbitals of cobalt only d_{z^2} seems to be significant for the considered interaction. After the optimization of the orbitals, only one of the cobalt d orbitals – $d_{x^2-y^2}$ – has an occupation number close to zero (0.03) while the other three share an occupation number of about two (1.97-1.99) what indicates that the unpaired electron doesn't prefer to reside on the cobalt centre. The d_{z^2} orbital overlaps with one of the antibonding π^* orbitals of the oxygen molecule what results with a bonding σ orbital and a corresponding antibonding σ^* orbital and an unchanged second π^* orbital as given in Figure 3.4.3.

Table 3.4.3 Comparison of energies of three spin states at BP86, B3LYP, TPSSh functionals, CASSCF, and NEVPT2 level of theory. All energies are in kcal/mol.

2S+1	E ^{BP86}	E ^{B3LYP}	E ^{TPSSh}	E ^{CASSCF}	E ^{NEVPT2}
2	0.0	0.0	0.0	0.0	0.0
4	28.5	23.5	10.9	19.8	26.3
6	48.1	33.8	39.2	94.6	101.5

**Figure 3.4.3** Molecular orbital diagram for the $\text{Co}(\text{tfa})_2(\text{H}_2\text{O})(\text{O}_2)$ system. The Co- O_2 σ -bonding and antibonding (σ^*) orbitals are formed from the interaction between the $3d_{z^2}$ and π^* orbitals. The second π^* orbital of O_2 remains nearly unchanged. σ , σ^* and π^* orbitals of the $\text{Co}(\text{tfa})_2(\text{H}_2\text{O})(\text{O}_2)$ system are presented on the right with corresponding occupation numbers.

The wave function of the system consists mainly of the configurations $(\sigma)^2(\pi^*)^1(\sigma^*)^0$ (96%), and $(\sigma)^0(\pi^*)^1(\sigma^*)^2$ (3%). This means that the unpaired electron resides at the oxygen moiety as it was the case in the DFT calculations. Moreover, from the orbital pictures given in Figure 3.4.3 it is obvious that the σ -bond between cobalt and oxygen is mainly composed of the π^* orbital of oxygen with only a small $3d_{z^2}$ contribution. Such a result suggests that the system is best described as a superoxide O_2^- forming a dative σ bond to an empty cobalt d_{z^2} orbital. Therefore, this interaction could be depicted as $\text{Co}^{\text{III}}(\text{S}=0)\leftarrow\text{O}_2^-(\text{S}=1/2)$ with formal oxidation state of cobalt atom being III. It is also worth noting that among the three orbitals presented here, only the antibonding σ^* has some contribution on the *trans*-located tfa-ligand. This observation may serve to explain low reactivity of cobalt chelates having a redox potential higher than $\text{Co}(\text{tfa})_2$ (higher than 0.5 eV) in aerobic oxidations.²⁵¹ For example introduction of a second trifluoromethyl group on each tfa ligand is expected to increase the redox potential of the system up to 1.0 eV and the system should no longer activate an oxygen molecule.²⁵¹ This is probably due to stabilization of the antibonding σ^* orbital by more electron withdrawing substituents. This prediction is under current experimental investigation.

3.4.5 OXYGEN UPTAKE PROCESS

So far, we have shown that the active catalyst with a superoxo ligand has a low spin doublet state. To investigate key steps in dioxygen binding to the cobalt complex, we first analyzed the ground state of $\text{Co}(\text{tfa})_2(\text{H}_2\text{O})$, which has not yet been reported from experimental studies. The [bis(trifluoromethyl-(+)-camphorato(-1))]cobalt(II) derivative, $\text{Co}(\text{tfc})_2$ (cf. Scheme 3.4.1), which crystallizes from aqueous THF as hydrated monotetrahydrofuran adduct, shows a magnetic moment of $\mu_{\text{eff}} = 1.5 \mu_{\text{B}}$ at room temperature (298 K), which points to an electronic low spin configuration.²⁵² In order to obtain more information on electronic properties of $\text{Co}(\text{tfa})_2(\text{H}_2\text{O})$, we optimized the structure of the d^7 -cobalt (II) complex in the low spin doublet and in the high spin quartet state. The structures of the two electronic configurations of $\text{Co}(\text{tfa})_2(\text{H}_2\text{O})$ are shown in Figure 3.4.4. According to the Table 3.4.4 the low spin state is higher in energy by only 0.8 kcal/mol using the BP86 functional, while this energy gap increases to 7.4 kcal/mol for the TPSSH functional and reaches the highest value of 11.6 kcal/mol, when the B3LYP functional is applied [this corresponds to the B3LYP value for the doublet-quartet energy gap of 16.9 kcal/mol in the $\text{Co}(\text{acac})_2(\text{H}_2\text{O})$ complex²⁵³]. Interestingly, the charge at the cobalt atom in the ground state geometry is +1.4 and thus increased by only 0.2 compared to the situation where is bound to dioxygen. When we performed a multireference calculation involving all five d orbitals of cobalt with seven electrons, we obtained a relative stabilization of the quartet state by 20.0 kcal/mol at NEVPT2 level of theory. A twofold higher value (46.8 kcal/mol) was obtained at the CASSCF level. Such a method sensitivity of the energy difference between high and low spin transition metal complexes is a well-known problem.^{254,255} It is caused by a much larger contribution of dynamic correlation in the low spin state, due to a high number of paired electrons and larger interpair correlation contribution with the ligands because of the shorter bond distances (e.g. in Figure 3.4.4 the $\text{Co}-\text{OH}_2$ distance is about 0.1 Å shorter in the doublet state in comparison to the quartet state).

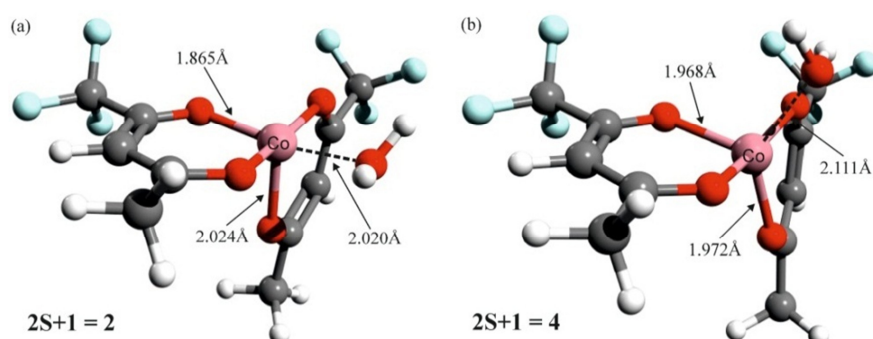


Figure 3.4.4 Structures of the $\text{Co}(\text{tfa})_2(\text{H}_2\text{O})$ complex optimized at two spin states - (a) doublet and (b) quartet state.

Table 3.4.4 Comparison of selected data for the $\text{Co}(\text{tfa})_2(\text{H}_2\text{O})$ complex optimised at two spin states. All energies are in kcal/mol. Used acronyms: sd - spin density, ch - charge.

$2S+1$	E^{BP86}	E^{B3LYP}	E^{TPSSh}	E^{CASSCF}	E^{NEVPT2}	sd(Co)	ch(Co)
2	0.8	11.6	7.4	46.8	20.0	1.0	1.2
4	0.0	0.0	0.0	0.0	0.0	2.6	1.4

We examined the oxygen uptake by the cobalt catalyst for all possible spin states, because relative energies of optimized geometries are strongly method-dependent. To study dioxygen binding to $\text{Co}(\text{tfa})_2(\text{H}_2\text{O})$, we iteratively optimized structures at fixed cobalt-oxygen distances for different spin states. The energy/distance correlations obtained from this part of the study are shown in Figure 3.4.5.

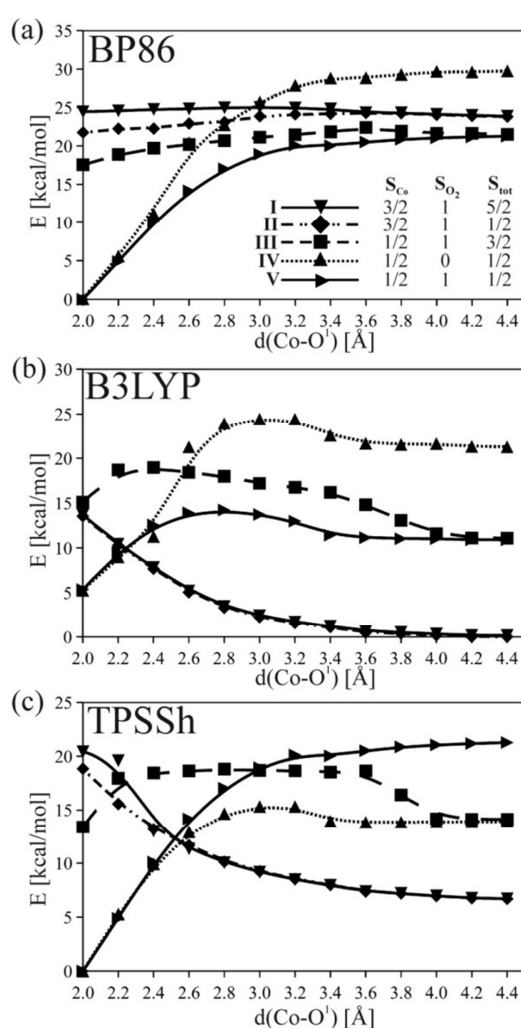


Figure 3.4.5 Functional dependency of potential energies for dioxygen binding to $\text{Co}(\text{tfa})_2(\text{H}_2\text{O})$ starting from triplet oxygen and different spin states of the cobalt complex (a-BP86, b-B3LYP, c-TPSSh). Curves for different spin arrangements I-V (compare Table 3.4.2) are defined by the spin state of cobalt (S_{Co}), oxygen molecule (S_{O_2}) and the total spin of the system (S_{tot}).

In the calculations with the BP86 functional the energy difference between the optimized doublet and quartet states of the $\text{Co}(\text{tfa})_2(\text{H}_2\text{O})$ complex are small (Table 3.4.4). Thus, the energy of triplet oxygen adducts to all possible spin configurations of $\text{Co}(\text{tfa})_2(\text{H}_2\text{O})$ for Co-O distances over 3.0 Å are close in energy. In general, exact exchange favours the high spin state of the $\text{Co}(\text{tfa})_2(\text{H}_2\text{O})$ complex, while dynamic correlation stabilizes the low spin state. Therefore, the doublet-quartet energy separation is more pronounced in case of the hybrid functionals. Taking into account the optimized ground state geometries for the respective spin states, we calculated the energy difference ΔE between the lowest state at long Co-O distance and the lowest state at short, fully optimized distance. ΔE of the oxygen activation process is -21.3 kcal/mol for the BP86 functional and -6.8 kcal/mol in case of the TPSSh functional. B3LYP predicts the oxygen activation being an endothermic process with $\Delta E=+5.2$ kcal/mol. Such an overestimated stabilization of high spin states is well known and can be decreased by tuning the amount of Hartree-Fock (HF)-exchange.⁸³ As we have already included three functionals in this study, each with different amount of HF-exchange contribution, we can illustrate its influence on the energetics of O_2 binding to the $\text{Co}(\text{tfa})_2(\text{H}_2\text{O})$ complex (see Figure 3.4.6), leading to an almost linear correlation. We also compared the results obtained with the DFT functionals to wave function based NEVPT2(9,7) calculations for a system at large Co-O separation (15.0Å) and we subtracted the lowest sextet energy from the energy of the doublet ground state adduct. In the NEVPT2 calculations $\Delta E=+3.7$ kcal/mol was obtained. This value, however, should be treated with care because we observed a trend of stabilization of the adduct with increasing basis set, i.e. a decrease of ΔE (see Table 3.4.5). With the fairly large def2-TZVPP basis set on the cobalt atom, we still did not achieve the limit of the NEVPT2 method. Thus, the real ΔE value is most probably closer to 0 kcal/mol (or even below) but can be accessed only with extremely large basis sets as has recently been systematically investigated for Fe(II).²⁵⁶

Table 3.4.5 Basis set dependence of the NEVPT2(9,7) energy change upon O_2 binding to the $\text{Co}(\text{tfa})_2(\text{H}_2\text{O})$ complex.

Basis set		ΔE [kcal/mol]
<i>Co, O atoms</i>	<i>C, H, F atoms</i>	
def2-SVP	def2-SVP	17.0
def2-TZVP	def2-SVP	7.1
def2-TZVP	def2-TZVP	6.4
def2-TZVPP	def2-TZVP	3.7

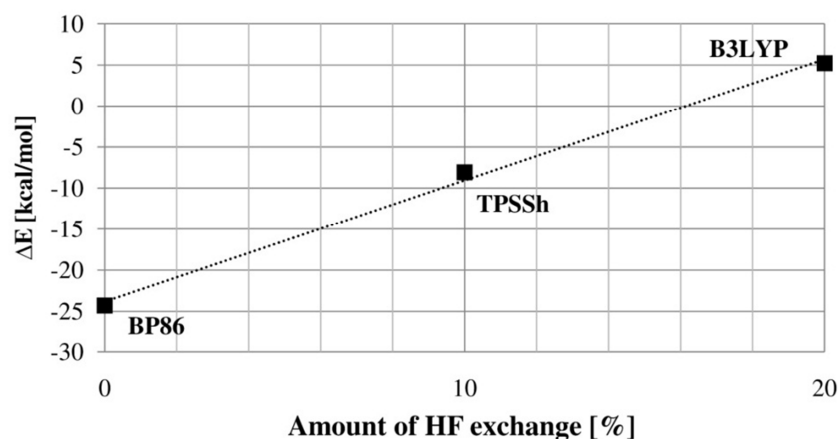


Figure 3.4.6 Linear dependency of the energy change during the oxygen activation process (ΔE) upon varying the amount of Hartree-Fock exchange in the functional (BP86 - 0%, TPSSh - 10%, B3LYP - 20%).

Recently, Rybak-Akimova et al.²⁵⁷ used a specially designed, penta-coordinated lacunar cyclidene cobalt(II) complexes in order to evaluate the Co-O₂ activation barrier. Their very low value of 1-2 kcal/mol can be addressed to the fact that the initial catalyst was already in low, doublet spin state while in our case the system has to undergo a spin reorganization process. In our case – at BP86 level of theory – a spin-degenerate system at long distance goes barrier-less directly to the low spin product. On the other hand, B3LYP and TPSSh functionals show a spin-reorganization region between 2.2 and 2.5 Å where the spin-pairing process is taking place with an activation barrier in range of 5-10 kcal/mol. It is possible that the adduct follows the doublet potential energy surface all the time, two-state or multistate reactivity^{258,259} which plays an important role in organometallic chemistry, e.g. for iron enzymes, such as Cytochrome P450, can also occur for this system. The formation of a superoxo moiety bound to Co(III) is similar to O₂ uptake by heme²⁶⁰ and non-heme iron enzymes.^{261,262} In case of heme,²⁶⁰ Fe(II) is in its high spin state at long distances while the electronic structure at short distances is best described as open shell singlet with one unpaired electron at Fe(III) in low spin state and the second located on the superoxo moiety. In several non-heme iron enzymes,²⁶¹ Fe(III) is in its high spin state after O₂ uptake. In such complexes, the lowest state is a septet state but for most reactions a transition to a close by quintet state is necessary, and activation barriers up to 10 kcal/mol were reported for dioxygen activation. Nevertheless, because of the method sensitivity, it is not possible to estimate whether for the cobalt complex formation of the adduct is barrier free or not. However, we only studied the gas phase reaction so far. In solution it is more likely that O₂ has to replace a solvent molecule at the sixth coordination site. In that case the complex might be in low spin configuration under reaction conditions.

3.4.6 CONCLUSIONS

The electronic ground state of $\text{Co}(\text{tfa})_2(\text{H}_2\text{O})$ in the gas phase, and presumably in nonpolar solvents, is a quartet state [high spin Co(II)]. As dioxygen approaches to bind to the cobalt complex, the quartet state couples with a triplet oxygen molecule to form a sextet, a quartet, or a doublet spin state with the high-spin state being again the lowest in energy. Dioxygen binding to $\text{Co}(\text{tfa})_2(\text{H}_2\text{O})$ occurs in a bent end-on manner. At the equilibrium distance for the bond between cobalt and the coordinated dioxygen molecule, $\text{Co}(\text{tfa})_2(\text{H}_2\text{O})(\text{O}_2)$ has a doublet ground state with the unpaired electron residing on the oxygen moiety, in a nearly unchanged π^* orbital. The bond between cobalt and oxygen can be described as a dative bond of a superoxo dioxygen molecule to a formal cobalt(III) ion. It was pointed out that the ligands will have influence on the Co-O bond strength by a *trans*-effect via modification of σ and σ^* orbitals.

The mechanistic analysis of the oxygen uptake process by $\text{Co}(\text{tfa})_2(\text{H}_2\text{O})$ is method sensitive. The reaction is exothermic by -21.3 kcal/mol for dioxygen binding on the BP86-level of theory and endothermic by 5.2 kcal/mol, if we use the B3LYP functional. The functional dependence of the results is attributed to differences in dynamic correlation energy by the methods, which highly contributes to the stabilization of the low spin state of cobalt(II). For the same reason, the NEVPT2 value of 3.7 kcal/mol is probably still too high. The energy change upon dioxygen activation on the catalyst is probably close to zero.

At a cobalt-oxygen distance of 2.2-2.5 Å, spin-reorganization occurs, which is an important aspect for oxidation catalysis, since effective catalysis by cobalt-complexes that formally change oxidation states from +II to +III and back to +II generally is only feasible, if the electronic configuration at cobalt is low spin. Depending on the functional used the activation is a barrier free process (BP86 functional) or has a small activation barrier up to 10 kcal/mol in case of B3LYP.

An interesting structural feature of *cis*- $\text{Co}(\text{tfa})_2(\text{H}_2\text{O})(\text{O}_2)$ is the ability of the dioxygen entity to form a hydrogen bond to the aqua-ligand, and presumably also to a bound alkenol. In the proposed mechanism for the oxidative cyclization, hydrogen atom abstraction from the alkenol toward the bound dioxygen entity has been put forward as one of the important steps to explain conversion of the alkenol into cyclic ether.

4 SUMMARY

In this thesis four challenging problems concerning metal- or metalloid-containing systems were carefully studied in order to explain their properties, reactivities and selectivities. The first project focused on the dialkylzinc additions to unsaturated aldehydes. The reaction was proved to have bimetallic intermediates. The experimentally observed non-linear effect was addressed to the differences in stability of various zinc-ligand aggregates. Furthermore, the differences in regioselectivity between cinnamaldehyde and *N*-formylbenzylimine were traced back to the differences in the π -conjugation of both compounds. In contrary, the stereoselectivity of the reaction was controlled by the paracyclophane unit as well as by bulky substituents in the side-chain of the ligand. Based on these findings, a set of modifications for the ligand system were proposed and tested *in silico*. One of the compounds is expected to be superior to any previous catalysts. An important outcome from this study is the survey of methods used in calculations of reaction barrier heights. It is shown that economic DFT calculations, when extended by empirical dispersion corrections allow for the prediction of stereoselectivities. However, the prediction of the regioselectivities is a much more demanding task and only a consistent treatment of electron correlation can yield qualitative agreement with experimental findings. In this case, the computationally more expensive – but even for large systems still applicable – LPNO-CEPA/1 approach seems to be an efficient and reliable choice.

In the second project systems with significantly elongated bonds were studied. Germanium ($\text{Ge}_{14}[\text{Si}(\text{SiMe}_3)_3]_5\text{Li}_3(\text{THF})_6$) and tin ($\text{Sn}_4\text{Si}[\text{Si}(\text{SiMe}_3)_3]_4(\text{SiMe}_3)_2$) cluster compounds appeared to be interesting examples of stable molecules with a number of undercoordinated atoms (three instead of four coordination partners for Ge or Sn) that are too far from each other to form a normal bond but are close enough to expect some kind of interaction. In both systems rhombic M_4R_6 (M = Ge, Sn; R – ligand) entities were found and the spin situation between two bridgehead atoms is best described as singlet biradicaloid. Moreover, an important contribution of the quantum-chemical studies was the demonstration that the stretching of the bond is not solely responsible for the observed biradicaloid character because the orientation and size of the ligands can also cause transitions between a radicaloid, a simple bounded system and a biradical with a quasi-degenerate singlet and triplet state. Furthermore, these calculations clearly show the limit of the applicability of single reference methods like DFT. Indeed, a more sophisticated treatment of static correlation, e.g. by using CASSCF wave functions is needed in order to describe the electronic state of such systems properly.

Smaller cluster compounds of nickel were considered in the next step. Experimental measurements concerning the dimer and the trimer are rather limited and are inconsistent with many theoretical findings. Within this work a benchmark study was performed on the Ni_2 molecule, and the bond length was calculated to be 2.22 Å with a corresponding vibrational

frequency of 286 cm^{-1} . The NEVPT2 method was shown to provide data that is in excellent agreement with MRACPF results. The perturbation approach was used to estimate the electronic ground state including spin-orbit interactions. It was found to be 0_g^+ in agreement with experiment. Moreover, it was pointed out that the TPSSh functional when combined with a broken symmetry approach provides bond lengths similar to those obtained with the NEVPT2 method. According to the literature, the bond is elongated by 0.1 \AA upon electron attachment to the nickel dimer. This effect was observed both at the NEVPT2 and the TPSSh level and the bond expansion was addressed to the occupation of a σ^* orbital by the excess electron. A similar analysis was performed in the case of the nickel trimer. The NEVPT2 and TPSSh calculations agree that the ground state of the neutral cluster has a triangular geometry and a quintet spin state. However, at the NEVPT2 level the anion has clearly a linear form while the TPSSh functional shows linear and triangular isomers to be nearly equal in energy. The final distinction can be made by measuring the O-H stretching vibration in the systems where the nickel cluster is solvated by two ethanol molecule. According to TPSSh calculations, the difference between the O-H stretching frequencies of the two ethanol molecules will be much smaller ($\sim 15\text{ cm}^{-1}$) for the linear isomer than for the triangular geometry ($\sim 90\text{ cm}^{-1}$). Upcoming experimental IR studies should clearly be able to distinguish between these two forms.

Similar problems with DFT methods were encountered in the last application covered by this work. The aim was to analyse the molecular oxygen activation process by cobalt(II) diketonate complexes like bis[trifluoroacetylacetonato(-1)]cobalt(II) $[\text{Co}(\text{tfa})_2]$. This reaction is the first step in a mild and cheap aerobic oxidation of alkenols into functionalized tetrahydrofurans (molecules of high biological activity). However, various mechanisms can be proposed depending on the electronic structure of the adduct. We found, that the isolated catalyst with one water molecule $[\text{Co}(\text{tfa})_2(\text{H}_2\text{O})]$ has a high spin quartet state. As dioxygen approaches the cobalt atom, the quartet state couples with a triplet dioxygen molecule and forms a sextet, a quartet, and a doublet spin state with the high-spin state being the lowest in energy. At the equilibrium Co–O₂ distance of 1.9 \AA , $\text{Co}(\text{tfa})_2(\text{H}_2\text{O})(\text{O}_2)$ has a doublet superoxo Co(III) ground state with the unpaired electron residing on the oxygen moiety, in a nearly unchanged O₂ π^* orbital. Here, it should be emphasised that even if DFT properly describes the electronic ground states of the catalyst and adduct, the relative spin state energies are, however, highly dependent on the functional used. A clear distinction would not be possible without NEVPT2 multireference calculations.

The calculations presented in this work established a solid base for further investigations concerning large metal- and metalloid-containing systems. The results evidently show that there is a great need to go beyond DFT in such computations. Elongated bonds or near-degeneracy problems within $3d$ transition metals are certainly the limit of single reference methods. In such cases, the CASSCF approach together with an inexpensive estimation of the

remaining correlation energy (NEVPT2) was proven to be as reliable as the CI-based methods. Moreover, the regioselectivity prediction in reactions involving only closed shell species requires a consistent treatment of electron correlation in the transition states which can have very different structures. The progress made with efficient and accurate approximations permits the use of high-level wave function based methods like CEPA for molecules with over 100 atoms, even with a decent basis set. Through the careful evaluation of our calculations, the stereoselectivity was shown to be properly described with most of the modern DFT functionals when augmented with dispersion corrections. In this work also a number of predictions concerning the chemical structures and their reactivities have been made. The provided quantitative data can be directly compared to the perspective experimental studies what will certainly assist the deep understanding of the metal-based catalytic processes.

5 ZUSAMMENFASSUNG (IN GERMAN)

In der vorliegenden Arbeit wurden verschiedene metallhaltige Komplexe und metalloide Clusterverbindungen mit Hilfe quantenchemischer Methoden untersucht. Dadurch war es unter anderem möglich, die Eigenschaften und die Reaktivität dieser Systeme zu verstehen sowie die Selektivität bei Reaktionen zu erklären.

Die erste Fragestellung befasste sich mit der Addition von Dialkylzink an ungesättigte Aldehyde. Hier konnte gezeigt werden, dass die Reaktion über bimetallische Intermediate verläuft. Der im Experiment beobachtete nicht-lineare Effekt kommt dabei durch die Stabilitätsunterschiede verschiedener Zink-Ligand-Aggregate zustande. Darüberhinaus konnte gezeigt werden, dass die Unterschiede in der Regioselektivität von Zimtaldehyd und N-Formylbenzylimin auf der unterschiedlichen π -Konjugation beruhen. Die Stereoselektivität der Reaktion selbst wird durch die Paracyclophan-Einheit sowie durch sterisch anspruchsvolle Substituenten in der Seitenkette des Liganden kontrolliert. Basierend auf diesen Erkenntnissen wurden mehrere Modifikationen für den Liganden vorgeschlagen und *in silico* überprüft. Eine dieser Verbindungen sollte allen bisher verwendeten Katalysatoren überlegen sein. Ein weiteres wichtiges Ergebnis ist der erhaltene Überblick über die Qualität verschiedener quantenchemischer Methoden für die Berechnung von Reaktionsbarrieren. Dichtefunktionalberechnungen sind beispielsweise zur Vorhersage der Stereoselektivität geeignet, sofern eine empirische Korrektur für Dispersionswechselwirkungen berücksichtigt wird. Im Gegensatz dazu ist die Vorhersage von Regioselektivitäten deutlich schwieriger und für die qualitative Übereinstimmung mit experimentellen Daten ist eine konsistente Beschreibung der Elektronenkorrelation erforderlich. Eine geeignete Wahl hierfür könnte die in dieser Arbeit verwendete LPNO-CEPA/1-Methode darstellen, welche zwar deutlich rechenintensiver, aber dennoch für große Systeme anwendbar ist.

Im Rahmen des zweiten Projekts wurden metallhaltige Systeme mit deutlich aufgeweiteten Bindungsabständen untersucht. Ausgewählte Clusterverbindungen mit Germanium ($\text{Ge}_{14}[\text{Si}(\text{SiMe}_3)_3]_5\text{Li}_3(\text{THF})_6$) und Zinn ($\text{Sn}_4\text{Si}[\text{Si}(\text{SiMe}_3)_3]_4(\text{SiMe}_3)_2$) sind interessante Beispiele für stabile Verbindungen, bei denen einige Atome eine Koordinationszahl von drei anstatt von vier aufweisen. Der Abstand zwischen den dreifach koordinierten Atomen ist einerseits zu groß für die Ausbildung einer gewöhnlichen Bindung, aber andererseits klein genug um eine Wechselwirkung zu erwarten. Bei beiden genannten Systemen liegen rhombische M_4R_6 -Einheiten ($\text{M} = \text{Ge}, \text{Sn}$; $\text{R} = \text{Ligand}$) vor und die elektronische Situation zwischen den beiden subvalenten Atomen lässt sich am besten als Singulett-Biradikaloid beschreiben. Mit Hilfe der quantenchemischen Untersuchungen konnte gezeigt werden, dass die Aufweitung der Bindung nicht allein für den beobachteten biradikaloiden Charakter verantwortlich ist. Vielmehr können durch die Orientierung und die Größe der Liganden Übergänge zwischen radikaloiden, gebundenen Zuständen und echten Biradikalen mit quasi-

entarteten Singulett- und Triplett-Zuständen verursacht werden. Des Weiteren wurde anhand dieser Berechnungen die Grenze der Anwendbarkeit von Eindeterminanten-Ansätzen wie DFT deutlich. Für die korrekte Beschreibung des elektronischen Zustands solcher Systeme ist eine angemessene Berücksichtigung der statischen Korrelation, beispielsweise durch CASSCF-Verfahren, notwendig.

Im dritten Teil der Arbeit wurden kleinere Nickelcluster untersucht. Für das Dimer und das Trimer liegen bisher nur wenige experimentelle Daten vor, welche jedoch nicht im Einklang mit den meisten Berechnungen sind. Im Rahmen der vorliegenden Arbeit wurde daher eine Benchmark-Studie für das Ni₂-Molekül durchgeführt. Für die Bindungslänge ergab sich ein Wert von 2.22 Å und die Schwingungsfrequenz beträgt 286 cm⁻¹. Die NEVPT2-Methode liefert hierbei Daten, welche in sehr guter Übereinstimmung mit den MRACPF-Ergebnissen sind. Der störungstheoretische Ansatz wurde verwendet, um den elektronischen Grundzustand unter Berücksichtigung von Spin-Bahn-Wechselwirkungen zu bestimmen. In Übereinstimmung mit dem Experiment konnte ein 0_g⁺-Zustand zugeordnet werden. Darüberhinaus wurde gezeigt, dass das TPSSh-Funktional im Rahmen des Broken-Symmetrie-Ansatzes ähnliche Bindungslängen wie die NEVPT2-Methode ergibt. Nach Literaturangaben verlängert sich die Bindung im Nickel-Dimer um 0.1 Å durch Anlagerung eines Elektrons. Dieser Effekt konnte sowohl mit NEVPT2 als auch mit TPSSh reproduziert werden und beruht auf der Besetzung eines σ*-Orbitals durch das zusätzliche Elektron. Ähnliche Untersuchungen wurden für das Nickel-Trimer durchgeführt. Hier ergaben die NEVPT2- und TPSSh-Berechnungen, dass der Grundzustand des neutralen Clusters eine dreieckige Geometrie und einen Quintett-Zustand besitzt. Für das entsprechende Anion konnte mit NEVPT2 eindeutig eine lineare Geometrie zugeordnet werden, während im Fall von TPSSh das lineare und das dreieckige Isomer ähnliche Energien aufweisen. Eine Möglichkeit zur Unterscheidung beider Spezies bietet die Messung der O-H-Streckschwingungsfrequenz im System [Ni₃(EtOH)₂]⁻. Gemäß den TPSSh-Berechnungen unterscheiden sich die Frequenzen der beiden O-H-Streckschwingungen im Fall des linearen Isomers weniger (~15cm⁻¹) als bei der dreieckigen Geometrie (~90cm⁻¹). Zukünftige IR-Experimente sollten daher in der Lage sein, die Geometrie eindeutig zu bestimmen.

Beim letzten Anwendungsprojekt traten im Zusammenhang mit DFT-Methoden ähnliche Schwierigkeiten auf. Das Ziel war es hier, den Aktivierungsprozess von molekularem Sauerstoff durch Kobalt(II)diketonat-Komplexe wie [Co(tfa)₂] zu analysieren. Diese Reaktion ist der erste Schritt in einer milden und kostengünstigen aerobischen Oxidation von Alkenolen zu funktionalisierten Tetrahydrofuranen (Moleküle mit hoher biologischer Aktivität). Jedoch sind abhängig von der elektronischen Struktur des Addukts verschiedene Mechanismen denkbar. Es konnte gezeigt werden, dass ein Komplex aus einem Katalysatormolekül mit einem Wassermolekül [Co(tfa)₂(H₂O)] einen Quartett-Grundzustand besitzt (High-Spin-Zustand). Durch Annäherung des Sauerstoffmoleküls (Triplett) an das Kobaltatom können der

Quartett- und der Triplett-Zustand zu einem Sextett-, einem Quartett- und einem Dublett-Zustand koppeln, wobei der High-Spin-Zustand energetisch am günstigsten ist. Beim Gleichgewichtsabstand (Co–O₂ 1.9 Å) weist der Co(tfa)₂(H₂O)(O₂)-Komplex einen Dublett-Grundzustand auf, wobei sich das ungepaarte Elektron in einem nahezu unveränderten π*-Orbital des Sauerstoffmoleküls befindet. An dieser Stelle muss betont werden, dass die DFT-Methode zwar den Grundzustand des Katalysators und des Addukts richtig wiedergibt, aber dass die relativen Energien der einzelnen Spinzustände stark vom verwendeten Funktional abhängen. Für zuverlässige Ergebnisse sind daher NEVPT2-Berechnungen erforderlich.

Die in Rahmen dieser Arbeit durgeführten quantenchemischen Berechnungen bilden eine zuverlässige Grundlage für weitere Untersuchungen an großen metall- und metalloidgehaltigen Systemen. Die Ergebnisse verdeutlichen, dass standardmäßig verwendete Dichtenfunktionalmethoden für die gegebenen Fragestellungen oftmals nicht ausreichen. Aufgeweitete Bindungen und nahezu entartete Zustände bei 3d-Übergangsmetallen stellen dabei die Grenze für die Anwendbarkeit von Eindeterminanten-Ansätzen dar. Für diese Fälle wurde gezeigt, dass die NEVPT2-Methode (CASSCF-Verfahren mit Abschätzung der fehlenden Korrelationsenergie) vergleichbar gute Ergebnisse liefert wie CI-basierte Methoden. Zudem erfordert die Vorhersage der Regioselektivität für Reaktionen, selbst wenn nur closed-shell Spezies auftreten, eine konsistente Beschreibung der Elektronenkorrelation in den Übergangszustände, da hier sehr unterschiedliche Strukturen vorliegen können. Durch Fortschritte hinsichtlich der Effizienz können korrelierte wellenfunktionbasierte Methoden wie CEPA für Moleküle mit mehr als 100 Atomen auch in Kombination mit sinnvollen Basissätzen angewendet werden. Anhand der sorgfältigen Auswertung der Ergebnisse dieser Arbeit konnte gezeigt werden, dass die Stereoselektivität bereits mit den meisten Dichtenfunktionalen richtig wiedergegeben werden kann, sofern Dispersionswechselwirkung berücksichtigt werden. Im Rahmen der vorliegenden Arbeit wurden zudem mehrere Vorbesagen bezüglich der Struktur und der Reaktivität ausgewählter Verbindungen gemacht. Diese Daten werden für die Auswertung zukünftiger Experimente hilfreich sein und somit zum tieferen Verständnis metallbasierter Katalyseprozesse beitragen.

6 PODSUMOWANIE (IN POLISH)

W niniejszej pracy doktorskiej poruszone zostały cztery złożone problemy dotyczące układów chemicznych zawierających metale lub metaloidy. Badania miały na celu dokładne przebadanie ich właściwości, reaktywności oraz selektywności. Pierwszy projekt skupiał się na addycjach dialkilocynku do nienasyconych aldehydów. Zostało potwierdzone, że w reakcji występują bimetaliczne produkty przejściowe. Zaobserwowany eksperymentalnie efekt nieliniowy został powiązany z różnicami w stabilności potencjalnych agregatów ligand-alkilocynk. Ponadto, zaobserwowane różnice w regioselektywności pomiędzy aldehydem cynamonowym a *N*-formylobenzyliminą zostały wyjaśnione na bazie różnic w stopniu π -skoniugowania obu związków. Stwierdzono, że stereokonfiguracja produktu jest kontrolowana wyłącznie poprzez jednostkę paracyklofanową oraz przyłączone do niej podstawniki powodujące dużą zawadę steryczną. Na podstawie tych wyników zaproponowano serię modyfikacji badanego ligandu i przetestowano je *in silico*. Jeden ze związków okazał się być bardziej selektywny od innych używanych w omawianej reakcji. Ważnym wynikiem tych badań jest test metod używanych do obliczeń wysokości barier energetycznych w reakcjach chemicznych. Obliczenia metodą DFT okazały się wystarczające dla określenia stereoselektywności reakcji ale tylko w wypadku gdy w obliczeniach zostały uwzględnione empiryczne poprawki na oddziaływania dyspersyjne. W celu ilościowego przewidzenia regioselektywności reakcji niezbędne jest spójne traktowanie korelacji elektronowej. W tym przypadku, dużo bardziej wymagająca metoda LPNO-CEPA/1, ciągle jednak możliwa do użycia w przypadku dużych układów, okazała się być odpowiednim wyborem.

W drugim projekcie przebadane zostały układy w których niektóre wiązania chemiczne są wyjątkowo rozciągnięte. Związki klastrkowe germanu ($\text{Ge}_{14}[\text{Si}(\text{SiMe}_3)_3]_5\text{Li}_3(\text{THF})_6$) i cyny ($\text{Sn}_4\text{Si}[\text{Si}(\text{SiMe}_3)_3]_4(\text{SiMe}_3)_2$) okazały się być ciekawymi przykładami stabilnych cząsteczek posiadających atomy, które nie są do końca wysyczone wiązaniami (trzy, zamiast czterech wiązań w przypadku Ge i Sn). Te trójskoordynowane atomy znajdują się za daleko od siebie by utworzyć normalne wiązanie pojedyncze, jednak są na tyle blisko by oczekiwać jakiś rodzaj oddziaływania. W obu układach znaleziono rombony system M_4R_6 ($\text{M} = \text{Ge}, \text{Sn}$; R – ligand), w którym układ spinów jest najlepiej określany jako singletowy ‘biradicaloid’ (stan pomiędzy wiązaniem pojedynczym a dwurodnikiem o multipletowości 1). Ponadto ważnym wkładem niniejszych obliczeń kwantowo-chemicznych była demonstracja faktu, że na pojawienie się oddziaływania typu ‘biradicaloid’ ma wpływ nie tylko wydłużenie wiązania pomiędzy atomami ale także orientacja i rozmiar ligandów. Zmiana tych parametrów może powodować przejście między oddziaływania typu ‘biradicaloid’, zwykłym wiązaniem pojedynczym a trypletowym dwurodnikiem. Dodatkowo obliczenia jasno pokazują limit stosowalności metod jednowyznacznikowych takich jak DFT. Dużo bardziej wyszukane

metody uwzględniające korelację statyczną, np. CASSCF, są niezbędne aby opisać stan elektronowy badanych układów.

W kolejnym kroku przeprowadzono obliczenia dla małych klasterów składających się z atomów niklu. Liczba eksperymentalnych wyników dla dimeru i trimeru niklu jest raczej znikoma i w wielu przypadkach niezgodna z danymi teoretycznymi. W tej pracy przeprowadzono obliczenia testowe dla cząsteczki Ni₂. Długość wiązania w tym układzie została oszacowana na 2.22 Å a odpowiadająca jej częstość drgań na 286 cm⁻¹. Metoda NEVPT2 okazała się być w doskonałej zgodności z wynikami otrzymanymi na poziomie MRACPF. Podejście perturbacyjne zostało także użyte w celu oszacowania elektronowego stanu podstawowego z uwzględnieniem oddziaływań spin-orbita. Zgodnie z wynikami, stanem podstawowym dimeru niklu jest 0_g⁺ co zgadza się z danymi eksperymentalnymi. Wykazano także, że funkcjonal TPSSh w połączeniu z podejściem ‘złamanej symetrii’ (od ang. *broken symmetry*) jest zgodny z wynikami otrzymanymi na poziomie NEVPT2. Jak wskazują badania eksperymentalne, podczas przyłączenia elektronu do cząsteczki Ni₂ wiązanie między atomami ulega wydłużeniu o 0.1 Å. Efekt ten został zaobserwowany na poziomie NEVPT2 i TPSSh a jego wyjaśnienie związane jest z przyłączeniem nadmiarowego elektronu do orbitalu σ*. Podobna analiza została przeprowadzona w przypadku trimeru niklu. Obliczenia metodami NEVPT2 i TPSSh wskazują, że stan podstawowy neutralnego trimeru ma geometrię trójkątną i kwintetowy stan spinowy. Na poziomie NEVPT2 anion tej cząsteczki przyjmuje strukturę liniową podczas gdy według obliczeń TPSSh oba izomery, trójkątny i liniowy, mają podobną energię. Ostateczne rozróżnienie będzie prawdopodobnie możliwe poprzez pomiar częstości drgań wiązania O-H w kompleksie, w którym klasterek niklu jest solwatowany przez dwie cząsteczki alkoholu etylowego. Zgodnie z obliczeniami TPSSh, różnica w drganiu rozciągającym O-H dwóch cząsteczek alkoholu będzie dużo mniejsza (~15 cm⁻¹) dla izomeru liniowego niż dla geometrii trójkątnej (~90 cm⁻¹). Badania IR powinny bez problemu rozróżnić obie formy.

Podobne problemy z metodami DFT zostały napotkane w ostatnim projekcie prezentowanym w tej pracy. Celem była tutaj analiza procesu aktywacji tlenu molekularnego przez kompleksy kobaltu(II) takie jak bis[trifluoroacetylacetonato(-1)]kobalt(II) [Co(tfa)₂]. Reakcja ta stanowi pierwszy etap w łagodnym i tanim aerobowym utlenianiu alkenoli do funkcjonalizowanych tetrahydrofuranów, cząsteczek o dużej aktywności biologicznej. Różne mechanizmy tej przemiany mogą zostać zaproponowane w zależności od struktury elektronowej adduktu. Zgodnie z obliczeniami izolowany katalizator z jedną cząsteczką wody [Co(tfa)₂(H₂O)] jest kompleksem wysokospinowym (kwartet). Kiedy cząsteczka tlenu zbliża się do atomu kobaltu, stan kwartetowy sprzęga się ze stanem trypletowym tlenu co daje stan sekstetowy, kwartetowy i dubletowy. W tym przypadku konfiguracja z pięcioma niesparowanymi elektronami (sekstet) jest najniżej energetyczna. Równowagowa długość wiązania Co–O₂ wynosi 1.9 Å a molekula Co(tfa)₂(H₂O)(O₂) posiada dubletowy stan podstawowy, gdzie atom

kobaltu jest formalnie opisywany jako Co(III) a grupa tlenowa posiada charakter ponadtlenkowy. Niesparowany elektron znajduje się na atomach tlenu na prawie nie zmienionym orbitalu σ^* O₂. Należy podkreślić, iż metoda DFT poprawnie opisuje podstawowy stan elektronowy katalizatora i adduktu, jednak relatywne energie poszczególnych stanów spinowych są zależne od użytego funkcjonału. Jasna separacja poszczególnych stanów nie byłaby możliwa bez wieloreferencyjnych obliczeń metodą NEVPT2.

Zaprezentowane obliczenia dają podstawę dla dalszych obliczeń dla dużych układów chemicznych zawierających metale i metaloidy. Otrzymane wyniki jasno pokazują potrzebę wyjścia poza metodę DFT dla takich kompleksów. Wydłużone wiązania czy problemy degeneracji poziomów energetycznych w przypadku metali trzeciej grupy układu okresowego stanowią bez wątpienia limit stosowalności metod jednowyznacznikowych. W takich przypadkach wykazane zostało, że użycie metody CASSCF wraz z perturbacyjnym przybliżeniem pozostałej energii korelacyjnej (NEVPT2) daje wyniki porównywalne do metod bazujących na oddziaływaniu konfiguracji (CI). Dodatkowo przewidzenie regioselektywności reakcji chemicznej, w której biorą udział tylko związki bez niesparowanych elektronów, wymaga spójnego traktowania korelacji elektronowej gdyż stany przejściowe mogą mieć bardzo różne struktury. Wyraźny postęp jaki poczynił się w przypadku wydajnych i dokładnych przybliżeń w chemii kwantowej pozwala dziś na prowadzenie obliczeń dokładnymi metodami bazującymi na funkcji falowej, takimi jak CEPA, dla cząsteczek zawierających ponad 100 atomów, ciągle w odpowiednio dużej bazie funkcyjnej. Poprzez dokładny test metod obliczeniowych pokazano, że stereoselektywność reakcji chemicznej może być przewidziana z użyciem większości funkcjonałów DFT ale tylko wtedy, gdy dodane zostaną empiryczne poprawki na energię dyspersyjną. Ponadto, wynikiem niniejszej pracy są przewidywania dotyczące struktury badanych układów chemicznych oraz ich reaktywności. Otrzymane dane mogą być bezpośrednio porównane z nadchodzącymi wynikami eksperymentalnymi co z pewnością pomoże w dogłębnym zrozumieniu procesów katalitycznych z udziałem kompleksów metalicznych.

7 ACKNOWLEDGEMENTS

It was a great pleasure for me to spend this three fruitful years here at KIT. First of all, I would like to thank my supervisor PD Dr. Karin Fink for her guidance, constructive criticism, inspiration and for being the most patient person I know.

This PhD thesis would certainly not be possible without Prof. Dr. Willem Klopper who gave me the opportunity to work in his group. He was always very helpful and created a stimulating scientific atmosphere.

I would like to sincerely thank Andrew Atkins, Tilmann Bodenstein, Angela Bihlmeier, Dorota Jakubczyk, and Michael Harding whose corrections and comments significantly improved this work.

I am thankful to all present and past members of the theoretical chemistry group who accompanied me during the last exciting years. It is hard to imagine a more friendly and helpful environment at work.

I would also like to thank all my scientific collaborators, Prof. Dr. Stefan Bräse, Prof. Dr. Markus Gerhards, Prof. Dr. Jens Hartung, Dr. Jan Paradies, Prof. Dr. Andreas Schnepf, and their groups for bringing my interests to the exciting chemical problems that are, in part, presented in this work.

Special thanks go to Andrew Atkins, Sylwia Sekuła-Neuner and Konstantinos Vogiatzis for making my stay in Karlsruhe unforgettable. I also thank all my friends in Poznań and Zielona Góra who always supported me, even being so far away.

I give thanks to my dear parents for their love and care throughout my life. Thank you for always believing in me. *Dziękuję!*

Finally, I thank my dear girlfriend Dorota for all her love and support during these challenging years and exciting scientific collaboration.

8 ACRONYMS

BSSE	Basis set superposition error
CASPT2	Complete active space perturbation theory at 2 nd order
CASSCF	Complete active space self-consistent field
CC	Coupled cluster
CEPA	Coupled electron pair approximation
CI	Configuration interaction
CSF	Configuration state function
DFT	Density functional theory
DKH	Douglas-Kroll-Hess
ECP	Effective core potential
FCI	Full configuration interaction
GGA	Generalised gradient-corrected approximation
HF	Hartree-Fock
HOMO	Highest occupied molecular orbital
IEPA	Independent electron pair approximation
LDA	Local density approximation
LPNO	Localised pair natural orbital
LUMO	Lowest unoccupied molecular orbital
MCSCF	Multiconfigurational self-consistent field
MPn	Møller-Plesset perturbation theory at n -th order
MRACPF	Multireference average coupled-pair functional
MRCI	Multireference configuration interaction
NEVPT2	n -Electron valence state perturbation theory at 2 nd order
NO	Natural orbital
PNO	Pair natural orbital
RI	Resolution of identity
ROHF	Restricted open-shell Hartree-Fock
SCF	Self-consistent field
SCS	Spin-component scaled
TS	Transition state
UHF	Unrestricted Hartree-Fock

9 COPYRIGHT PERMISSIONS

The Chapter 3 contains in part material that has already been published in peer-reviewed journals. The copyright permissions for published material are granted from the right owners and the details are as follow:

- results, tables and figures from the subchapter 3.1 are reproduced in part with permissions from:
 - S. Ay, R. E. Ziegert, H. Zhang, M. Nieger, K. Rissanen, K. Fink, A. Kubas, R. M. Gschwind, S. Bräse, *NMR-Spectroscopic and Solid-State Investigations of Cometal-Free Asymmetric Conjugate Addition: A Dinuclear Paracyclophaneimine Zinc Methyl Complex*, J. Am. Chem. Soc. 2010, **132**, 12899. Copyright 2010 American Chemical Society.
 - Kubas, S. Bräse, K. Fink, *Theoretical Approach Towards the Understanding of Asymmetric Additions of Dialkylzinc to Enals and Iminals Catalysed by [2.2]Paracyclophane-Based N,O-Ligands*, Chem. Eur. J. 2012, DOI: 10.1002/chem.201103710. Copyright 2012 Wiley-VCH Verlag GmbH & KGaA.
- results, tables and figures from the subchapter 3.2 are reproduced in part with permissions from:
 - C. Schenk, A. Kracke, K. Fink, A. Kubas, W. Klopffer, M. Neumaier, H. Schnöckel, A. Schnepf, *The Formal Combination of Three Singlet Biradicaloid Entities to a Singlet Hexaradicaloid Metalloid $Ge_{14}[Si(SiMe_3)_3]_5[Li(THF)_2]_3$ Cluster*, J. Am. Chem. Soc. 2011, **133**, 2518. Copyright 2011 American Chemical Society.
 - C. Schrenk, A. Kubas, K. Fink, A. Schnepf, *[$Sn_4Si\{Si(SiMe_3)_3\}_4(SiMe_3)_2$]: A Model Compound for the Unexpected First-Order Transition from a Singlet Biradicaloid to a Classical Bonded Molecule*, Angew. Chem. Int. Ed. 2011, **50**, 7273. Copyright 2011 Wiley-VCH Verlag GmbH & KGaA.
- results, tables and figures from the subchapter 3.4 are reproduced in part with permissions from:
 - Kubas, J. Hartung, K. Fink, *How O_2 binds to bis(trifluoroacetylacetonato)cobalt(II) complex? Ab initio and DFT studies.*, Dalton Trans. 2011, **40**, 11289. Reproduced by permission of The Royal Society of Chemistry. Available on-line: <http://dx.doi.org/10.1039/C1DT10724K>.

10 LIST OF SCIENTIFIC PUBLICATIONS

1. A. Kubas, K. Fink, S. Bräse
Theoretical Approach Towards the Understanding of Asymmetric Additions of Dialkylzinc to Enals and Iminals Catalysed by [2.2]Paracyclophane-Based N,O-Ligands
Chem. Eur. J. 2012, DOI: 10.1002/chem.201103710.
2. C. Barth, D. Jakubczyk, A. Kubas, F. Anastassacos, G. Brenner-Weiß, K. Fink, U. Schepers, S. Bräse, P. Koelsch
Inter-kingdom Signaling: Integration, Conformation and Orientation of N-Acyl-L-Homoserine Lactones in Supported Lipid Bilayers
Langmuir 2012, DOI: 10.1021/la301241s.
3. L. Greb, P. Oña-Burgos, A. Kubas, F. C. Falk, F. Breher, Karin Fink, D. W. Stephan, J. Paradies
[2.2]Paracyclophane derived Bisphosphines for the Activation of Hydrogen by FLPs: Application in Domino Hydrosilylation/Hydrogenation of Enones
Dalton Trans. 2012, DOI: 10.1039/C2DT30374D.
4. D. Jakubczyk, C. Barth, A. Kubas, F. Anastassacos, P. Koelsch, K. Fink, U. Schepers, G. Brenner-Weiß, S. Bräse
Deuterium-labelled N-acyl-L-homoserine lactones (AHLs)—inter-kingdom signalling molecules—synthesis, structural studies, and interactions with model lipid membranes
Anal. Bioanal. Chem. 2012, **404**, 473.
5. M. Kubicki, A. Paul, A. Kubas, C. Jelsch, K. Fink, C. Lecomte
Density Analysis of 2-methyl-4-nitro-1-phenyl-1H-imidazole-5-carbonitrile: An Experimental and Theoretical Study of CN-CN Interactions
J. Phys. Chem. 2011, **115**, 12941.
6. A. Kubas, J. Hartung, K. Fink
How O₂ binds to bis(trifluoroacetylacetonato)cobalt(II) complex? Ab initio and DFT studies.
Dalton Trans. 2011, **40**, 11289.
7. C. Schrenk, A. Kubas, K. Fink, A. Schnepf
[Sn₄Si{Si(SiMe₃)₃}₄(SiMe₃)₂]: A Model Compound for the Unexpected First-Order Transition from a Singlet Biradicaloid to a Classical Bonded Molecule
Angew. Chem. Int. Ed. 2011, **50**, 7273.

8. C. Schrenk, A. Kubas, K. Fink, A. Schnepf
[Sn₄Si{Si(SiMe₃)₃}₄(SiMe₃)₂]: eine Modellverbindung für den unerwarteten Übergang erster Ordnung eines Singulett-Biradikaloids zu einem klassisch gebundenen System
Angew. Chem. 2011, **123**, 7411.
9. C. Schenk, A. Kracke, K. Fink, A. Kubas, W. Klopfer, M. Neumaier, H. Schnöckel, A. Schnepf
The formal combination of three singlet biradicaloid entities to a singlet hexaradicaloid metalloid Ge₁₄[Si(SiMe₃)₃]₅Li₃(THF)₆ cluster.
J. Am. Chem. Soc. 2011, **133**, 2518.
10. S. Ay, R. E. Ziegert, H. Zhang, M. Nieger, K. Rissanen, K. Fink, A. Kubas, R. M. Gschwind, S. Bräse
NMR-spectroscopic and solid-state investigations of cometal-free asymmetric conjugate addition: a dinuclear paracyclophaneimine zinc methyl complex.
J. Am. Chem. Soc. 2010, **132**, 12899.
11. A. Kubas, M. Hoffmann, B. Marciniak
Quantum chemical studies on substitution effects within silyl group in the silylative coupling of olefins
J. Mol. Model. 2010, **16**, 395.

11 BIBLIOGRAPHY

- ¹ IUPAC. Compendium of Chemical Terminology, 2nd ed. (the "Gold Book"). Compiled by A. D. McNaught and A. Wilkinson. Blackwell Scientific Publications, Oxford (1997). XML on-line corrected version: <http://goldbook.iupac.org> (2006-) created by M. Nic, J. Jirat, B. Kosata; updates compiled by A. Jenkins. ISBN 0-9678550-9-8. doi:10.1351/goldbook.
- ² T. H. Maugh II, *Science* 1983, **220**, 1032.
- ³ P. Schuster, *Complexity* 2005, **11**, 11.
- ⁴ D. Astruc, *Nanoparticles and Catalysis*, WILEY-VCH, Weinheim, ISBN 978-3-527-31572-7, 2008.
- ⁵ W. Kohn, L. J. Sham, *Phys. Rev.* 1965, **140**, A1133.
- ⁶ J. P. Perdew, K. Schmidt, *AIP Conf. Proc.* 2001, **577**, 1, doi: 10.1063/1.1390175.
- ⁷ N. E. Schultz, Y. Zhao, D. G. Truhlar, *J. Phys. Chem. A* 2005, **109**, 4388.
- ⁸ N. Drebov, R. Ahlrichs, *J. Chem. Phys.* 2011, **134**, 124308.
- ⁹ S. Grimme, C. Diedrich, M. Korth, *Angew. Chem. Int. Ed.* 2005, **45**, 625.
- ¹⁰ S. Niu, B. Hall, *Chem. Rev.* 2000, **100**, 353.
- ¹¹ W. M. C. Sameera, F. Maseras, *WIREs Comput Mol Sci* 2012, **2**, 375.
- ¹² J. N. Harvey, *Annu. Rep. Prog. Chem., Sect. C: Phys. Chem.* 2006, **102**, 203.
- ¹³ E. Schrödinger, *Ann. Physik* 1926, **79**, 361.
- ¹⁴ J. von Neumann, J. P. Wigner, *Physik. Z.* 1929, **30**, 467.
- ¹⁵ L. Piela, *Ideas of Quantum Chemistry*, Elsevier, ISBN 978-0444522276, 2006.
- ¹⁶ M. Born, J. R. Oppenheimer, *Ann. Physik* 1927, **84**, 457.
- ¹⁷ W. Ritz, *J. Reine Angew. Math.* 1909, **135**, 1.
- ¹⁸ J. Slater, *Phys. Rev.* 1930, **35**, 509.
- ¹⁹ C. Hättig, W. Klopper, A. Köhn, D. P. Tew, *Chem. Rev.* 2012, **112**, 4 and references therein.
- ²⁰ P. Pyykkö, *Chem. Rev.* 1988, **88**, 563.
- ²¹ R. Ahuja, A. Blomquist, P. Larsson, P. Pyykkö, P. Zalewski-Ejgierd, *Phys. Rev. Lett.* 2011, **106**, 018301.
- ²² P. A. M. Dirac, *Proc. R. Soc. London, Ser. A* 1929, **123**, 714.
- ²³ T. Saue, *ChemPhysChem* 2011, **12**, 3077.
- ²⁴ G. Breit, *Phys. Rev.* 1929, **36**, 553.
- ²⁵ G. Breit, *Phys. Rev.* 1930, **36**, 363.
- ²⁶ G. Breit, *Phys. Rev.* 1932, **39**, 616.
- ²⁷ J. Autsbach, *J. Chem. Phys.* 2012, **136**, 150902.
- ²⁸ W. Pauli, *Z. Phys.* 1927, **43**, 601.
- ²⁹ *An Introduction to Relativistic Quantum Chemistry in European Summer School in Quantum Chemistry, Book III*, 7th Ed., Per-Olof Widmark, Ed., Lund University, 2011.

- ³⁰ D. Ganyushin, F. Neese, *J. Chem. Phys.* 2006, **125**, 024103 and references therein.
- ³¹ B. A. Hess, C. M. Marian, U. Wahlgren, O. Gropen, *Chem. Phys. Lett.* 1996, **251**, 365.
- ³² C. Chang, M. Pelissier, M. Durand, *Phys. Scr.* 1986, **34**, 294.
- ³³ J.-L. Heully, I. Lindgren, E. Lindroth, S. Lundqvist, A.-M. Mårtensson-Pendrill, *J. Phys. B* 1986, **19**, 2799.
- ³⁴ E. van Lenthe, E. J. Baerends, J. G. Snijders, *J. Chem. Phys.* 1993, **99**, 4597.
- ³⁵ M. Douglas, N. M. Kroll, *Ann. Phys. (N.Y.)* 1974, **82**, 89.
- ³⁶ B. A. Hess, *Phys. Rev. A* 1986, **33**, 3742.
- ³⁷ A. Wolf, M. Reiher, B. A. Hess, *J. Chem. Phys.* 2002, **117**, 9215.
- ³⁸ M. Dolg, *Effective Core Potentials in Modern Methods and Algorithms of Quantum Chemistry*, Proceedings, 2nd Ed., J. Grotendorst (Ed.), John von Neumann Institute for Computing, Jülich, NIC Series, Vol. 3, ISBN 3-00-005834-6, 2000.
- ³⁹ F. Bloch, *Z. Phys.* 1928, **52**, 555.
- ⁴⁰ C. C. J. Roothan, *Rev. Modern Phys.* 1951, **23**, 69.
- ⁴¹ G. G. Hall, *Proc. Royal Soc. A* 1951, **205**, 541.
- ⁴² J. A. Pople, R. K. Nesbet, *J. Chem. Phys.* 1954, **22**, 571.
- ⁴³ M. W. Wong, L. Radom, *J. Phys. Chem.* 1995, **99**, 8582.
- ⁴⁴ C. C. J. Roothan, *Rev. Modern Phys.* 1960, **32**, 179.
- ⁴⁵ J. Almlöf, R. Ahlrichs, *Notes on Hartree-Fock Theory and Related Topics in European Summer School in Quantum Chemistry, Book I*, 7th Ed., Per-Olof Widmark, Ed., Lund University, 2011.
- ⁴⁶ T. Helgaker, P. Jørgsen, J. Olsen, *Molecular Electronic-Structure Theory*, John Wiley & Sons, Ltd., ISBN 0-461-96755-6, 2000.
- ⁴⁷ S. Grimme, *J. Chem. Phys.* 2003, **118**, 9095.
- ⁴⁸ S. Grimme, *J. Comput. Chem.* 2003, **24**, 1529.
- ⁴⁹ J. Antony, S. Grimme, *J. Phys. Chem. A* 2007, **111**, 4862.
- ⁵⁰ R. A. Bachorz, F. A. Bischoff, S. Höfener, W. Klopper, P. Ottinger, R. Leist, J. A. Frey, S. Leutwyler, *Phys. Chem. Chem. Phys.* 2008, **10**, 2758.
- ⁵¹ M. Gerenkamp, S. Grimme, *Chem. Phys. Lett.* 2004, **392**, 229.
- ⁵² T. Schwabe, S. Grimme, *Acc. Chem. Res.* 2008, **41**, 569 and references therein.
- ⁵³ A. Szabo, N. S. Ostlund, *Modern Quantum Chemistry: Introduction to Advanced Electronic Structure Theory*, 1st ed. rev. by McGraw-Hill Publishing 1989, republished by Dover Publications Inc., 1996.
- ⁵⁴ R. F. Fink, *J. Chem. Phys.* 2010, **133**, 174113 and references therein.
- ⁵⁵ E. Rossi, G. L. Bendazzoli, S. Evangelisti, D. Maynau, *Chem. Phys. Lett.* 1999, **310**, 530.
- ⁵⁶ P. O. Löwdin, *Phys. Rev.* 1955, **97**, 1474.
- ⁵⁷ W. Meyer, *Int. J. Quant. Chem.* 1971, **S5**, 59.
- ⁵⁸ W. Meyer, *J. Chem. Phys.* 1973, **58**, 1017.
- ⁵⁹ R. Ahlrichs, H. Lischka, V. Staemmler, W. Kutzelnigg, *J. Chem. Phys.* 1975, **62**, 1225.

- ⁶⁰ R. Ahlrichs, *Comp. Phys. Comm.* 1979, **17**, 31.
- ⁶¹ P. Rosmus, P. Botchwina, J. P. Maier, *Chem. Phys. Lett.* 1981, **84**, 71.
- ⁶² A. M. Semkow, P. Rosmus, H. Bock, P. Botschina, *Chem. Phys.* 1979, **40**, 377.
- ⁶³ H.-J. Werner, M. Schütz, *J. Chem. Phys.* 2011, **135**, 144116 and references therein.
- ⁶⁴ P. Pulay, *Chem. Phys. Lett.* 1983, **100**, 151.
- ⁶⁵ F. Neese, F. Wennmohs, A. Hansen, *J. Chem. Phys.* 2009, **130**, 113018.
- ⁶⁶ F. Neese, A. Hansen, D. G. Liakos, *J. Chem. Phys.* 2009, **131**, 064103.
- ⁶⁷ P. Hohenberg, W. Kohn, *Phys. Rev.* 1964, **136**, 864.
- ⁶⁸ J. C. Slater, *Phys. Rev.* 1951, **81**, 385.
- ⁶⁹ S. J. Vosko, L. Wilk, M. Nussair, *Can. J. Phys.* 1980, **1980**, 1200.
- ⁷⁰ A. D. Becke, *Phys. Rev. A* 1988, **38**, 3098.
- ⁷¹ J. P. Perdew, Y. Wang, *Phys. Rev. B* 1986, **33**, 8800.
- ⁷² A. D. Becke, *J. Chem. Phys.* 1988, **88**, 1053.
- ⁷³ J. P. Perdew, *Phys. Rev.* 1986, **B33**, 8822.
- ⁷⁴ J. P. Perdew, *Electronic Structure of Solids '91*, P. Ziesche and H. Eschring, Eds., Akademie Verlag Berlin, 1991.
- ⁷⁵ J. P. Perdew, K. Burke, M. Enzerhof, *Phys. Rev. Lett.* 1996, **77**, 3865.
- ⁷⁶ C. Lee, W. Yang, R. H. Parr, *Phys. Rev. B* 1988, **37**, 785.
- ⁷⁷ K. Eichkorn, O. Treutel, H. Öhm, M. Häser, R. Ahlrichs, *Chem. Phys. Lett.* 1995, **240**, 283.
- ⁷⁸ J. Tao, J. P. Perdew, V. N. Staroverov, G. E. Scuseria, *Phys. Rev. Lett.* 2003, **91**, 146401.
- ⁷⁹ D. C. Langreth, J. P. Perdew, *Solid State Commun.* 1975, **17**, 1425.
- ⁸⁰ O. Gunnarsson, B. I. Lundquist, *Phys. Rev. B* 1976m, **13**, 4274.
- ⁸¹ P. J. Stephens, F. J. Devlin, C. F. Chabalowski, M. J. Frisch, *J. Phys. Chem.* 1994, **98**, 623.
- ⁸² C. J. Cramer, *Essentials of Computational Chemistry*, 2nd Ed., John Wiley & Sons, ISBN 0-470-09182-7, 2007.
- ⁸³ J. N. Harvey, *DFT Computation of Relative Spin-State Energetics of Transition Metal Compounds in Structure and Bonding*, **112**, pp. 151, Heidelberg, 2004.
- ⁸⁴ T. Yanai, D. P. Tew, N. C. Handy, *Chem. Phys. Lett.* 2004, **393**, 51.
- ⁸⁵ S. Grimme, *J. Comput. Chem.* 2004, **25**, 1463.
- ⁸⁶ J. Hepburn, G. Scoles, R. Penco, *Chem. Phys. Lett.* 1975, **36**, 451.
- ⁸⁷ R. Ahlrichs, R. Penco, G. Scoles, *Chem. Phys.* 1977, **19**, 119.
- ⁸⁸ S. Grimme, *J. Comput. Chem.* 2006, **27**, 1787.
- ⁸⁹ S. Grimme, J. Antony, S. Ehrlich, H. Krieg, *J. Chem. Phys.* 2010, **132**, 154104.
- ⁹⁰ S. Grimme, *Wiley Interdisciplinary Reviews: Computational Molecular Science* 2011, **1**, 211.
- ⁹¹ U. Ryde, R. A. Mata, S. Grimme, *Dalton Trans.* 2011, **40**, 11176.
- ⁹² A. Tarnopolsky, A. Karton, R. Sertchook, D. Vuzman, J. M. L. Martin, *J. Phys. Chem. Lett.* 2008, **112**, 3.
- ⁹³ S. Grimme, *Org. Lett.* 2010, **12**, 4670.

- ⁹⁴ B. O. Roos, *The multiconfigurational (MC) self-consistent field (SCF) theory in European Summerschool in Quantum Chemistry 2011, Book II*, P.-O. Widmark, Ed., Lund University, 2011 and references therein.
- ⁹⁵ B. O. Roos, P. R. Taylor, P. E. M. Siegbahn, *Chem. Phys.* 1980, **48**, 157.
- ⁹⁶ K. Pierloot, *Calculations of Electronic Spectra of Transition Metal Complexes in Theoretical and Computational Chemistry: Computational photochemistry*, **16**, M. Olivussi, Ed., Elsevier, 2005 and references therein.
- ⁹⁷ V. Veryazov, P.-Å. Malmqvist, B. O. Roos, *Int. J. Quant. Chem.* 2011, **111**, 3329.
- ⁹⁸ K. Anderson, B. O. Roos, P.-Å. Malmqvist, P.-O. Widmark, *Chem. Phys.* 1994, **230**, 391.
- ⁹⁹ K. Anderson, P.-Å. Malmqvist, B. O. Roos, A. J. Sadlej, K. Wolinski, *J. Phys. Chem.* 1990, **94**, 5483.
- ¹⁰⁰ K. Anderson, P.-Å. Malmqvist, B. O. Roos, *J. Chem. Phys.* 1992, **96**, 1218.
- ¹⁰¹ S. T. Epstein, *The Variational Method in Quantum Chemistry*, Academic Press, 1974.
- ¹⁰² K. G. Dyall, *J. Chem. Phys.* 1995, **102**, 4909.
- ¹⁰³ C. Angeli, R. Cimiraglia, S. Evangelisti, T. Leininger, J.-P. Malrieu, *J. Chem. Phys.* 2001, **114**, 10252.
- ¹⁰⁴ C. Angeli, R. Cimiraglia, J.-P. Malrieu, *Chem. Phys. Lett.* 2001, **350**, 297.
- ¹⁰⁵ C. Angeli, R. Cimiraglia, J.-P. Malrieu, *J. Chem. Phys.* 2002, **117**, 9138.
- ¹⁰⁶ R. W. A. Havenith, P. R. Taylor, C. Angeli, R. Cimiraglia, K. Ruud, *J. Chem. Phys.* 2004, **120**, 4619.
- ¹⁰⁷ M. Atanasov, D. Ganyushin, K. Sivalingam, F. Neese, *A modern first-principles view on ligand field theory through the eyes of correlated multireference wavefunctions in Structure and Bonding*, **143**, D. M. Mingos, P. Day, J. P. Dahl, Eds., Springer Verlag, 2012 and references therein.
- ¹⁰⁸ P. E. Siegbahn, *Chem. Phys.* 1977, **25**, 197.
- ¹⁰⁹ P. E. Siegbahn, *Int. J. Quant. Chem.* 1983, **23**, 1869.
- ¹¹⁰ W. Meyer, *Modern Theoretical Chemistry*, H. F. Schaefer III, Ed., Plenum, New York, 1977.
- ¹¹¹ P. E. Siegbahn, *Int. J. Quant. Chem.* 1980, **18**, 1229.
- ¹¹² H.-J. Werner, E.-A. Reinsch, *J. Chem. Phys.* 1982, **76**, 3144.
- ¹¹³ R. Gdanitz, R. Ahlrichs, *Chem. Phys. Lett.* 1988, **143**, 413.
- ¹¹⁴ P. G. Szalay, R. J. Bartlett, *Chem. Phys. Lett.* 1993, **214**, 418.
- ¹¹⁵ S. R. Langhoff, E. R. Davidson, *Int. J. Quant. Chem.* 1974, **8**, 61.
- ¹¹⁶ P. G. Szalay, T. Müller, G. Gidofalvi, H. Lischka, R. Shepard, *Chem. Rev.* 2012, **112**, 108.
- ¹¹⁷ R. J. Bartlett, M. Musiał, *Rev. Mod. Phys.* 2007, **79**, 291 and references therein.
- ¹¹⁸ J. Paldus, J. Pittner, P. Čársky, *Multireference Coupled-Cluster Methods: Recent Developments in Recent Progress in Coupled Cluster Methods*, P. Čársky, J. Paldus, J. Pittner, Eds., **11**, Springer Verlag, 2010 and references therein.

- ¹¹⁹ T. Shiozaki, G. Knizia, H.-J. Werner, *J. Chem. Phys.* 2011, **134**, 034113 and references therein.
- ¹²⁰ T.-C. Jagau, *JUNQ* 2011, **1**, 4.
- ¹²¹ A. Schäfer, H. Horn, R. Ahlrichs, *J. Chem. Phys.* 1992, **97**, 2517.
- ¹²² K. Eichkorn, F. Weigend, O. Treutler, R. Ahlrichs, *Theor. Chem. Acc.* 1997, **97**, 119.
- ¹²³ F. Weigend, R. Ahlrichs, *Phys. Chem. Chem. Phys.* 2005, **7**, 3297.
- ¹²⁴ F. Weigend, M. Häser, H. Patzelt, R. Ahlrichs, *Chem. Phys. Letters* 1998, **294**, 143.
- ¹²⁵ F. Neese, E. F. Valeev, *J. Chem. Theory Comput.* 2011, **7**, 33 and references therein for ANOs.
- ¹²⁶ T. H. Dunning, K. A. Peterson, A. K. Wilson, *J. Chem. Phys.* 2001, **114**, 9244 and references therein.
- ¹²⁷ D. E. Woon, T. H. Dunning, *J. Chem. Phys.* 1995, **103**, 4572.
- ¹²⁸ S. F. Boys, F. Bernardi, *Mol. Phys.* 1970, **19**, 553.
- ¹²⁹ I. Mayer, *Int. J. Quantum Chem.* 1983, **23**, 341.
- ¹³⁰ S. F. Boys, I. Shavitt, University of Wisconsin, Rep WIS-AF-13, 1959.
- ¹³¹ R. A. Kendall, H. A. Früchtl, *Theor. Chem. Acc.* 1997, **97**, 158.
- ¹³² K. Eichkorn, O. Treutler, H. Öhm, M. Häser, R. Ahlrichs, *Chem. Phys. Letters* 1995, **242**, 652.
- ¹³³ F. Weigend, *Phys. Chem. Chem. Phys.* 2006, **8**, 1057.
- ¹³⁴ F. Weigend, *Phys. Chem. Chem. Phys.* 2002, **4**, 4285.
- ¹³⁵ F. Neese, F. Wennmohs, A. Hansen, U. Becker, *Chem. Phys.* 2009, **356**, 98.
- ¹³⁶ H. Eyring, *J. Chem. Phys.* 1935, **3**, 63.
- ¹³⁷ H. Eyring, *Trans. Faraday Soc.* 1938, **34**, 41.
- ¹³⁸ E. Wigner, *Trans. Faraday Soc.* 1938, **34**, 29.
- ¹³⁹ B. C. Garrett, *Theor. Chem. Acc.* 2000, **103**, 200 and references therein.
- ¹⁴⁰ R. Fletcher, *Practical Methods of Optimization*, 2nd Ed., John Wiley & Sons Ltd., ISBN 0-471-49463-1, 2000.
- ¹⁴¹ A. R. Leach, *Molecular Modelling Principles and Applications*, 2nd Ed., Pearson Education Ltd., ISBN 0-582-38210-6, 2001.
- ¹⁴² T. Helgaker, *Chem. Phys. Letters* 1991, **182**, 503.
- ¹⁴³ D. A. McQuarrie, J. D. Simon, *Molecular Thermodynamics*, University Science Books, ISBN 978-1891389054, 1999.
- ¹⁴⁴ F. Jensen, *Introduction to Computational Chemistry*, 2nd Ed., John Wiley & Sons Ltd., ISBN 0-470-01187-4, 2007.
- ¹⁴⁵ I. M. Alecu, J. Zheng, Y. Zhao, D. G. Truhlar, *J. Chem. Theory Comput.* 2010, **6**, 2872.
- ¹⁴⁶ V. Barone, M. Biczysko, J. Bloino, M. Borkowska-Panek, I. Carnimeo, P. Panek, *Int. J. Quant. Chem.* 2011, **112**, 2185 and references therein.
- ¹⁴⁷ Y.-Y. Chuang, D. G. Truhlar, *J. Chem. Phys.* 2000, **112**, 1221.

- ¹⁴⁸ TURBOMOLE, a development of University of Karlsruhe and Forschungszentrum Karlsruhe GmbH, 1989-2007, TURBOMOLE GmbH, since 2007; available from <http://www.turbomole.com>; accessed 31.05.2012.
- ¹⁴⁹ ORCA - an ab initio, DFT and semiempirical SCF-MO package. Developed by F. Neese, Bonn University and MPI Mülheim, Germany, available from <http://www.mpibac.mpg.de>; accessed 31.05.2012.
- ¹⁵⁰ MOLDEN a pre- and post processing program of molecular and electronic structure, written by G. Schaftenaar, available from <http://www.cmbi.ru.nl/molden/>; accessed 31.05.2012.
- ¹⁵¹ W. Humphrey, A. Dalke, K. Schulten, *J. Molec. Graphics* 1996, **14**, 33.
- ¹⁵² Avogadro: an open-source molecular builder and visualization tool. Version 1.00. Available on-line from <http://avogadro.openmolecules.net/>.
- ¹⁵³ L. Pu, H.-B. Yu, *Chem. Rev.* 2001, **101**, 757.
- ¹⁵⁴ S. J. Degrado, H. Mizutani, A. H. Hoveyda, *J. Am. Chem. Soc.* 2001, **123**, 755.
- ¹⁵⁵ S. Ay, M. Nieger, S. Bräse, *Chem. Eur. J.* 2008, **14**, 11539.
- ¹⁵⁶ S. Dahmen, S. Bräse, *J. Am. Chem. Soc.* 2002, **124**, 5940.
- ¹⁵⁷ M. Kitamura, S. Okada, S. Suga, R. Noyori, *J. Am. Chem. Soc.* 1989, **111**, 4028.
- ¹⁵⁸ D. Guillaneaux, S. H. Zhao, O. Samuel, D. Rainford, H. B. Kagan, *J. Am. Chem. Soc.* 1994, **116**, 9430.
- ¹⁵⁹ C. Girard, H. B. Kagan, *Angew. Chem. Int. Ed.* 1998, **37**, 2922.
- ¹⁶⁰ S. Ay, R. E. Ziegert, H. Zhang, M. Nieger, K. Rissanen, K. Fink, A. Kubas, R. M. Gschwind, S. Bräse, *J. Am. Chem. Soc.* 2010, **132**, 12899.
- ¹⁶¹ S. Kitamura, H. Oka, R. Noyori, *Tetrahedron* 1999, **55**, 3605.
- ¹⁶² M. Yamakawa, R. Noyori, *Organometallics* 1999, **18**, 128.
- ¹⁶³ B. Goldfuss, M. Steigelmann, S. I. Khan, K. N. Houk, *J. Org. Chem.* 2000, **65**, 77.
- ¹⁶⁴ J. Vázquez, M. A. Pericàs, F. Maseras, A. Lledós, *J. Org. Chem.* 2000, **65**, 7303.
- ¹⁶⁵ B. Goldfuss, M. Steigelmann, F. Rominger, *Eur. J. Org. Chem.* 2000, 1785.
- ¹⁶⁶ A. Klamt, G. Schüürmann, *J. Chem. Soc. Perkin Trans.* 1993, **2**, 799.
- ¹⁶⁷ Ertl, P.; Rohde, B.; Selzer, P. *J. Med. Chem.* 2000, **43**, 3714.
- ¹⁶⁸ Sinnokrot, M. O.; Sherrill, C. D. *J. Am. Chem. Soc.* 2004, **126**, 7690.
- ¹⁶⁹ K. B. Wiberg, P. R. Rablen, M. Marquez, *J. Am. Chem. Soc.* 1992, **114**, 8654.
- ¹⁷⁰ H. M. Badawi, *J. Mol. Struct. (Theochem)* 2002, **617**, 9.
- ¹⁷¹ D. Y. Afanas'yev, A. V. Prosyaniuk, *J. Mol. Struct. (Theochem)* 2005, **730**, 45.
- ¹⁷² M. Brahimi, Y. Belmiloud, D. Kheffache, *J. Mol. Struct. (Theochem)* 2006, **759**, 1.
- ¹⁷³ H. B. Bürgi, J. D. Dunitz, J. M. Lehn, G. Wipff, *Tetrahedron* 1974, **30**, 1563.
- ¹⁷⁴ I. Fleming, *Molecular Orbitals and Organic Chemical Reactions: Reference Edition*, John Wiley & Sons, Chichester, ISBN 978-047074658, 2010.
- ¹⁷⁵ F. M. Bickelhaupt, *J. Comp. Chem.* 1999, **20**, 114.
- ¹⁷⁶ W.-J. van Zeist, F. M. Bickelhaupt, *Org. Biomol. Chem.* 2010, **8**, 3118.

- ¹⁷⁷ A. E. Dorgio, K. Morokuma, *J. Am. Chem. Soc.* 1989, **111**, 4635.
- ¹⁷⁸ A. Schnepf, *New J. Chem.* 2010, **34**, 2079.
- ¹⁷⁹ H. Schnöckel, *Chem. Rev.* 2010, **110**, 4125.
- ¹⁸⁰ S. Scharfe, F. Kraus, S. Stegmaier, A. Schier, T. F. Fässler, *Angew. Chem. Int. Ed.* 2011, **50**, 3630 and references therein.
- ¹⁸¹ A. Schnepf, *Phosphorus Sulphur Silicon Relat. Elem.* 2004, **179**, 695.
- ¹⁸² A. Pacher, C. Schrenk, A. Schnepf, *J. Organomet. Chem.* 2010, **695**, 941.
- ¹⁸³ C. Schenk, A. Kracke, K. Fink, A. Kubas, W. Klopper, M. Neumaier, H. Schnöckel, A. Schnepf, *J. Am. Chem. Soc.* 2011, **133**, 2518.
- ¹⁸⁴ C. Schrenk, A. Kubas, K. Fink, A. Schnepf, *Angew. Chem. Int. Ed.* 2011, **50**, 7273.
- ¹⁸⁵ D. Nied, W. Klopper, F. Breher, *Angew. Chem. Int. Ed.* 2009, **48**, 1411.
- ¹⁸⁶ P. Pyykkö, M. Atsumi, *Chem. Eur. J.* 2009, **15**, 186.
- ¹⁸⁷ C. Drost, M. Hildebrand, P. Lönnecke, *Main Group Met. Chem.* 2002, **25**, 93.
- ¹⁸⁸ B. Metz, H. Stoll, M. Dolg, *J. Chem. Phys.* **2000**, *113*, 2563.
- ¹⁸⁹ R. Koch, T. Bruhn, M. Weidenbruch, *Theochem.* 2004, **680**, 91.
- ¹⁹⁰ X. Wang, Y. Peng, Z. Zhu, J. C. Fettinger, P. P. Power, J. Guo, S. Nagase, *Angew. Chem. Int. Ed.* 2010, **49**, 4593.
- ¹⁹¹ W. Kaim, B. Schwederski, *Bioanorganische Chemie*, 4. Auflage, Teubner Verlag, Wiesbaden, 2005.
- ¹⁹² P. M. Bialach, M. Braun, A. Lüchow, M. Gerhards, *Phys. Chem. Chem. Phys.* 2009, **11**, 10403.
- ¹⁹³ P. M. Bialach, A. Funk, M. Weiler, M. Gerhards, *J. Chem. Phys.* 2010, **133**, 194304.
- ¹⁹⁴ H. Wang, Y. G. Khait, M. R. Hoffmann, *Mol. Phys.* 2005, **103**, 263.
- ¹⁹⁵ C. W. Bauschlicher, Jr., Per E. M. Siegbahn, L. G. M. Pettersson, *Theor. Chim. Acta* 1988, **74**, 479.
- ¹⁹⁶ C. Angeli, R. Cimiraglia, *Mol. Phys.* 2011, **109**, 1503.
- ¹⁹⁷ C. Duboc, D. Ganyushin, K. Sivalingam, M.-N. Collomb, F. Neese, *J. Phys. Chem. A* 2010, **114**, 10750.
- ¹⁹⁸ R. Pou-Américo, M. Merchán, I. Nebot-Gil, P.-Å. Malmqvist, B. O. Roos, *J. Chem. Phys.* 1994, **101**, 4893.
- ¹⁹⁹ M. D. Morse, G. P. Hansen, P. R. R. Langridge-Smith, L.-S. Zheng, M. E. Gensic, D. L. Michalopoulos, R. E. Smalley, *J. Chem. Phys.* 1984, **80**, 5400.
- ²⁰⁰ J. C. Pinegar, J. D. Langenberg, C. A. Arrington, E. M. Spain, M. D. Morse, *J. Chem. Phys.* 1995, **102**, 666.
- ²⁰¹ J. Ho, M. L. Polak, K. M. Ervin, W. C. Lineberger, *J. Chem. Phys.* 1993, **99**, 8542.
- ²⁰² H. Wang, H. Haouari, R. Craig, J. R. Lombardi, D. M. Lindsay, *J. Chem. Phys.* 1996, **104**, 3420.
- ²⁰³ E. M. Spain, M. D. Morse, *J. Chem. Phys.* 1992, **97**, 4641.
- ²⁰⁴ C. J. Barden, J. C. Riestra-Kiracofe, H. F. Schaefer III, *J. Chem. Phys.* 2000, **113**, 690.

- ²⁰⁵ S. Yanagisawa, T. Tsuneda, K. Hirao, *J. Chem. Phys.* 2000, **112**, 545.
- ²⁰⁶ G. L. Gutsev, C. W. Bauschlicher Jr., *J. Phys. Chem. A* 2003, **107**, 4755.
- ²⁰⁷ C. V. Diaconu, A. E. Cho, J. D. Doll, D. L. Freeman, *J. Chem. Phys.* 2004, **121**, 10026.
- ²⁰⁸ G. L. Arvizu, P. Calaminici, *J. Chem. Phys.* 2007, **126**, 194102.
- ²⁰⁹ A. T. Barnes, H. E. Hallam, D. Jones, *Proc. R. Soc. Lond. A* 1973, **335**, 97.
- ²¹⁰ C. W. Bauschlicher, Jr., H. Partridge, S. R. Langhoff, *Chem. Phys. Lett.* 1992, **195**, 360.
- ²¹¹ M. Moskovits, D. P. DiLella, *J. Chem. Phys.* 1980, **72**, 2267.
- ²¹² D. I. Davlyatshin, L. V. Serebrennikov, A. V. Golovkin, *Russ. J. Phys. Chem. A* 2009, **83**, 2087.
- ²¹³ G.-L. Arvizu, P. Calaminici, *J. Chem. Phys.* 2007, **126**, 194102.
- ²¹⁴ B. N. Papas, H. F. Schaefer III, *J. Chem. Phys.* 2005, **123**, 074321.
- ²¹⁵ F. Calvayrac, *Comp. Mat. Sci.* 2000, **17**, 164.
- ²¹⁶ P. A. Derosa, J. M. Seminario, P. B. Balbuena, *J. Phys. Chem. A* 2001, **105**, 7917.
- ²¹⁷ S. E. Weber, P. Jena, *Chem. Phys. Lett.* 1997, **281**, 401.
- ²¹⁸ S.-R. Liu, H.-J. Zhai, L.-S. Wang, *J. Chem. Phys.* 2002, **117**, 9758.
- ²¹⁹ G. Ganteför, W. Eberhardt, *Phys. Rev. Lett.* 1996, **76**, 4975.
- ²²⁰ T. Mukaiyama, T. Yamada, *Bull. Chem. Soc. Jpn.* 1995, **68**, 17.
- ²²¹ R.A. Sheldon, *Top. Curr. Chem.* 1993, **163**, 23.
- ²²² D. Schröder, H. Schwarz, in *Essays in Contemporary Chemistry*, G. Quinkert M.V. Kisakürek, Eds., Wiley-VCH, Weinheim, ISBN 3-906390-28-4, 2001.
- ²²³ R.S. Drago, B.B. Corden, *Acc. Chem. Res.* 1980, **13**, 353.
- ²²⁴ N.J. Turro, *Modern Molecular Photochemistry*, University Science Books, Mill Valley, CA, ISBN 978-0935702712, 1991.
- ²²⁵ R.A. Sheldon, J.K. Kochi, *Metal-Catalyzed Oxidations of Organic Compounds*, Academic Press, New York, ISBN 978-0126393804, 1981.
- ²²⁶ A. Werner, A. Z. Mylius, *Z. Anorg. Allg. Chem.* 1898, **16**, 245.
- ²²⁷ G. A. Rodley, W. T. Robinson, *Nature* 1972, **235**, 438.
- ²²⁸ S. Tamagaki, Y. Kanamaru, M. Ueno, W. Tagaki, *Bull. Chem. Soc. Jpn.* 1991, **64**, 165.
- ²²⁹ M. Strašák, J. Kaválek, *J. Mol. Catal.* 1991, **66**, 239.
- ²³⁰ E.-G. Jäger, J. Knautd, M. Rudolph, M. Rost, *Chem. Ber.* 1996, **129**, 1041.
- ²³¹ N. J. Henson, P. J. Hay, A. Redondo, *Inorg. Chem.* 1999, **38**, 1618.
- ²³² A. Dedieu, M.-M. Rohmer, A. Veillard, *J. Am. Chem. Soc.* 1976, **98**, 5789.
- ²³³ M. Valko, R. Klement, P. Pelikán, R. Boča, L. Dlhán, A. Böttcher, H. Elias, L. Müller, *J. Phys. Chem.* 1995, **99**, 137.
- ²³⁴ J. Hartung, M. Greb, *J. Organomet. Chem.* 2002, **661**, 67.
- ²³⁵ S. Inoki, T. Mukaiyama, *Chem. Lett.* 1990, **1**, 67.
- ²³⁶ B. Menéndez Pérez, D. Schuch, J. Hartung, *Org. Biomol. Chem.* 2008, **6**, 3532.
- ²³⁷ D. Schuch, P. Fries, M. Dönges, J. Hartung, *J. Am. Chem. Soc.* 2009, **131**, 12918.
- ²³⁸ J. P. Wolfe, M. B. Hay, *Tetrahedron* 2007, **63**, 261.

- ²³⁹ B. M. Hoffman, D. L. Diemente, F. Basolo, *J. Am. Chem. Soc.* 1970, **92**, 61.
- ²⁴⁰ G. A. Rodley, W. T. Robinson, *Nature* 1972, **235**, 438.
- ²⁴¹ A. Bakac, H. Espendon, *J. Am. Chem. Soc.* 1990, **112**, 2273.
- ²⁴² J. Cho, R. Sarangi, H. Y. Kang, J. Y. Lee, M. Kubo, T. Ogura, E. I. Solomon, W. Nam, *J. Am. Chem. Soc.* 2010, **132**, 16977.
- ²⁴³ J. E. Newton, M. B. Hall, *Inorg. Chem.* 1984, **23**, 4627.
- ²⁴⁴ V. N. Staroverov, G. E. Scuseria, J. Tao, J. P. Perdew, *J. Chem. Phys.*, 2003, **119**, 12129.
- ²⁴⁵ V. N. Staroverov, G. E. Scuseria, J. Tao, J. P. Perdew, *J. Chem. Phys.* 2004, **121**, 11507.
- ²⁴⁶ M. Radoń, M. Srebro, E. Brocławik, *J. Chem. Theory Comput.* 2009, **5**, 1237.
- ²⁴⁷ K. Yamaguchi, *Chem. Phys. Lett.* 1975, **33**, 330.
- ²⁴⁸ L. Noodleman, *J. Chem. Phys.* 1981, **74**, 5737.
- ²⁴⁹ V. S. Bryantsev, W. A. de Jong, K. C. Cossel, M. S. Diallo, W. A. Goddard III, G. S. Groenewold, W. Chien, M. J. Van Stipdonk, *J. Phys. Chem. A* 2008, **112**, 5778 and references therein.
- ²⁵⁰ I. Bytheway, M. B. Hall, *Chem. Rev.* 1994, **94**, 639.
- ²⁵¹ K. Kato, T. Yamada, T. Takai, S. Inoki, S. Isayama, *Bull. Chem. Soc. Jpn.* 1990, **63**, 179.
- ²⁵² B. Menéndez Pérez, D. Schuch, J. Hartung, *From Cobalt(II)-Activated Molecular Oxygen to Hydroxymethyl-Substituted Tetrahydrofurans in Activating Unreactive Substrates. The Role of Secondary Interactions*, C. Bolm, E. Hahn, Eds., Wiley-VCH, ISBN 978-3-527-31823-0, 379-396, 2009.
- ²⁵³ P. Pietrzyk, M. Srebro, M. Radoń, Z. Sojka, A. Michalak, *J. Phys. Chem. A* 2011, **115**, 2316.
- ²⁵⁴ A. Domingo, M. A. Carvajal, C. De Graaf, *Int. J. Quant. Chem.* 2010, **110**, 331.
- ²⁵⁵ G. Ganzenmüller, N. Berkaine, A. Fouqueau, M. E. Casida, M. Reiher, *J. Chem. Phys.*, 2005 **122**, 234321.
- ²⁵⁶ M. Kepenekian, V. Robert, B. Le Guennic, C. De Graaf, *J. Comput. Chem.* 2009, **30**, 2327.
- ²⁵⁷ E. V. Rybak-Akimova, M. Masarwa, K. Marek, P. R. Warburton, D. H. Bush, *Chem. Commun.* 1996, 1451.
- ²⁵⁸ S. Shaik, D. Kumar, S. P. de Visser, A. Altun, W. Thiel, *Chem. Rev.* 2005, **105**, 2279.
- ²⁵⁹ D. Schröder, S. Shaik, H. Schwarz, *Acc. Chem. Res.* 2000, **33**, 139.
- ²⁶⁰ K. P. Jensen, U. Ryde, *J. Biol. Chem.* 2004, **279**, 14561.
- ²⁶¹ A. Bassan, T. Borowski, P. E. M. Siegbahn, *Dalton Trans.* 2004, **20**, 3153.
- ²⁶² M. Lundberg, K. Morokuma, *J. Phys. Chem. B* 2007, **111**, 9380.